Assessing Coastal Plain Wetland Composition using Advanced Spaceborne Thermal Emission and Reflection Radiometer Imagery

Eva Pantaleoni

Dissertation submitted to the faculty of Virginia Polytechnic Institute and State University in partial fulfillment of the requirements for the degree of

Doctor of Philosophy
In
Crop and Soil Environmental Science

John M. Galbraith, Co-chair
Randolph H. Wynne, Co-chair
James B. Campbell
Laurence W. Carstensen
W. Lee Daniels

May 3, 2007
Blacksburg, Virginia

Keywords: ASTER, wetlands, multi-temporal analysis, logit model, CART, Sub-pixel analysis

Assessing Coastal Plain Wetland Composition using Advanced Spaceborne Thermal Emission and Reflection Radiometer Imagery

Eva Pantaleoni

ABSTRACT

Establishing wetland gains and losses, delineating wetland boundaries, and determining their vegetative composition are major challenges that can be improved through remote sensing studies. We used the Advanced Spaceborne Thermal Emission and Reflection Radiometer (ASTER) to separate wetlands from uplands in a study of 870 locations on the Virginia Coastal Plain. We used the first five bands from each of two ASTER scenes (6 March 2005 and 16 October 2005), covering the visible to the short-wave infrared region (0.52-2.185µm). We included GIS data layers for soil survey, topography, and presence or absence of water in a logistic regression model that predicted the location of over 78% of the wetlands. While this was slightly less accurate (78% vs. 86%) than current National Wetland Inventory (NWI) aerial photo interpretation procedures of locating wetlands, satellite imagery analysis holds great promise for speeding wetland mapping, lowering costs, and improving update frequency. To estimate wetland vegetation composition classs, we generated a classification and regression tree (CART) model and a multinomial logistic regression (logit) model, and compared their accuracy in separating woody wetlands, emergent wetlands and open water. The overall accuracy of the CART model was 73.3%, while for the logit model was 76.7%. The CART producer's accuracy of the emergent wetlands was higher than the accuracy from the multinomial logit (57.1% vs. 40.7%). However, we obtained the opposite result for the woody wetland category (68.7% vs. 52.6%). A McNemar test between the two models and NWI maps showed that their accuracies were not statistically different. We conducted a sub-pixel analysis of the ASTER images to estimate canopy cover of forested wetlands. We used top-of-atmosphere reflectance from the visble and near infrared bands, Delta Normalized Difference Vegetation Index, and a tasseled cap brightness, greenness, and wetness in linear regression model with canopy cover as the dependent variable. The model achieved an adjusted-R^2 of 0.69 (RMSE = 2.7%) for canopy cover less than 16%, and an adjusted-R^2 of 0.04 (RMSE = 19.8%) for higher canopy cover values. Taken together, these findings suggest that satellite remote sensing, in concert with other spatial data, has strong potential for mapping both wetland presence and type.

DEDICATION

To my husband, Alexei

ACKNOWLEGEMENTS

I would like to thank Dr. Galbraith, my CSES advisor, for his support and help over these years at Virginia Tech. He introduced me to the CSES family, and taught me soil science always with great enthusiasm. I will never forget our adventurous field trips! A special thank to my Forestry advisor, Dr. Wynne, who has always provided me with challenging suggestions and comments of extreme importance to develop and complete my research. Thanks to my committee members: Dr. Daniels, Dr. Campbell and Dr. Carstensen for their precious suggestions, and Dr. Daniels especially for his encouragement every time I was running into his office with a new problem!

A huge thank to Patricia Donovan, with whom I spent a wonderful time in the GIS lab. Pat never negated me her help, being a fantastic friend that I will certainly never forget.

I would like to thank also all the CSES staff and student (especially lab 250…. thanks for the good time, the cakes, and the coffee …I felt like at home with you all!). I really want to acknowledge Sybil Phoenix and Sue Brown: without you I would be still lost in the VT bureaucracy!!!

More than everybody, I need to thank my husband, Alexei Ovtchinnikov. You have taught me how to never give up, in research and in life. This research is dedicated to you, Alexei.

TABLE OF CONTENTS

LIST OF TABLES

LIST OF FIGURES

1 INTRODUCTION

1.1 BACKGROUND

Section 404 of the Federal Water Pollution Control Act (Public Law 92-500, 33 U.S.C. 1251) of 1972 brought about a change in the way wetlands were regarded. Public Law 92-500 legislation is also referred to as the U.S. Clean Water Act (CWA). The CWA established that no discharge of dredged or fill material can be permitted if a practical alternative exists that is less damaging to the aquatic environment or if the Nation's waters would be significantly degraded. This legislation moved federal agencies to focus their attention on identify always more accurately the location of aquatic habitats (e.g. wetlands), in order to produce appropriate policy and guidance (Environmental Laboratory, 1987), and in order to develop and interpret environmental criteria utilizable in evaluating permit applications. When a practical alternative to discharging and filling is impossible, the government requires the construction of new wetlands as needed to mitigate for wetland losses. Wetland mitigation has become the leading tool for combating wetland loss in the U.S. (Mitsch and Gosselink, 1993; Cole and Shafer, 2002).

In 1986, the Emergency Wetland Resource Act directed the National Wetlands Inventory (NWI), part of the U.S. Fish and Wildlife Service (FWS), to map and produce digital wetland databases for the USA, including information on the characteristics, extent, and status of the Nation’s wetlands and deepwater habitats. Currently, NWI utilizes 1:40,000 aerial photography for performing stereoscopic photo-interpretation of areas and delineation of wetland boundaries. The specific and unique features that a wetland must have to be jurisdictional and protected make the job of identifying wetlands especially difficult. In addition to the hydrophytic vegetation component, a wetland is characterized by a wetness regime whose hydroperiod insures the dominant growth and reproduction of hydrophytes, which is also one of the factors for the development of hydric soils. The NWI procedure for detecting and mapping wetlands generally meets prescribed standards (Wilen et al., 2002), and it is widely accepted. However, this procedure has some weaknesses such as high costs due to the panel of people required both for digitizing the aerial photographs and field validating the wetlands; and delay in estimating gains and losses of wetlands due to the large time required to update maps.

NWI maps do not show all wetlands since the maps are derived from aerial photo-interpretation with varying limitations due to scale, photo quality, inventory techniques, and other factors. Consequently, the maps tend to show wetlands that are easily identified from aerial photos, soil maps, and topographic maps. In general, the older NWI maps prepared from 1970s-era black and white photography (1:80,000 scale) tend to be very conservative, with many forested and drier-end emergent wetlands not mapped. Maps derived from color infrared photography (less than 5% of the nation) tend to yield more accurate results except when this photography was captured during a dry year, making wetland identification difficult (Tiner, 1999).

Even though NWI maps are widely used as reference data for scientists, little research has been reported that quantifies how many wetlands are actually not on NWI maps. Swartwout et al. (1981) reported 15% omission error in wetland vegetation classification in Massachusetts. In Nevada, Werner (2005) found that 42% of surveyed palustrine wetlands were not found on the NWI maps. More than half of these were meadows (55%), while the rest were primarily scrub-shrub wetland (21%) or forested (20%) wetlands. Stolt and Baker (1995) reported that NWI did not adequately inventory wetlands in the Blue Ridge physiographic region of central Virginia. About 109 hectares of jurisdictional wetlands were located by field mapping in the same study areas where NWI had indicated only 17 hectares of wetland occurrence. Most of the published research supports the accuracy of the NWI maps, assessing that over 90% of the times that NWI identifies as wetland, it is in fact a wetland (Kuzilla et al., 1991; Stolt and Baker, 1995; Kudray and Gale, 2000). Unfortunately, there is no information verifying the overall national effectiveness of NWI maps to estimate the number and area of wetlands (Stolt and Baker, 1995; Galbraith et al., 2003).

Satellite imagery offers an alternative approach to use of aerial photography for wetland detection. Observation from space satellites offers a unique opportunity to acquire information at broad scale and to parameterize environmental models (Foody and Curran, 1994; Yamagata, 1999). The value in remote sensing for the study of the Earth lies in the representation of details not visible to humans by other means. One major advantage of remotely sensed data over both analog and digital aerial photography and field collection is the ability to investigate various types of environmental changes in an

easy, fast and cost effective way. Satellite remote sensing can identify the wetland resource as to type, characterize the general wetland land cover type, identify sub-emergent and emergent wetlands, and supply details about wetlands over large or inaccesible areas (Lyon and McCarthy, 1995). Although wetlands are among the most productive and important ecosystems of the world, few studies using remote sensing data have been conducted to monitor changes or functionality in inland freshwater wetlands (Carter et al., 1979; Wickware and Howarth, 1981).

Although single images have been used to discriminate broad bottomland forest types by focusing upon static classification schemes of community composition (Jensen et al., 1987, Hodgson et al., 1988), multi-temporal satellite imagery has been preferred (Bolstad and Lillesand, 1992; Wolter et al. 1995; Townsend and Walsh, 2001). Forested wetland mapping using only multispectral-based remote sensing techniques has proven to be problematic due to the moderate pixel resolution, such as the 30x30 m pixel resolution of Landsat (Jacobson et al., 1987; Federal Geographic Data Committee, 1992; Tiner, 1999). An improvement in discriminating different wetland vegetation types has come with the application of hyperspectral data and radar (Bajjouk et al., 1998; Silvestri et al., 2002).

Geographic Information Systems (GIS) can be used to combine digital information about soils, hydrography, vegetation, and topography with remote sensing for improving the determination and identification of wetlands. NWI, digital color infrared orthophotography, digital topographic maps, Soil Survey Geographic Data Base (SSURGO) survey maps, and Digital Elevation Models (DEMs) have been extensively used for wetland mapping and assessment of wetland functions (O'Hara, 2001; Sugumaran et al., 2004; Dosskey et al., 2005; McCauley and Jenkins, 2005). However, existing public domain digital data sets have limitations for finding small wetlands and wetlands covered by dense tree canopies. A combination of remote sensing and GIS data analysis to locate and delineate wetlands seems advantageous given the complexity of wetlands and the necessity of combining environmental aspects, such as type of soil and vegetation cover; that the two tools would not be able to identify when considered alone.

1.2 OBJECTIVES

In the United States, the main source of information on wetlands is the NWI, which derived from either manual or partially automated digitizing of aerial photographs. This study proposed an alternative methodology for mapping and recognizing wetland types and characteristics, using an experimental satellite sensor, ASTER.

The first experiment evaluated the ability of ASTER and GIS data layers to separate wetlands from uplands in the Coastal Plain of Virginia. A second study focused more closely at determining wetland type. The third study was conducted by zooming into pixels, to determine the amount of wetland canopy cover contained in each pixel. In specific, this study presents three objectives:

1) to explore the ability of raw ASTER bands and GIS data layers to map the presence and absence of wetlands using a logistic regression model;

2) to compare the ability of a parametric (classification and regression tree) and non-parametric (multiple logistic regression) models in differentiating among woody wetlands, emergent wetlands, open water habitat, and uplands; and

3) to quantify the amount of canopy cover in wetlands at the sub-pixel level using ASTER and remote sensing indices through a regression analysis.

1.3 DISSERTATION ORGANIZATION

This dissertation is organized in six chapters. The first chapter includes the background of the research, and the objectives of three studies. The second chapter is an independent literature review of concepts related to the whole study. The third, fourth, and fifth chapters provide an independent abstract, introduction, materials and methods, result and conclusion section for each of the three internal studies. The last chapter consists of a general summary, conclusion, and reccomendation for future research on the application of ASTER to wetlands.

2 LITERATURE REVIEW

2.1 HISTORY OF WETLAND LOSSES AND PROTECTION

Many of the Earth's wetlands are located within the permafrost areas in the northern hemisphere. Russia, Canada and the United States (mainly in Alaska) have the largest area of wetlands (Brady and Weil, 1999). The exact amount of wetlands in humid climates and tropical zones is not known, nor is the wetland area within arid regions (Yamagata and Sugita, 1999).

At the time of European settlement, wetlands may have occupied a third of the land surface within the southern part of the United States (Dahl 1990). Nearly half of Louisiana and Florida may have been wetlands. The landscape in these regions, as in most of the eastern United States, has been altered dramatically over the past 200 years. Wetlands have been associated with mosquitos and the diseases they carry (malaria, yellow fever), have been reported as a hazard to transportation, and as a refuge for hostile humans and animals. Hence, wetland drainage has been justified to solve these hazards and to develop terrains more suitable as agriculture and forestry resources, and have been filled or otherwise altered to construct commercial and urban developments, transportation networks, and navigational facilities (Tiner 1996).

In 1754, South Carolina authorized the drainage of Cacaw Swamp for agricultural use (Beauchamp, 1987). Areas of the Great Dismal Swamp in Virginia and North Carolina were surveyed in 1763 so that canals could be constructed for water transportation routes and logging activities. In the early 1900s, the Florida Legislature passed the Swamp and Overflowed Lands Grant Act; drainage districts were formed and by the late 1920s most of the wetlands in South Florida were drained by canals designed to reclaim land. Hewes and Frandson (1952) described the prairie pothole region landscape as follows: "low knolls are separated by saucer-like depressions, in which empounded water often stands the year around ... in the main rainwater which falls upon the uplands has to escape by seepage or evaporation. Little ponds and marshes are found in almost innumerable places scattered all over the county." In the same period, the slogan "every acre to its best use" was a common justification for draining wetlands

(Staunton, 1950). In the early 1600s, the area that was to become the conterminous United States contained approximately 90 million hectares of wetlands. About 42 million hectares remained as of the mid-1980s (Dahl and Johnson, 1991).

Only in recent years have steps been taken to restore and protect wetlands. Beginning in 1972, with passage of the Federal Water Pollution Control Act, Congress responded to judicial action and public pressures to protect the nation's waters, interpreted to include any waters that may affect interstate commerce, and recently reinterpreted to include waters connected to navigable waters (Downing et al., 2003). The objective of the Act was to restore and maintain the chemical, physical, and biological integrity of the navigable or permanent water. At that time, the law had not directly addressed wetlands. With the Federal Water Pollution Control Act was amended in 1977, and is now commonly known as the Clean Water Act (CWA). Wetlands were legally included in the definition of navigable water (U.S.E.P.A., 2002).

Section 404 of the CWA is the only legislation that directly links the CWA to wetlands; it authorizes the U.S. Army Corps of Engineers (COE) to issue or deny permits that deposit dredge or fill material in the nation's waters; mandates the COE to develop regulations and jurisdiction in wetlands; and authorizes the U.S. Environmental Protection Agency (EPA) to participate in development of regulations and to review or deny COE permits. In 1986, the Emergency Wetland Resource Act directed the U.S. Fish and Wildlife Service (FWS) to map and produce a digital wetlands database for the United States. Currently the National Wetlands Inventory (NWI), as part of the FWS, produces information on the characteristics, extent, and status of the nation's wetlands and deepwater habitats. This information is available to federal, state, and local agencies, as well as academic institutions and the public.

2.2 WETLANDS

There is no a single definition of wetland used by all agencies, scientists, policymakers, or landowners for all purposes (Heimlich et al., 1998). There is often disagreement or misunderstanding about what the term "wetland" means, which can create confusion in discussing the state of wetland resources and changes in wetland policy (Smith, 1997). "Wetlands" is a general term used to describe areas which are neither entirely terrestrial

nor totally aquatic. These areas vary from the majestic cypress swamps of the southern United States to shallow, unimpressive depressions which hold water for only a few weeks out of the year. Wetlands have unique hydrologic characteristics that result in soils and plant and animal communities that have special adaptations to live in or use the wetland environment (Messina and Conner, 2000). Among the most widely used definitions of wetlands are the CWA definition and the Cowardin Definition.

2.3 CLEAN WATER ACT WETLAND DEFINITION

Wetlands identified for regulation by the Clean Water Act are often referred to as "jurisdictional wetlands" (Messina and Conner, 2000). In section 40 CFR 230.41 of the CWA, it states that "Wetlands consist of areas that are inundated or saturated by surface or ground water at a frequency and duration sufficient to support, and that under normal circumstances do support, a prevalence of vegetation typically adapted for life in saturated soil conditions" (U.S.E.P.A., 1977). This definition is not complete enough to use as a field identification guide, so the COE and other federal agencies produced the 1987 Corps of Engineers Wetland Delineation Manual (Environmental Laboratory, 1987) to describe in detail the identification and delineation of jurisdictional wetlands. The '87 Manual requires that at least one positive wetland indicator be present for each of the following criteria: hydric soils, hydrophytic vegetation, and wetland hydrology, as described below. Supplementary guidance has been issued and the '87 Manual has been updated several times. There is no any wetland inventory associated with the Clean Water Act; on the contrary, wetlands are delineated on a site-specific basis (Messina and Conner, 2000).

2.4 HYDRIC SOILS

A hydric soil is defined by the National Technical Committee for Hydric Soils as a soil that formed under conditions of saturation, flooding, or ponding long enough during the growing season to develop anaerobic conditions in the upper part (59 Fed. Reg. 35680, 1994). The Natural Resources Conservation Service (NRCS) was responsible for maintaining a list of soil survey map units that contain hydric soils in the United States

(Messina and Conner, 2000). The lists of hydric soils were created by using criteria based on selected soil properties documented in Soil Taxonomy and the Soil Survey Manual (Soil Survey Staff, 1999). The list of hydric soils contains any soil whose range of properties includes any of the hydric soil criteria. The list and the criteria are being phased out of use by both NRCS and COE, and are being replaced by field indicators and a technical standard. The field indicators are morphological properties known to be associated with soils that meet the definition of a hydric soil; they are essential for hydric soil identification because once formed, they persist in the soil during both wet and dry seasonal conditions.

2.5 HYDROPHYTIC VEGETATION

Hydrophytes are plants growing in water or on a substrate that is at least periodically deficient in oxygen due to saturation and microbial reduction. Hydrophytes have morphological, physiological and reproductive adaptations that allow them to thrive in inundated or saturated soils where non-hydrophytes (upland plants) cannot (Eggers et al., 1997). It is essential to have knowledge of plant species when delineating wetlands (Mitsch and Gosselink, 1993). The vegetation criterion in jurisdictional wetland definition requires an area to have over 50 percent of its dominant species classified as wetland adapted plants. The presence of a particular plant does not indicate wetland conditions unless the vegetation dominance, hydrology, and soil criteria are met.

The FWS developed a national list of plant species that may occur in wetlands. The plants have been separated into five categories based on their likely occurrence in wetlands (Reed, 1988):

i. *Obligate wetland* (OBL) plants occur almost always under natural conditions in wetlands (> 99% of the time).
ii. *Facultative wetland* (FACW) plants usually occur in wetlands (67-99% of the time) but are occasionally found in uplands.
iii. *Facultative* (FAC) plants are equally likely to occur in wetlands or uplands (34-66% of the time).

iv. *Facultative Upland* (FACU) plants usually occur in uplands, but are occasionally found in wetlands (1-33% of the time).

v. *Obligate Upland* (UPL) plants almost always occur (> 99% of the time) in uplands.

2.6 HYDROLOGY

Wetland hydrology refers to the inflow and outflow of water through a wetland and its interaction with other site factors. Wetland hydrology occurs in areas where the soil is saturated or inundated with ground or surface water within 30 cm of the surface for long enough during the growing season to create anaerobic conditions and to exclude the growth of plants which are not adapted for life in saturated soils. Inundation or saturation in the root zone must be long enough to create hydric soils and promote the growth and reproduction of hydrophytic vegetation (Messina and Conner, 2000).

The Wetland Delineation Manual provides a list of indicators for identifying wetland hydrology. Field indicators are evidence of present or past hydrologic events (Environmental Laboratory, 1987). Indicators are divided in primary and secondary indicators. Any of these primary indicators are considered evidence of wetland hydrologic characteristics, while secondary indicators are supplemental to support evidence of wetland hydrology. Soil saturation is generally observed with field survey. Primary indicators for recorded data and field observations include:

1. Visual observation of inundation (surface flooding), or
2. Visual observation of saturation (evidence of periodic saturation within 12" of the surface), or
3. Watermarks or staining on bark of woody vegetation, or
4. Drift lines, "high tide" lines of debris left by previous high water events, or
5. Sediment deposits, including deposits of algae, or
6. Drainage patterns within wetlands, or
7. Oxidized root channels in the soil (orange-reddish "halos" surrounding the channels of live roots).

Secondary indicators include:

1. Water stained leaves, or
2. Local soil survey hydrology data for identified soils, or
3. Fact neutral test, or
4. Bare soil areas.

2.7 COWARDIN SYSTEM OF WETLAND DEFINITION

According to Cowardin et al. (1979) wetlands are lands transitional between terrestrial and aquatic systems where the water table is usually at or near the surface or the land is covered by shallow water. For purposes of this classification, wetlands must have one or more of the following three attributes: (1) at least periodically, the land supports hydrophytes, (2) the substrate is predominantly undrained hydric soil, and (3) the substrate is non-soil and is saturated with water or covered by shallow water at some time during the growing season of each year.

The Cowardin classification system is based on a hierarchical structure that groups wetlands according to ecologically similar characteristics. The Cowardin system was developed to be applicable both to ground based information and remote sensing methods. The Cowardin system excludes uplands, but it includes both aquatic and terrestrial habitats. It is considered to be the easiest of the existing national wetland classification systems to use for wetland map preparation, and it is the national standard system for wetland classification (Mader, 1991). The FWS and NWI use the Cowardin wetland types, which include: swamps, freshwater, brackish water, and saltwater marshes, bogs; vernal pools, periodically inundated salt flats; intertidal mudflats, wet meadows, wet pastures, springs and seeps, portions of lakes, ponds, rivers and streams, and all other areas which are periodically or permanently covered by shallow water, or dominated by hydrophytic vegetation, or in which the soils are predominantly hydric in nature (Cowardin et al., 1979). On the other hand, the COE 87 manual uses the CWA definition, which includes “swamps, marshes, bogs, and similar areas” (Environmental Laboratory, 1987).

2.8 THE NATIONAL WETLAND INVENTORY

Survey methods and wetland definitions have varied over the years, making an estimate of wetland trends nearly impossible. The most recent nationwide estimate is from the National Wetlands Inventory (NWI), the fourth major inventory of the nation's wetlands (Messina and Conner, 2000).

The operational phase of the NWI involves wetland mapping, status and trend analysis. The main product of the NWI is large scale (1: 24,000) maps that show the location, shape, and characteristics of wetlands and deepwater habitats on U.S. Geological Survey base topographic maps (NWI, 1995). For some regions of Alaska and desert regions in the West, smaller scale maps are produced (Tiner, 1996). Priorities for mapping have been based on the needs of the FWS, and other federal and state agencies, dependent on the availability of funds and quality aerial photography (Wilen and Pywell, 1992). National estimates of wetland status and trends are made at 10 year intervals, depending on funding. The estimates are used to evaluate the effectiveness of federal programs and policies, identify national and regional problems, and increase public awareness (NWI, 1995).

NWI utilizes conventional photo-interpretation techniques, using aerial photographs at scales from 1:40,000 to 1:80,000, and for the earliest maps at 1:133,000. Color-infrared photography (scale 1:58,000 and 1:40,000) is considered the best tool for mapping wetlands, especially if the photographs are taken during the late winter.

At the beginning of its operation, NWI utilized the National High Altitude Photography (NHAP) program, which was in effect from 1978 to 1988. NHAP photographs were taken simultaneously with two cameras, one containing black-and-white film, the other color infrared. An NHAP black-and-white photograph covered about 334 km^2, and because of the longer focal length in the second camera, an NHAP color-infrared photograph covered about 176 km^2.

The National Aerial Photography Program (NAPP) was established in 1987 to coordinate aerial photography for the United States among Federal and State agencies. Taken from aircraft flying nominally at about 6100 m above the terrain, each NAPP photograph covers about 83 km^2. The change from the smaller 1:58,000 to the larger

1:40,000 scale increased the cost of mapping but also improved map accuracy and detail (Messina and Conner, 2000).

In conducting the inventory and preparing maps, the NWI undertakes seven major steps (Tiner, 1996), and requires team work:

1) review aerial photographs to identify evident wetlands, typical wetlands, and problematic areas,
2) select and visit sites for field checking in the above areas,
3) review field trip results by stereoscopically viewing inspected sites on aerial photographs,
4) make stereoscopic photo-interpretation of study area, delineate wetland boundaries, and classify each wetland according to the Cowardin classification system,
5) perform quality control at regional and national level,
6) prepare draft 1:24,000 scale wetland maps, and
7) coordinate interagency (federal and state) review of draft maps and conduct field checking and produce final NWI maps.

2.9 AERIAL PHOTOGRAPHS AND SATELLITE IMAGERY

Although aerial photography is commonly used in wetland mapping, photo-interpretation is not a simple task (Tiner, 1996). Wetlands are not always permanently flooded or saturated, and the degree of wetness of the soil complicates the interpretation of the landscape. NWI currently uses stereoscopic photographs in order to detect depressional wetlands and facilitate identification of certain sloping wetlands. Unfortunately, wetlands do not form only in depressions: they can be found on broad flats and gently sloping areas (Tiner, 1996).

Other photo-interpretation problems occur when the vegetation of drier wetlands is not dramatically different from that of adjacent upland areas, and ecotone zones are difficult to establish. Further, small changes in elevation may cause large variations in the hydrologic characteristics of wetlands (Warthon et al., 1982; White et al., 1983; Hupp, 1986).

More then half of the wetlands in the United States are forested (Frayer et al, 1983). They are ecologically valuable since they moderate downstream flooding, maintain water quality, control pollution, and provide habitats for wildlife (Warthon et al, 1982); hence it is critical to identify them. Mapping forested wetlands is especially difficult because of the presence of broad ecotones, areas of transition in which communities grade into another across complex geomorphic, edaphic, and hydrologic gradients (Warthon et al. 1982; Sharitz and Mitsch 1993; Rice and Peet 1997; Townsend and Walsh 2001). Using traditional aerial photography for delineating forested wetlands can be extremely challenging. The spectral characteristics of a forest wetland canopy are not sharply different from upland forest canopies. Also, the canopy hides the hydrological characteristic of the soil below, in addition to understory vegetation and topographic features of the ground, all which are key parameters for determining a wetland. To facilitate the recognition of deciduous forested wetland, leaf-off photographs are generally used, even though the interpreter has to consider precipitation condition or period of drought prior the photographic overflights. However, wetlands may be characterized by the presence of evergreen species, such as Pond pine (*Pinus serotina*), Loblolly Bay (*Gordonia lasianthus*), and Sweetbay magnolia (*Magnolia Virginiana*). In this case, the recognition of wetlands relies on differences in spectral signatures between upland and wetland evergreen vegetation, and on the availability of elevation data.

Aerial photography is not always practical for collecting regional information or information requiring continual validation, because of the cost and logistical difficulties associated with capturing the data (Jensen et al., 1987; Johnston and Barson, 1993; Harvey and Hill, 2001). An alternative way of detecting wetlands is implementing the use of remote sensing from satellite imagery.

With the availability of moderate resolution Landsat Thematic Mapper (TM) data in 1982, interest has been drawn to its use in wetland vegetation mapping by means of a computer-assisted approach (Dottavio and Dottavio, 1984; Jensen et al., 1987). Different approaches and different sensors have been applied. Ackleson and Klemas (1987) obtained Landsat TM and Landsat Multispectral Scanner (MSS) imagery for the Guinea Marsh located in lower Chesapeake Bay to compare the ability between the platforms to detect two species of submergent aquatic vegetation. They found no substantial

differences between the TM and MSS imagery for discriminating among vegetation classes, but substantial improvements in classification accuracy were achieved for the Landsat TM data set when water depth measurements were included in the analysis (Ackelson and Klemas, 1987). Jacobson et al. (1987) used Landsat TM data to achieve greater than 90% accuracy for lacustrine systems when compared to NWI maps. However, only 25% accuracy was obtained for seasonally and temporally flooded emergent wetlands, and no more than 25% of the wetlands under 0.8 ha in size were identified. The use of single images has been implemented for discriminating broad bottomland forest types focusing upon static classification schemes of community composition. Jensen et al. (1987) used a 'cluster busting' technique that allowed important wetland vegetation to be identified. However, there is evidence in the literature that intra-annual satellite imagery provides significant improvements in the detail and accuracy of wetland classification, by capturing the phenological changes throughout the growing season. Satellite images, collected during different season of the same year, enhance the ability to discriminate between wetland vegetation types (Mackey, 1990), and multi-temporal data can help evaluate hydrological, phenological and compositional changes across seasons and between years. Hodgson et al. (1988) used inter-annual change detection for the Savannah River Site in South Carolina for distinguishing between cypress-tupelo (*Taxodium-Nyssa*) forests and other bottomland hardwood forests. Mackey (1990) used eleven dates of SPOT data along with near-concurrent vertical aerial photographic and phenological data for 1987-1989 to determine seasonal and annual changes in a 400 ha southeastern freshwater marsh. He reported that early April through mid-May was the best time to discriminate among bald cypress/water tupelo (T*axodium distichum L.Rich./Nyssa acquatica L.)* swamp forest and the non-persistent water primrose (*Ludwigia spp.*) and persistent cattail (*Typha spp.*) stands in this wetland.

The possibility of discriminating among vegetation composition allows hierarchical classification of the vegetation, matching the logical structure of most plot-based floristic classification systems (Townsend and Walsh, 2001). It is advantageous to combine the information derived from satellite sensors with existing GIS data sets that already identify soil features characteristic of wetlands. Several authors have reported

improved land-cover classification accuracy by integrating spatial environmental data with satellite imagery (Civco, 1989; Welch et al., 1992). Bolstad and Lillesand (1992) incorporated spatial data into a rule-based model for land-cover classification of Landsat-TM imagery, and increased land-cover classifcation accuracies by 12% over classification of TM data alone.

Several models have been developed in order to improve the suitability of multispectral imagery for detecting wetlands.. An example is the Soil-Vegetation-Water index developed by Yamagata and Sugita (1999) for monitoring land cover change in the Kushiro wetland, in Japan, using Landsat TM images. Researchers have also successfully used the tasseled cap transformation as another method for discriminating soil moisture content. The tasseled cap transformation has been developed for Landsat, IKONOS, and recently for ASTER (Wang and Sun, 2005). Nevertheless, mapping different kind of vegetation using multispectral images remains difficult. Optical sensors have been used to map wetland vegetation in the Amazon (Mertes et al., 1996; Novo and Shimabukuro, 1997). Thick vegetation covering underlying waters and clouds or smoke frequently obscured the ground, limiting the quality of maps of the study area. In addition, the moderate resolution of Landsat (30x30 m) emphasizes detection of non-wetland cover, omitting wetlands as a class or significantly underestimating wetland area (Hansen et al., 2000; Loveland et al., 2000; Hess et al., 2003).

Among the large number of satellite sensors launched by the National Aeronautics and Space Administration (NASA) and the European Space Agency (ESA) in the last decade, the most commonly used method for detecting wetlands are the radar systems. Radar systems are both passive and active microwave sensors, and one of their biggest advantages is that they are little influenced by clouds and smoke (Travaglia and Macintosh, 1997). On the contrary, they can penetrate the vegetation canopy, and they have been proven to be useful for wetlands mapping (Melack and Hess, 1998). Bourgeau-Chavez et al. (2002) demonstrated that multi-band synthetic aperture radar (SAR) data can be used to map wetlands with an accuracy of about 74%.

Improvements in detecting wetlands and discriminating among different vegetation and soils have been shown by the recent application of classification techniques to airborne hyperspectral data (Bajjouk et al., 1998; Silvestri et al., 2002). At

the end of a study in the Orbetello Lagoon, in Italy, Alberotanza et al. (1999) affirmed that airborne imaging spectrometers are presently capable of returning clearly distinct spectral signatures, directly comparable with field spectral measurements. Hirano et al. (2003) found hyperspectral analysis suitable for discriminating forest and herbaceous communities, with accuracies ranging from 74% to 95% in discriminating tree species in red, black and white mangrove communities.

The use of hyperspectral and radar images for wetland mapping is not free from difficulties and limitations from a practical standpoint (Hirano et al., 2003). One difficulty is the complexity of image-processing procedures that are required before the image data can be effectively used for automated classification of wetland vegetation. A second equally important difficulty is the high cost of the data.

The cost to undertake a survey varies greatly depending on the size of the area to be flown, the pixel resolution chosen, and the number of spectral bands that are to be collected. An average project is charged for the time committed to the project, the time required to preprocess the data collected, and for incurred expenses such as airfare, hotels, shipping, etc. In addition, surveys that are scheduled can be canceled because of weather conditions, and the deadline of a project can shift considerably (Hyperspectral Data International, 2004), delaying project and increasing overall costs.

Airborne methods can provide more detailed information about habitat mapping, and the choice of commissioning either digital or photographic sensors depends on the staff cost and the urgency of data acquisition. Color aerial photography is cheaper than digital airborne scanner data if the staff costs are considerably less than $150 per day (Mumby et al., 1999).

In this research, the Advanced Spaceborne Thermal Emission and Reflection Radiometer (ASTER) sensor was used as the source of remote sensing data. ASTER was launched on the Terra Platform as part of NASA's Earth Observing System in December 1999. It has the potential to overcome the limitations in wetland mapping due to its fine resolution of 15x15 m in the visible and near infrared spectral range, and a total of 14 bands. ASTER is an on-demand sensor, and scenes may be available monthly. The cost of ASTER scenes is relatively low compared to other satellite imagery. ASTER data have successfully been used for monitoring volcanic activities, climatic changes, urban

environmental problems, glaciers and fire monitoring (Stefanov et al., 2001; Ford et al., 2003), but little research on wetland applications has been reported (Kato et al., 2001).

In conclusion, even though aerial photography has been a favored tool for operational wetland mapping, satellite remote sensing techniques have the potential for matching the results obtained using aerial photography, with the advantage of improving timeliness and cost.

3 A LOGIT MODEL FOR PREDICTING WETLAND LOCATION USING ASTER AND GIS

3.1 ABSTRACT

Data from the Advanced Spaceborne Thermal Emission and Reflection Radiometer (ASTER) were used to develop a logistic regression model to predict the location of wetlands in the Coastal Plain of Virginia. We used the first five bands from two ASTER scenes (spanning 0.52-2.18 μm) covering the same area, acquired 6 March 2005 and 16 October 2005. To improve the accuracy of the model, we included GIS data layers representing hydric soils and water. The resulting model predicted the location of over 78% of total wetlands, highlighting the potential of models incorporating ASTER data for speeding the wetland mapping process, lowering costs of map production, and improving wetland mapping accuracy.

3.2 INTRODUCTION

According to the state summary from the National Water Summary on Wetland Resources, Virginia has about 1 million acres of wetlands, and about three-quarters are non-tidal wetlands (Dahl and Allord, 1997). In recent years, function and value of wetlands have shifted from being purely economical to being more environmentally oriented. Several studies highlight the importance of wetlands regarding water quality and water holding capacity (Bruland and Richardson, 2004), as well as sediment retention (Llewellyn et al., 1995). In addition, wetlands are important feeding, breeding, and drinking areas for wildlife, and provide a stopping place refuge for waterfowl (Burdick et al., 1989; Lillesand and Kiefer, 2004).

In 1977, the U.S. Clean Water Act (CWA) established that no discharge of dredged or fill material into waters of the United States can be permitted if a practical alternative exists that is less damaging to the aquatic environment or if the Nation's waters would be significantly degraded (U.S. Army Corps of Engineers, 1995). This legislation required federal agencies to focus their interest into more accurate identification of location of aquatic habitats (e.g. wetlands) in order to produce

appropriate policy and guidance (Environmental Laboratory, 1987), and in order to develop and interpret environmental criteria utilizable in evaluating permit applications. In 1986, the Emergency Wetland Resource Act directed the National Wetlands Inventory (NWI), part of the U.S. Fish and Wildlife Service, to map and produce digital wetland databases for the USA, including information on the characteristics, extent, and status of the Nation's wetlands and deepwater habitats. NWI uses 1:40,000 aerial photography for performing a stereoscopic photo-interpretation of an area, and delineating wetland boundaries. There are several problems with the current process, including: high costs due to the personnel needed both for digitizing the aerial photographs and for field validation of the wetlands; delays in estimating gains and losses of wetlands due to the extensive time required to update maps (about ten years), and omission error estimated to vary from 35% (Werner, 2005) to 85% (Stolt and Baker, 1995).

An alternative method of detecting wetlands is through the use of satellite imagery. Single images have been used for discriminating broad bottomland forest types, focusing upon static classification schemes of community composition (Jensen et al., 1987; Hodgson et al. 1988), but multi-temporal satellite imagery has been generally preferred (Bolstad and Lillesand, 1992; Wolter et al. 1995; Townsend and Walsh, 2001). However, forest wetland mapping using only multispectral-based remote sensing techniques has proven to be problematic (Jacobson et al., 1987; Tiner, 1990; Federal Geographic Data Committee [FGDC], 1992). Optical sensors have been used to map wetland vegetation in the Amazon (Novo and Shimabukuro, 1997), but vegetation covering underlying waters, and cloud, haze or smoke frequently obscuring the ground were limitations. In addition, the relatively moderate resolution of some sensors, such as Landsat, emphasizes non-wetland cover, omitting wetlands as a class or significantly underestimating wetland area (Defries et al., 2000; Loveland et al., 2000; Hess et al., 2003).

The Advanced Spaceborne Thermal Emission and Reflection Radiometer (ASTER) offers the potential to reduce issues associated with spatial resolution. Moreover, it may lower costs and time for updating maps. ASTER is an on-demand sensor that has been successfully implemented in monitoring volcanic activities, climatic changes, urban environmental problems, glacier retreat and fire monitoring (Stefanov et

al., 2001; Ford et al., 2003), but little research on wetlands has been reported (Kato et al., 2001).

Details of the sensor are provided in table 3.1. The sensor consists of three subsystems: visible and near-infrared (VNIR), short wave infrared (SWIR), and thermal infrared (TIR) subsystems.

Table 3.1. Characteristics of the ASTER instrument.

Characteristic	VNIR[1]	SWIR[2]	TIR[3]
Spectral Range	Band 1: 0.520 - 0.600 µm Band 2: 0.630 - 0.690 µm Band 3: 0.760 - 0.860 µm Band 3: 0.760 - 0.860 µm	Band 4: 1.600 - 1.700 µm Band 5: 2.145 - 2.185 µm Band 6: 2.185 - 2.225 µm Band 7: 2.235 - 2.285 µm Band 8: 2.295 - 2.365 µm Band 9: 2.360 - 2.430 µm	Band 10: 8.125 - 8.475 µm Band 11: 8.475 - 8.825 µm Band 12: 8.925 - 9.275 µm Band 13: 10.250 - 10.950 µm Band 14: 10.950 - 11.650 µm
Ground Resolution	15 m	30 m	90 m
Data Rate (Mb/sec)	62	23	4.2
Cross-track Pointing (°)	±24	±8.55	±8.55
Swath Width (km)	60	60	60

§[1] Visible and near infrared
[2] Short wave infrared
[3] Thermal infrared

In this study we used the VNIR and the SWIR subsystems. VNIR operates in three spectral bands at visible and near-IR wavelengths, with a resolution of 15 m. The SWIR subsystem operates in six spectral bands in the near-infrared region through a single, nadir-pointing telescope that provides 30-m resolution. One of the disadvantages of ASTER is that the sensor does not observe the spectral range between 0.450 and 0.520 micrometers. This range, commonly known as the blue band (or Band 1 in Landsat TM) provides increased penetration of water bodies and it is also capable of differentiating soil and rock surfaces from vegetation (Quinn, 2001). Moisture greatly influences the reflection of shortwave radiation from soil surfaces in the SWIR (1.100–2.500 µm) region of the spectrum (Bowers and Hanks, 1965; Skidmore et al., 1975). Lobell and Asner (2002) described a relatively robust relationship between degree of saturation and SWIR

reflectance, estimating that soil moisture based on a general model of SWIR reflectance contained only half the uncertainty of estimates based in the VNIR.

The first objective of this study was to explore the ability of raw ASTER bands in predicting wetland location using a logistic regression model (logit). Our second objective was to quantify the improvement of the model when additional variables were introduced. We initially selected five GIS variables: digital soil data obtained from the Soil Survey Geographic Database (SSURGO), hydrographic data obtained from the U.S. National Hydrography Dataset (NHD), a 10 m digital elevation model, the slope of the terrain, and a wetness index map computed by dividing the tangent of the slope of the terrain over the catchment area (Gessler et al., 1995). Our third objective was to compare our results with NWI data.

3.3 DATA AND METHODS

3.3.1 STUDY AREA

Our area of interest was located on the Coastal Plain of Virginia (figure 3.1). The Coastal Plain consists of fluvial and marine deposits, primarily non-lithified. The oldest sediments were deposited during the Cretaceous, much younger deposits are found near the coastline (5,000-25,000 years ago) (Eick, 2006). Most of the terrain is nearly level with slow run off. The elevation has a median of 33 m above the mean sea level, with a maximum elevation of 105 m. Numerous rivers and streams cross the Coastal Plain. Their sinuous patterns create environments favorable for wetlands of varied natures: emergent, scrub and shrub, and forested wetlands. The Coastal Plain is characterized also by mineral flat wetlands, whose locations are independent from the vicinity to streams. Even though urbanization and agriculture have greatly reduced these wetlands, the Coastal Plain is the region that contains more than 70% of all the wetlands in Virginia (Tiner and Finn, 1986).

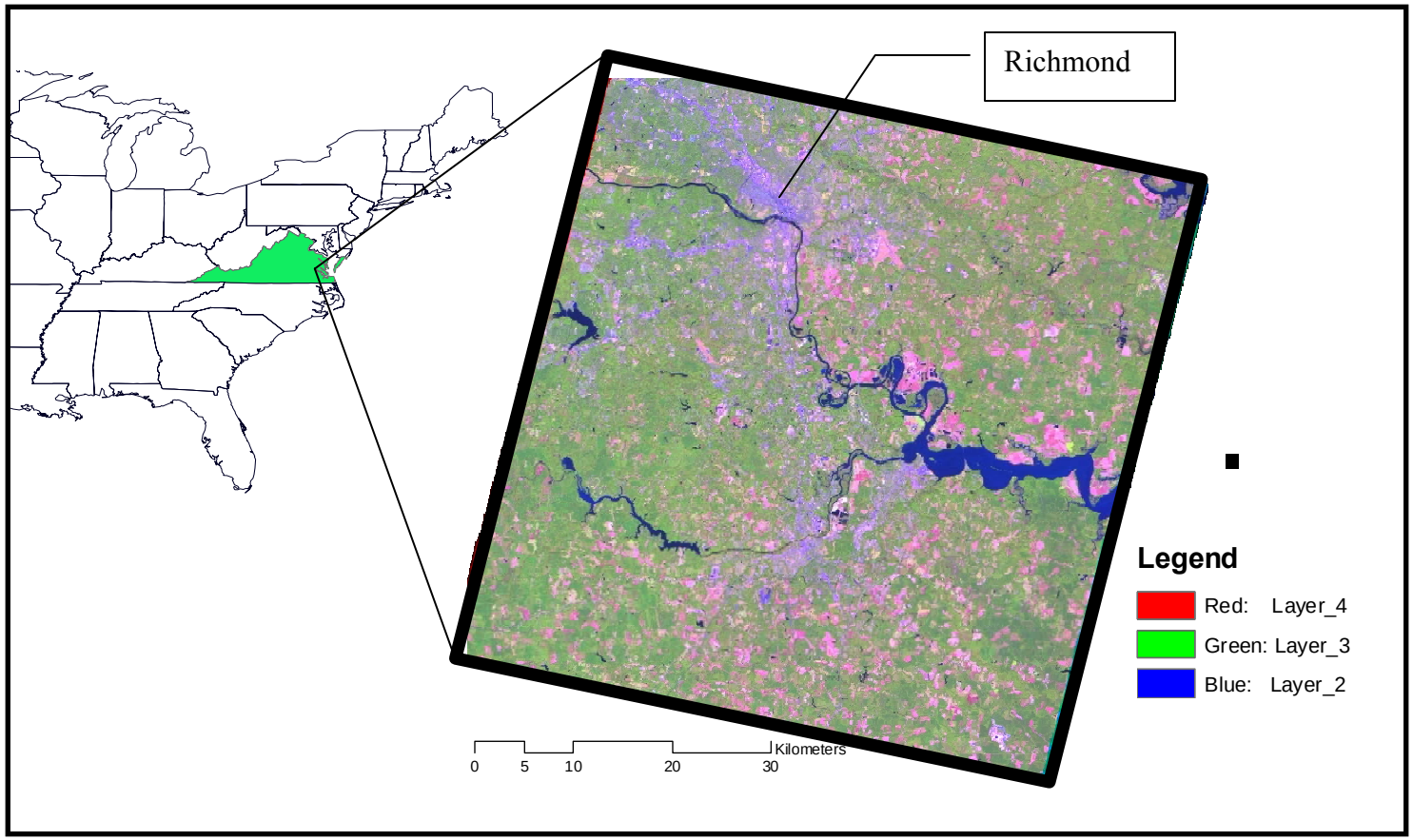

Figure 3.1. Map of the study area as obtained from the 16 October 2005 ASTER image, and its location within Virginia (in green). Layer 4 = 1.600 - 1.700 µm 7, Layer 3 = 0.760-0.860 µm, Layer 2 = 0.630-0.690 µm.

3.3.2 ASTER

We based this study on the analysis of two ASTER images. One image was collected on 6 March 2005, the second image on 16 October 2005 (respectively AST_L1B.3: 2028411439, and AST_L1B.3:2028019676). We chose these two scenes for the following reasons. The first week of March is important in the hydrologic cycle of wetlands since the water table has risen to the surface, increasing the moisture content of the soil. The height of the water table is critical for wetland survivals and detection. The water table has to reach surface to provide the necessary habitat for the growth and reproduction of hydrophytic vegetation. In March, leaves have not yet appeared on trees, allowing a spectral analysis of the soil moisture. The October date was chosen because the vegetation has started putting on its autumn colours, favouring discrimination between wetland and upland vegetation, and vegetation within wetlands.

Even though the multispectral range of ASTER bands covers values between 0.520 μm and 2.430 μm, in this study we used only the bands covering the spectrum from the visible to shortwave infrared range (0.520-2.185μm, Band 1 to Band 5). The choice of this range was dictated by the fact that higher value bands are affected by spectral crosstalk phenomena (Iwasaki and Tonooka, 2005), and we were advised to use ASTER images produced in the last five years (K. Thome, personal communication, June 2005).

At the pre-processing stage, we georeferenced the images to the Universal Transverse Mercator 1983 North American Datum (UTM NAD 83) using a first order polynomial transformation. We selected twenty ground control points (RMSE = 0.80 m) and twenty check points (RMSE = 0.85 m). We converted each ASTER band to top-of-atmosphere reflectance using solar irradiance values provided by the ASTER science team (K. Thome, personal communication, June 2005). Table 3.2 shows the solar irradiance value for the ASTER bands. We masked out clouds and their shadows via digitizing using ERDAS Imagine® 9.0 (Leica Geosystems LLC, Norcross, GA, USA). We resampled the bands to 15 m to match the pixel resolution of the first three ASTER bands.

Table 3.2. Solar irradiance values for ASTER.

Band	Solar Irradiance (W/m^2 micrometer)
1	1846.9
2	1546.0
3	1117.6
4	232.5
5	80.32
6	74.92
7	69.20
8	59.82
9	57.32

3.3.3 GIS DATA LAYERS

The Soil Survey Geographic Database (SSURGO) provided the most detailed level of soil information. SSURGO was designed primarily for farm and ranch, landowner/user, township, county, and parish natural resource planning and management. We reclassified the SSURGO soil data in order to obtain a binary set of hydric vs. non-hydric soils. The distinction was based on the percentage of hydric composition established by NRCS within each map unit. Soils having a hydric composition greater than 85% were classified as 'hydric'; soils that had a composition lower than 55% were classified as 'non-hydric'. We checked the location of the soils with a hydric composition between 55% and 85% using topographic maps and fine resolution digital orthophotos (scale 1:1,200 and 1:2,400). Soils with this range of hydric composition were typically found either in urban areas (hence, 'non-hydric') or on river-beds (hence, 'hydric').

The hydrographical data were collected from the NHD, a comprehensive set of digital spatial data. It contains information about surface water features such as lakes, ponds, streams, rivers, springs and wells. The NHD is based upon the content of USGS Digital Line Graph (DLG) hydrography data integrated with reach-related information

from the Environmental Protection Agency Reach File Version 3 (USGS, 2005). As continuous GIS data layers, we used a 10 m digital elevation model (DEM) developed from the Virginia Base Mapping Program (VBMP). The VBMP DEMs provide the highest resolution terrain model currently available in the Commonwealth of Virginia (Futrell and Sforza, 2004). The data came as three-dimensional elevation mass points spaced across the surface on a regular grid or at random intervals as necessary for properly modeling the earth surface (VBMP, 2003), and were grouped in tiles. About 900 tiles covered our study area, for a total of 90,000 points. A comprehensive TIN was created using the 3-D Analyst Extension™ in ArcMap 9.1® (Environmental Systems Research Institute, Inc., Redlands, CA, USA), and subsequently converted to a grid file to obtain a DEM with a 10 m horizontal resolution. We tested the vertical accuracy of the DEM using the geodetic control network provided by the U.S. National Geodetic Survey (table 3.3), as suggested by Maune et al. (2001).

Table 3.3. Vertical accuracy of the DEM generated from the VBMP dataset compared to the geodetic control network points.

RMSE (m)	Mean (m)	Median (m)	Skew	Std. Dev.	# of Points
1.96	0.43	0.20	1.87	1.92	773

We calculated the slope of the terrain from the DEM using the Spatial Analysis tool in ArcMap 9.1® (Environmental Systems Research Institute, Inc., Redlands, CA, USA), and the wetness index as the ratio between the tangent of the slope of the terrain and the catchment area (Gessler et al., 1995). The calculations for the catchment area and the slope were performed using ArcView 3.2® (Environmental Systems Research Institute, Inc., Redlands, CA, USA). The catchment area is commonly computed on grids using flow direction algorithms that treat the flow as coming from point source at the pixel center (Chirico et al., 2005).

3.3.4 EXPERIMENTAL DESIGN AND FIELD VALIDATION

We randomly sampled 870 points over the study area. Appendix A shows the coordinates of the points. We labelled the points either as wetland or upland[1] using topographic maps and high resolution digital orthophotographs obtained from the VBMP. The digital orthophotographs were based on true color, leaf-off photography acquired in 2002 at one of three scales: 1:4,800 in rural areas, 1:2,400 in urban and suburban areas, and 1:1,200 in areas where localities chose the option to purchase the higher accuracy product (VBMP, 2003). Figure 3.2 shows the orthotile grid for the study area.

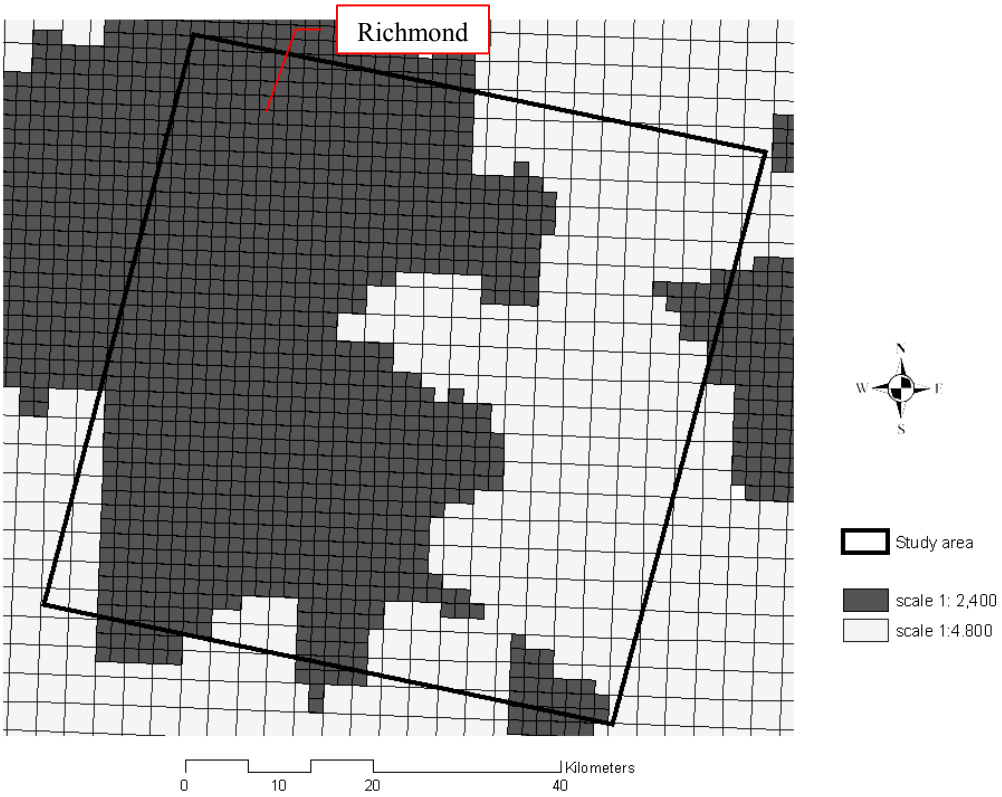

Figure 3.2. Virginia Base Mapping Program orthotile grid. The gray tiles have a scale of 1:2,400; the white tiles have a 1:4,800 scale. The black frame indicates the location of the study area.

[1] In this study, we refer to upland as any land that is not a wetland.

We identified uncertain points with the help of a panel of GIS and wetland experts. We randomly subdivided the points into two groups. The first group, containing 211 upland points and 263 wetland points, was used for developing the logit model. The second group, containing 164 upland points and 228 wetland points, was utilized for testing the model.

We performed a field survey on 15% of the total points. 95% of the sites were correctly identified. We tested for possible spatial autocorrelation using the Moran's I index (Moran, 1950), because parametric models rely on the assumption of independence of errors. Moran's I is a weighted product-moment correlation coefficient, where the weights reflect geographic proximity. The Moran's I index varies between -1 and +1. Values of I larger than 0 indicate positive spatial autocorrelation; values smaller than 0 indicate negative spatial autocorrelation. In order to determine whether a deviation of I from its expectation is statistically significant, one relies on the asymptotic distribution of I, which is Gaussian with mean -1/(n-1) and variance σ_I^2 (Schabenberger and Pierce, 2001). To reject the null hypothesis of no spatial autocorrelation, the observed z-score must be higher than the $z_{\alpha/2}$ cutoff of a standard Gaussian distribution. GEODA® software (University of Illinois, Urbana-Champaign, IL, USA) was used for calculating Moran's I and to compute the variance σ_I^2 in a randomized approach, where the $Z(s_i)$ are considered fixed and are randomly permuted. The results from this test are shown in table 3.4. The values of I are very close to zero. However, comparing the empirical distribution to the theoretical distribution, the p-values show a statistically significant positive correlation for most of the variables when water is included in the model, and for most of the October bands when water is excluded from the model. We decided to proceed with the analysis, recognizing that our results may be slightly influenced by autocorrelation.

Table 3.4. Moran's I values, expected I, standard deviation, Z-score, and p-value for each variable for the original set of data (a), and a set of data that does not contain the water category (b).

a)

Variable	Moran's I	E(I)	Sd	Z-score	P-value
Wetness Index	0.016	-0.002	0.0225	0.827	0.092
March Band 3	0.019	-0.002	0.0231	0.926	0.199
October Band 5	0.024	-0.002	0.0235	1.145	0.147
October Band 2	0.032	-0.002	0.0233	1.502	0.077
October Band 1	0.032	-0.002	0.0216	1.583	0.066
March Band 4	0.034	-0.002	0.0232	1.586	0.067
October Band 4	0.038	-0.002	0.0231	1.749	0.054
March Band 5	0.042	-0.002	0.0233	1.893	0.040
DEM	0.063	-0.002	0.0233	2.820	0.010
March Band 1	0.064	-0.002	0.0231	2.903	0.010
March Band 2	0.064	-0.002	0.0228	2.904	0.009
NHD	0.066	-0.002	0.0232	2.966	0.002
October Band 3	0.082	-0.002	0.0236	3.593	0.002
SSURGO	0.088	-0.002	0.0237	3.819	0.001
Slope	0.166	-0.002	0.0245	6.886	0.001

b)

Variable	Moran's I	E(I)	Sd	Z-score	P-value
October Band 2	0.032	-0.003	0.0266	1.305	0.101
October Band 5	0.031	-0.003	0.0243	1.412	0.091
October Band 1	0.033	-0.003	0.0240	1.488	0.091
March Band 3	0.040	-0.003	0.0245	1.735	0.027
October Band 4	0.049	-0.003	0.0252	2.071	0.038
March Band 4	0.054	-0.003	0.0251	2.259	0.015
Wetness Index	0.051	-0.003	0.0218	2.477	0.015
March Band 5	0.066	-0.003	0.0257	2.681	0.007
March Band 1	0.069	-0.003	0.0249	2.904	0.012
March Band 2	0.072	-0.003	0.0248	3.024	0.007
DEM	0.076	-0.003	0.0253	3.123	0.005
October Band 3	0.085	-0.003	0.0261	3.372	0.006
NHD	0.085	-0.003	0.0248	3.560	0.001
SSURGO	0.103	-0.003	0.0259	4.089	0.001
Slope	0.205	-0.003	0.0254	8.181	0.001

3.3.5 THE LOGIT MODEL

The discrete choice model, developed by McFadden (1974), is often referred as the multinomial logistic regression model or logit model. The assumption behind logistic regression is that the probability of a dependent variable taking the value of 1 follows a logistic curve (Wrigley, 1985). We chose a binomial logit model because only two outcomes were possible: wetland vs. not wetland. The binomial logit model is expressed as follows:

$$P(d=1|x)=\frac{\exp^{\beta' x_i}}{1+\exp^{\beta' x_i}} \qquad \textbf{[Equation 3.1]}$$

where d is the dependent variable, x is the set of independent variables, and β represents the coefficients derived from the logit model. In this study, the categorical binomial dependent variable takes the value of 1 when it is wetland, and zero when it is upland.

The logit model was developed in SAS® 9.1.3 (Statistical Analysis System Institute Inc., Cary, NC, USA) using the PROC LOGISTIC procedure.

3.4 RESULTS

We initially developed a logistic regression model for every ASTER band separately in order to observe the relationship between each band and the presence of wetlands. Table 3.5 show the overall accuracy obtained using each single band, and the producer's (P) and user's accuracy (U) (Lillesand and Kiefer, 2004) when water is included in the model. The producer's accuracy indicates how well pixels of the given cover type are classified. The user's accuracy indicates the probability that a pixel classified in a given class actually represents that class on the ground (Lillesand and Kiefer, 2004). The overall trend, which varied quite a bit among bands and dates, revealed little commission error for wetlands, but many were missed. At a probability level of 90%, the March scene had some influence in detecting wetlands. March Band 3 had the highest accuracies, followed by Band 4 and 5.

Table 3.5. Estimate values and accuracy rate for each individual March ASTER band (a) and October band (b) from an in-sample analysis when water is included in the model. *P* = producer's accuracy; *U* = user's accuracy.

a)

Variable	Band 1	Band 2	Band 3	Band 4	Band 5
Estimate value	-14.29 (p < 0.0001)	-19.97 (p < 0.0001)	-38.43 (p < 0.0001)	-23.57 (p < 0.0001)	-36.10 (p < 0.0001)

Accuracy rate at 90% probability level

Overall accuracy	47.2		44.7		74.6		63.9		60.2	
	P	*U*	*P*	*U*	*P*	*U*	*P*	*U*	*P*	*U*
Wetland accuracy	7.0	100	7.0	94.4	59.3	96.9	39.7	97.7	33.9	97.4
Upland accuracy	100.0	44.7	99.6	44.6	96.8	63.2	99.3	55.0	98.6	52.7

Accuracy rate at 95% probability level

Overall accuracy	40.7		40.9		68.8		59.2		55.5	
	P	*U*	*P*	*U*	*P*	*U*	*P*	*U*	*P*	*U*
Wetland accuracy	0.0	100	0.5	100	48.9	94.5	31.5	97.2	24.9	100
Upland accuracy	100	42.6	100	42.5	97.9	58.6	99.6	51.6	100	49.5

b)

Variable	Band 1	Band 2	Band 3	Band 4	Band 5
Estimate value	-1.725 (p < 0.0001)	-3.293 (p < 0.0001)	-3.556 (p < 0.0001)	-5.720 (p < 0.0001)	-8.794 (p < 0.0001)

Accuracy rate at 90% probability level

Overall accuracy	40.7		40.7		40.7		36.1		40.7	
	P	*U*	*P*	*U*	*P*	*U*	*P*	*U*	*P*	*U*
Wetland accuracy	0.0	-	0.0	-	20.2	95.7	13.0	100	7.0	100
Upland accuracy	100	42.5	100	42.5	97.2	43.5	100	45.9	100	44.3

Accuracy rate at 95% probability level

Overall accuracy	40.7		40.7		40.7		40.7		40.7	
	P	*U*	*P*	*U*	*P*	*U*	*P*	*U*	*P*	*U*
Wetland accuracy	0.0	100	0.5	100	15.9	96.5	7.0	98.2	7.0	100
Upland accuracy	100	42.6	100	42.5	97.9	58.6	99.6	51.6	100	49.5

As expected, the accuracy increased once all bands were used in the model (table 3.6, part a). At a 90% probability level, the producer's accuracy is 60.6%. The producer's accuracy decreased to 50% at a 95% probability level. Table 3.6 (part b) shows results obtained once the water category is excluded. This comparison was necessary because open water fell into the wetland category using this classification scheme, but is easily identified using multispectral data that includes the reflective infrared. The overall accuracy decreased by about 4% at both confidence levels. The wetland producer's accuracy was about 12% lower, confirming our suspicion that inclusion of open water in the wetlands category inflated the accuracy. The inversely related user's accuracies for wetlands (high) and uplands (low) confirms the general trend toward overclassifying uplands.

Table 3.6. Accuracy rates obtained using all the 10 ASTER bands in the logit model when the original set of data (a) is considered, and (b) when water is excluded from the model. *P* = producer's accuracy; *U* = user's accuracy.

a)

Probability level	*90%*		*95%*	
Overall Accuracy	74.5		69.0	
	P	*U*	*P*	*U*
Wetland Accuracy	60.6	96.4	50.6	97.3
Upland Accuracy	96.0	51.5	97.6	48.3

b)

Probability level	*90%*		*95%*	
Overall Accuracy	70.4		64.0	
	P	*U*	*P*	*U*
Wetland Accuracy	48.2	97.4	34.8	99.3
Upland Accuracy	96.0	49.8	97.6	49.5

In order to identify which band contributes most to the model, we computed the marginal effect (table 3.7). The marginal effect is the change in probability of detecting a wetland for a one standard deviation change in each respective independent variable from its median value. Band 3 had the highest marginal effect (7.277). The other bands had a much lower value. Band 1 was also negative, meaning an inverse correlation with the predicted probability; however it was the second highest marginal value (-2.466).

Considering the October scene, the marginal effect of all the bands was low with respect to the March scene. This result is in agreement with the fact that each individual October band does not have any power in identifying wetlands. The high marginal effect of March Band 3 may be influenced by the statistically significant spatial autocorrelation found in presence of water. However, the spatial autocorrelation should positively influence also the October bands, but we observe that the marginal effect of the October scene is close to none.

Table 3.7. Marginal effect of the ASTER bands.

Band #	1	2	3	4	5
March					
Standard Deviation	0.077	0.085	0.087	0.091	0.050
Marginal Effect	-2.466	1.337	7.277	0.394	-0.056
October					
Standard Deviation	0.081	0.090	0.125	0.124	0.075
Marginal Effect	0.297	0.272	0.240	0.501	-1.102

Before introducing all the GIS data in the logistic regression model, we performed a canonical discriminant analysis to test the significance of each variable in separating wetlands from uplands. The canonical discriminant analysis finds linear combinations of the quantitative variables that provide maximal separation between the classes. The canonical discriminant analysis was performed in SAS, using PROC CANDISC. The CANDISC procedure computes squared Mahalanobis distances between class means, and performs both univariate and multivariate one-way analyses of variance. Appendix B provides the SAS code used for the canonical discriminant analysis and the %PLOT macro to plot pairs of canonical variables to aid visual interpretation of group differences (figure 3.3 and 3.4).

We computed the canonical analysis twice. The first time, we considered all the training points, including the water category. The second time, we computed the analysis excluding the water category, so that the direct effect of water on the correlation was observed. The results were not significantly different.

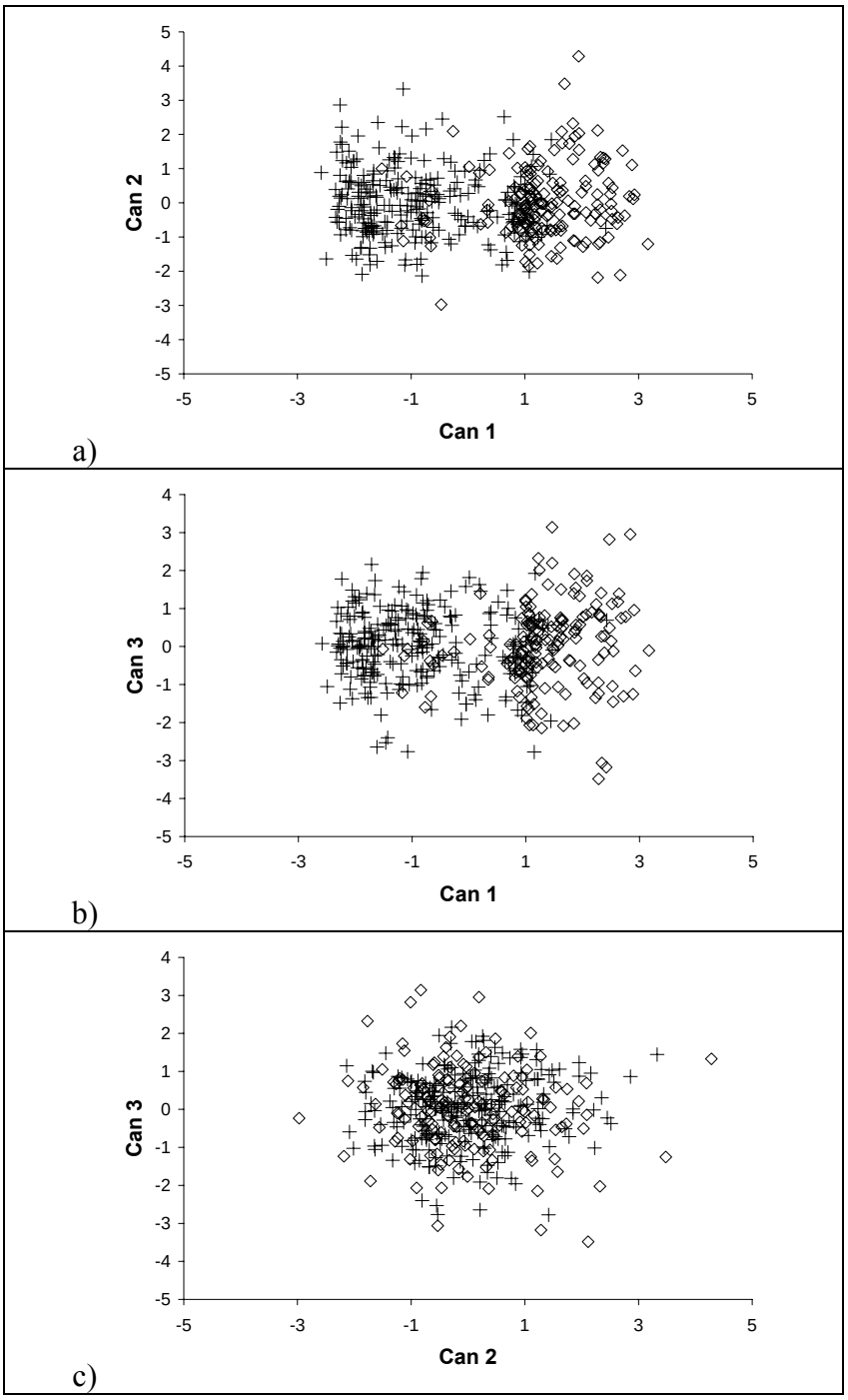

Figure 3.3. Plot of the canonical variables from the original dataset. Canonical variable 1 (Can 1) vs. canonical variable 2 (Can 2)(a); canonical variable 1 (Can 1) vs. canonical variable 3 (Can 3) (b); canonical variable 3 (Can 3) vs. canonical variable 2 (Can 2)(c). The cross symbol represents upland, and the diamond symbol represents wetland.

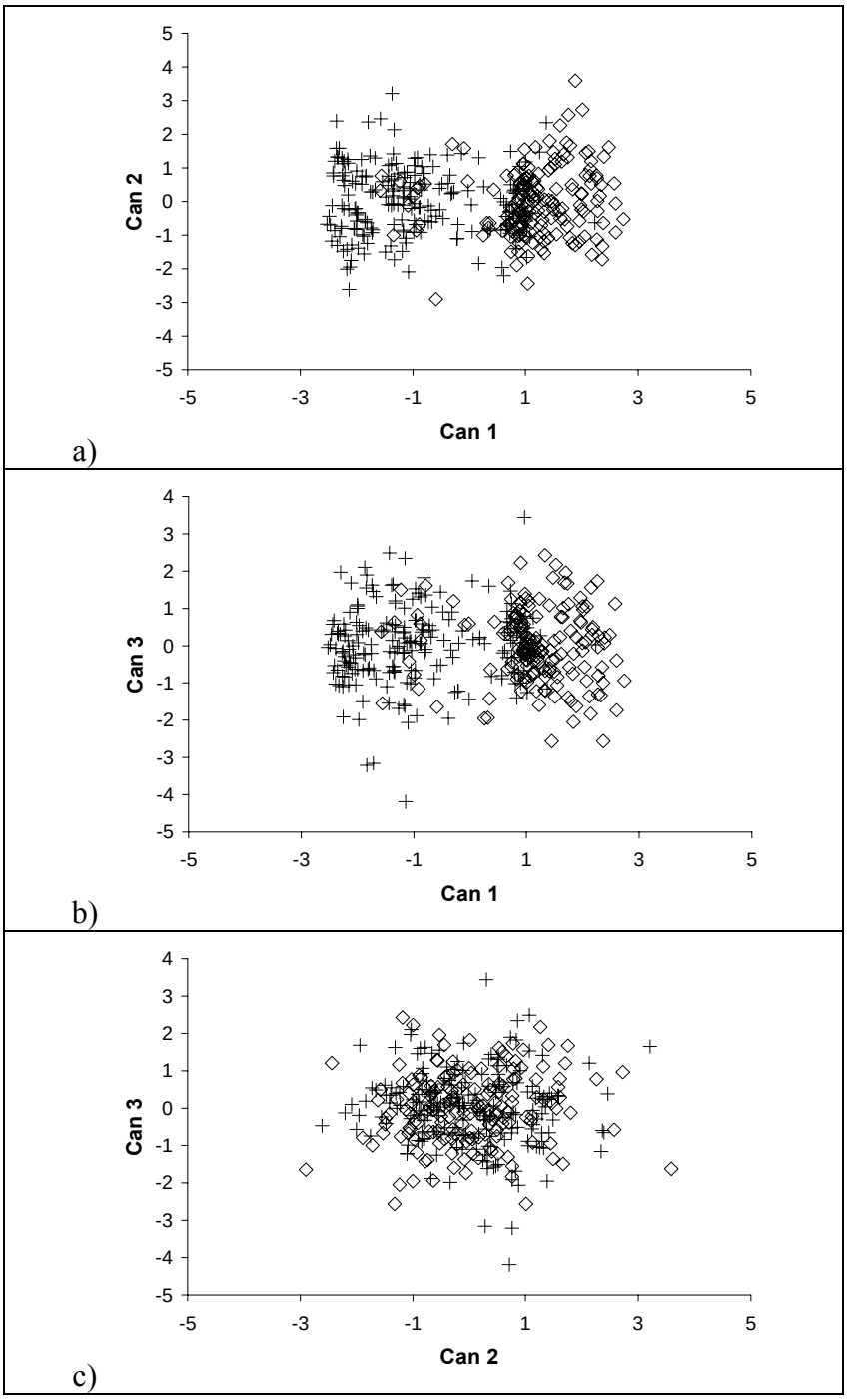

Figure 3.4. Plot of the canonical variables from the dataset when the water is not included. Canonical variable 1 (Can 1) vs. canonical variable 2 (Can 2) (a); canonical variable 1 (Can 1) vs. canonical variable 3 (Can 3) (b); canonical variable 3 (Can 3) vs. canonical variable 2 (Can 2) (c). The cross symbol represents upland, and the diamond symbol represents wetland.

Table 3.8 shows the canonical variate correlation between the first canonical variate (Can1) and the independent variables in case of presence (a) and absence of water (b). We considered the first canonical variable only because it was able to separate uplands from wetlands, whether the water category was included or not.

Higher values in table 3.8 signify higher correlations. SSURGO soil data had the highest correlation with Can1 (0.876), followed by Band 3 from the March scene, which had a negative correlation (-0.803), and the NHD water data had a positive value (0.725). The other variables had lower correlation values, meaning that they did not have the same power in separating wetlands from uplands. When water was excluded from the analysis, the results did not change. SSURGO soil data remained the variable with the highest correlation value (0.897), followed by March Band 3, and NHD water data.

Table 3.8. Canonical variate correlation of Can1 with the 15 variables used in the logit model. Water category is included (a); water category is excluded (b).

a)		*b)*	
March		*March*	
Band 1	-0.520	Band 1	-0.539
Band 2	-0.592	Band 2	-0.566
Band 3	-0.803	Band 3	-0.776
Band 4	-0.684	Band 4	-0.626
Band 5	-0.620	Band 5	-0.550
October		*October*	
Band 1	-0.359	Band 1	-0.401
Band 2	-0.355	Band 2	-0.394
Band 3	-0.421	Band 3	-0.264
Band 4	-0.594	Band 4	-0.527
Band 5	-0.550	Band 5	-0.487
SURGO	0.876	SURGO	0.897
NHD	0.725	NHD	0.694
DEM	-0.583	-DEM	0.528
Slope	-0.153	-Slope	0.156
WI	0.315	WI	0.263

Because of the proven significant contribution of March Band 3 over the other ASTER bands, we selected only Band 3 to be combined with the SSURGO soil data and the NHD water data in two other logit models.The first included the water category; the second excluded the water category. Each time, the model was tested on an out-of-sample dataset (table 3.9). The out-of-sample results are slightly different than the in-sample results using only March Band 3. However, when water is excluded from the model, the out-of-sample results are higher at both 90% and 95% probability level than the results obtained joining all the ASTER bands into the model. Since March Band 3 was not affected by spatial autocorrelation in absence of the water category ($p = 0.027$), we can affirm that spatial autocorrelation does not inflate the power of March Band 3. Also, even though March Band 3 easily measure the water category, it is also able to detect over 56% of wetlands that are not open water.

Adding the GIS data layers one by one to the model having originally only March Band 3, we observed that the producer's accuracy rate for wetland prediction increased significantly when NHD water data was added into the model. At a 90% CI, NHD water data raised the accuracy rate 17% with the water category, and 15% without. On the other hand, SSURGO soil data did not have the same influence. With water, it increased the producer's accuracy rate 8%, without water 2%. The commission error for uplands varies between 30% and 40% when the GIS data layers are added to the model. The addition of the binary variables together did not increase the accuracy rate more than what NHD water was able to do by itself. When water was included in the analysis, the model had the highest producer's accuracy rate both at CI equal to 90% and 95%. When water was excluded, the model did not show any significant difference from the model that included only the NHD and March Band 3. Figure 3.5 shows a map of the classification obtained from the model when SSURGO soil and NHD water data are included. The map can be compared to the March Band 3 image (figure 3.6). The James River is completely identified, and so are the swamps associated with its sinuous path. In the center of the figure is Turkey Island, an area characterized by palustrine wetlands. The area has a greater than 90% probability of being wetland. The accuracy becomes lower at the stream level. The model does not appear to misclassify agricultural or urban areas as wetlands.

Table 3.9. Accuracy rates derived from an out-of-sample test. The values show the increase of accuracy once SSURGO soil and NHD water are added to the model containing only March Band 3. The results are shown in presence (a) and absence (b) of the water. *P* = producer's accuracy; *U* = user's. accuracy.

a) With water

	Band 3				SSURGO				NHD				SSURGO + NHD			
Probability Level	90%		95%		90%		95%		90%		95%		90%		95%	
Overall Accuracy	76.9		71.2		80.6		70.2		86.0		83.4		86.5		83.4	
	P	*U*	*P*	*U*	*P*	*U*	*P*	*U*	*P*	*U*	*P*	*U*	*P*	*U*	*P*	*U*
Wetland Accuracy	60.2	93.8	48.8	89.5	68.3	99.2	60.0	94.8	77.5	99.4	72.5	99.2	78.8	98.5	73.0	100
Upland Accuracy	94.4	63.8	91.1	56.2	95.5	66.1	98.2	52.3	97.6	76.1	98.2	68.6	97.0	76.6	97.6	76.1

b) Without water

	Band 3				SSURGO				NHD				SSURGO + NHD			
Probability Level	90%		95%		90%		95%		90%		95%		90%		95%	
Overall Accuracy	70.2		73.6		76.2		68.1		84.6		81.7		84.3		81.7	
	P	*U*	*P*	*U*	*P*	*U*	*P*	*U*	*P*	*U*	*P*	*U*	*P*	*U*	*P*	*U*
Wetland Accuracy	56.5	93.3	42.9	96.2	58.6	99.0	40.9	98.2	72.9	95.5	66.9	99.1	72.9	99.1	67.4	98.1
Upland Accuracy	94.3	51.4	98.0	48.6	95.7	63.1	98.2	60.1	97.6	76.4	98.2	65.3	97.0	66.4	97.6	70.6

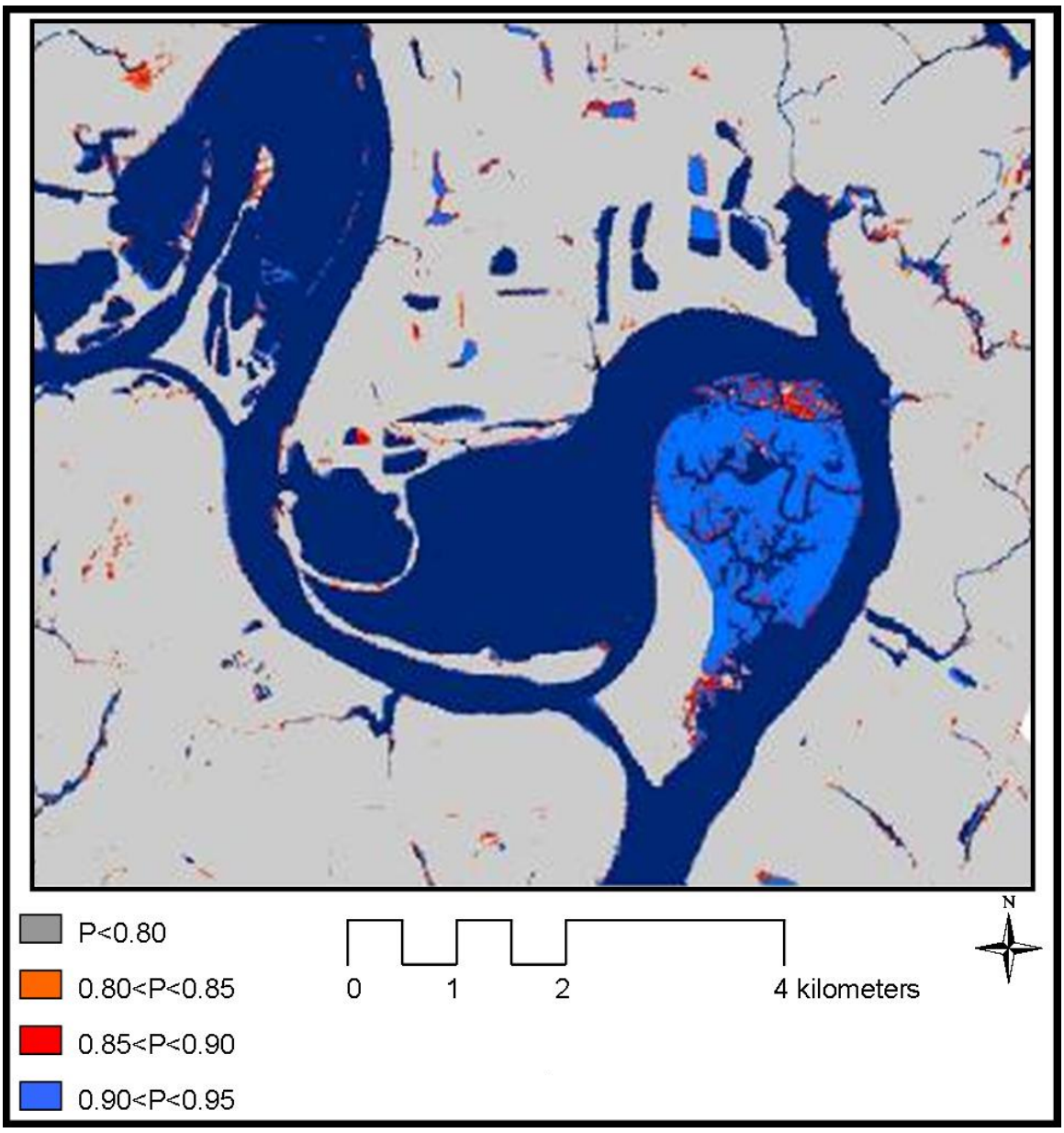

Figure 3.5. Wetland classification as resulted from inputing SSURGO soil, NHD water, and March Band 3 into the binary logit model. The legend shows the probability of accurately mapping wetlands for a subset of the study area.

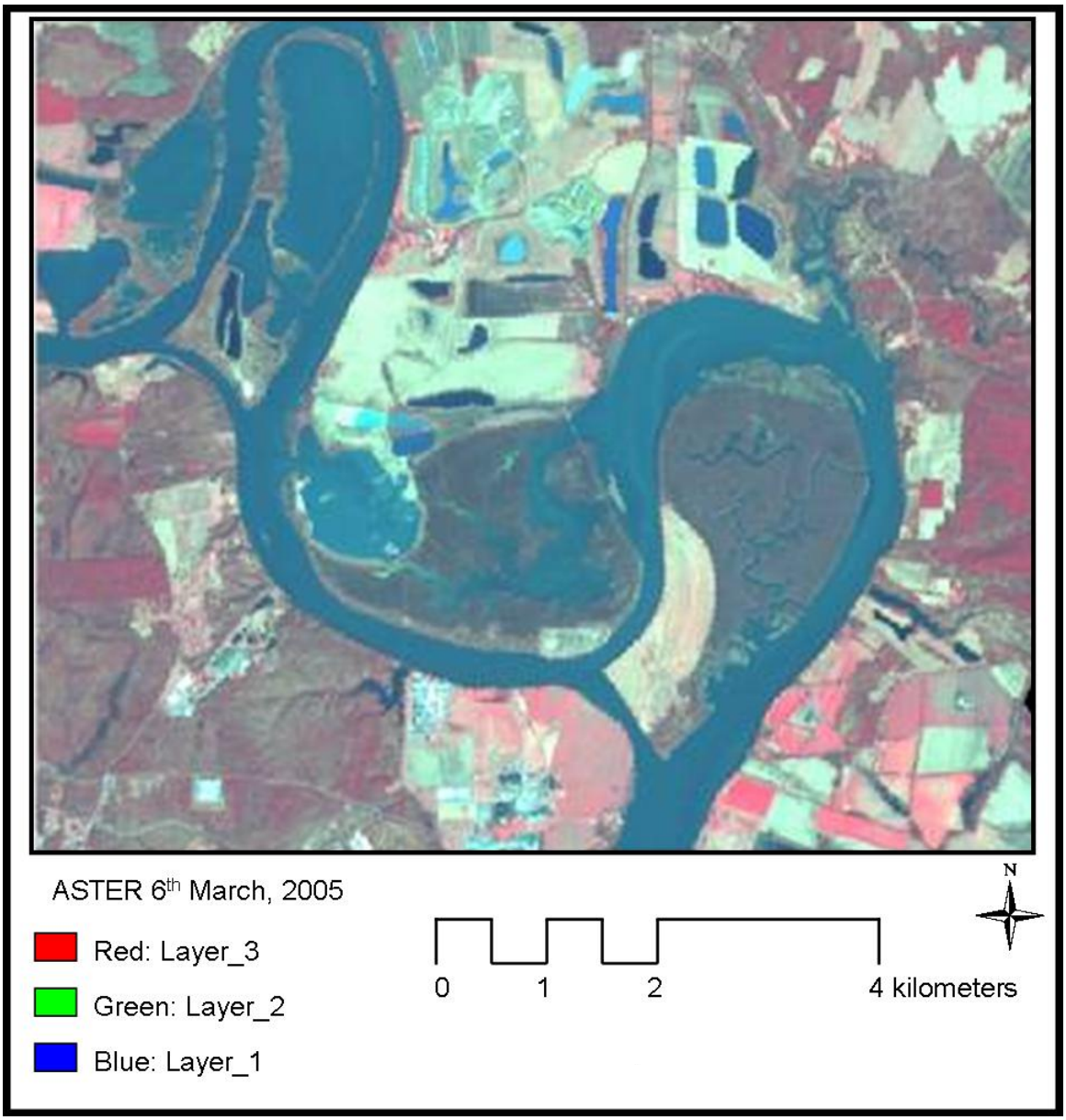

Figure 3.6. ASTER scene of a subset of the study area taken on 6 March 2005.

3.4.1 ANALYSIS OF MISCLASSIFIED WETLANDS

In order to identify the reasons for misclassification, we extracted the incorrectly classified points and examined each point using digital orthophotos. Table 3.10 shows the causes of misclassification both for wetlands and uplands. Woody wetlands had the highest misclassification. Even though the image was acquired during a leaf-off month, several wetlands present evergreen forest cover that may obfuscate the standing water and soil beneath the canopy.

A second reason for misclassification was related to georectification. The random points were classified as belonging either to uplands or wetlands by looking at their position on aerial photographs. Because of the large study area (60 x 60 km), it was not possible to mosaic all the orthophotos and georeferenced them to the ASTER image. As such, we anticipate that positional error was a factor leading to decreased accuracies, though we are uncertain of its importance.

Table 3.10. Cause of misclassification and percentage of misclassified wetlands based on location and type of wetland.

Location/ Wetland Category	Cause of Misclassification
Woody Wetlands	Tree canopy cover (94%); Georectification (6%)
Emergent Wetlands	Dry soil; Georectification
Ponds/Streams	Georectification, sediments in settling ponds, size
Uplands	Ponding of agricultural fields, parking lots; Georectification

3.4.2 NWI ACCURACY

We used the same set of point data for testing the accuracy of NWI in classifying wetlands. The overall accuracy (table 3.11) of NWI is higher than the one reached by our final model, which included March Band 3, SSURGO and NHD data. In addition, the producer's and user's accuracy values were high. The McNemar test (McNemar, 1947) in table 3.12 also showed that the NWI classification is more accurate than our final model ($\chi^2 = 21.35$, p-value < 0.0001).

Table 3.11. Error matrix obtained using data from NWI.

Category	Wetland	Upland	Row Total	Producer's accuracy	User's accuracy
Wetland	204	21	225	86.6	98.5
Upland	3	164	167	98.8	88.6
Column Total	207	185	392		
Overall accuracy	92.8				

Table 3.12. McNemar test between the NWI data and the results from the logit model obtained from the use of ASTER March Band 3, NHD, and SSURGO data at 90% probability level.

McNemar's Test	
χ^2	21.35
p-value	< 0.0001
Kappa	0.73

3.5 DISCUSSION AND CONCLUSIONS

The first objective of this study was to test the ability of the ASTER sensor in detecting the location of wetlands. The sensor was able to capture 60.6% of the total wetlands with a probability level of 90%. March Band 3 (NIR) proved to be the most useful. The utility of March Band 3 was inversely correlated with the presence of wetland, i.e. the higher the NIR signal, less likely a pixel would be labeled "wetland". This result may seem surprising, but it is in accord with the work of Slaughter et al. (2001) and Hunt and Rock (1989), who showed the NIR band to be capable of detecting soil and plant moisture content, and with the work of Tan et al. (2003), that found the near infrared band to be the most indicative sign of vegetation leaf health status. The negative correlation of wetland vegetation and the NIR band was due to the absence of vegetation on wetlands at the time when the March scene was taken. The NIR band signaled the wet ground beneath the canopy that was not formed yet.

This study does not agree with Mackey (1990) who reported that an inter-season analysis is necessary for properly detecting wetlands. Even though a multi-temporal analysis of the data should in theory help identify the hydrological, phonological and compositional changes that are typical of wetland areas, results from this study prove that the March scene was the only one required.

NHD water is the GIS variable that contributed the most to the wetland identification accuracy. NHD water is a publicaly available dataset that we strongly suggest for use in wetland studies. SSURGO data were initially thought to be the most useful data because of a key property that they track: the individual hydric soils. However, SSURGO was proven to be less valuable than NHD water. The SSURGO data show limitations that can be connected to the age of the data, and to the unkown location of the hydric soils within each soil map unit. SSURGO data were surveyed and produced in the late 1980s. Since then, the land has been subject to many changes that cannot be revealed by SSURGO. For example, the low contribution to the model is probably caused by the presence of agricultural lands where SSURGO indicated hydric soil. In addition, as noted above, the hydric composition identified by the SSURGO dataset does not specify the spatial location of the composition within the soil map unit area. The hidric

composition may be concentrated within a depressional area or randomly spread throughout the unit area. The only way to assess it would be a field survey, which is not feasable over our study area due to its large extent.

From canonical discriminant analysis, it appears that elevation is a marginal factor in determining wetlands. An elevation model that is more accurate than the one provided in this study might be of further help in predicting location of wetlands. The wetness index was not helpful either. A wetness index generated from a finer grid size (2 and 4 m grid cell) is not very different from one generated from a 10 m DEM (Zhang and Montgomery, 1994), but it is significantly different from one generated from a 30 m DEM. Thus, it may be worthwhile to use a higher resolution DEM to indicate elevation patterns, but not to use it for generating a more accurate wetness index.

Our conclusions are that ASTER has the potential to be successfully used to identify wetlands in the Coastal Plain of Virginia, as it has a spatial and spectral resolution that allows discrimination between uplands and wetlands. The Coastal Plain region in nearby states is similar in its characteristics, thus, we do not see any reason why our model could not be applied in states other than Virginia. Lands that are topographically different from the Coastal Plain may be subject to different results. We speculate that a more undulating topography would increase the probability of locating wetlands, and the DEM and wetness index would be more efficient than in the Coastal Plain.

With our model, we predict up to 78% of all the wetlands when the p-value is set to 0.1. This study proves that the results are statistically different from the results achieved by NWI on the same study area. NWI presents an omission error of 14% on wetlands, whereas our model omits about 27% of the wetlands. Even though the difference is significant, the accuracy of our model is balanced by factors such as time and costs. The traditional way of manually digitizing wetland maps implies high production costs due to the team of scientists that have to be employed. The use of ASTER images requires only one workstation and one analyst. The maps produced as a result of this research are not suitable for land management decisions at the parcel level. However, the wetlands identified with our model are almost always wetlands when field-

verified. As such, costs could be reduced by using a two-stage process (e.g., ASTER then high-resolution orthoimagery).

In addition, ASTER may speed the map updating process from ten years to one. That is, maps may be produced every time a March image is available for the location of interest. However, the on-demand and still experimental nature of ASTER may limit the availability of scenes over time and space, and the availability of imagery with similar (or better) spatial resolution appears to be beneficial.

4 A COMPARISON OF CART AND LOGISTIC REGRESSION FOR MAPPING WETLAND TYPES IN THE COASTAL PLAIN OF VIRGINIA USING THE ASTER SENSOR

4.1 ABSTRACT

Frequent mapping of wetlands is extremely important for monitoring gains and losses in these valuable ecosystems. This study compared a non-parametric and a parametric model for discriminating among uplands (non-wetlands) and three types of wetlands: woody wetlands, emergent wetlands, and open water. Spring (6 March 2005) and fall (16 October 2005) satellite images obtained from the Advanced Spaceborne Thermal Emission and Reflection Radiometer (ASTER) and GIS data layers formed input for a classification and regression tree (CART) and a multinomial logistic regression (logit) analysis. The overall accuracy of the CART model was 73.3%. The overall accuracy of the logit model was 76.7%. The accuracies were not statistically different from each other (McNemar $\chi^2 = 0.89$, $p = 0.34$). The CART producer's accuracy of the emergent wetlands was higher than the accuracy from the multinomial logit (57.1% vs. 40.7%), whereas woody wetlands identified by the multinomial logit model presented a producer's accuracy higher than the one from the CART model (68.7% vs. 52.6%). The producer's accuracy indicates how well pixels of the given cover type are classified. A McNemar test between the two models and NWI maps showed that their accuracies are not statistically different. Overall, these two models provided promising results, even though they are not sufficiently accurate to replace completely current methods of wetland mapping based on feature extraction on high-resolution orthoimagery.

4.2 INTRODUCTION

Like any other natural environment, wetlands are subject to changes over time due to natural events such as floods and hurricanes that modify their shape and size, and by human activities that have replaced wetlands with agricultural and urban land. Accurate and up-to-date wetland maps are important for evaluating gains and losses of these valuable ecosystems and for enabling governmental agencies to produce suitable policy

and release appropriate permits to the public. The accuracy of a map depends on the protocols that have been used to produce it, including the source data. Currently the National Wetland Inventory (NWI) provides the highest detail wetland maps available to the public. The main product of the NWI is large scale (1:24,000) maps that show the location, shape, and characteristics of wetlands and deepwater habitats. NWI utilizes conventional photo-interpretation techniques, using aerial photographs at scales from 1:40,000 to 1:80,000, and, for the earliest maps, at 1:133,000 to locate and map wetlands in the United States.

In this study, we use data from the Advanced Spaceborne Thermal Emission and Reflection Radiometer. ASTER is an imaging instrument flying on Terra, a satellite launched in December 1999 as part of NASA's Earth Observing System. ASTER consists of three separate instrument subsystems (table 4.1): the visible and near infrared (VNIR), the shortwave infrared (SWIR), and the thermal infrared (TIR). The VNIR subsystem operates in three spectral bands at visible and near-infrared wavelengths, with a resolution of 15 m. It consists of two telescopes: one nadir-looking with a three-spectral-band detector, and the other backward-looking with a single-band detector. The backward-looking telescope provides a second view of the target area in Band 3 (0.76-0.86 μm) for stereo observations. The SWIR subsystem operates in six spectral bands in the near-IR region through a single, nadir-pointing telescope that provides 30 m resolution. The TIR subsystem operates in five bands in the thermal infrared region using a single, fixed-position, nadir-looking telescope with a resolution of 90 m. The ASTER instrument is still being corrected and improved. Dr. Thome of the Remote Sensing Group, University of Arizona, recommended using ASTER images produced in the last three years (K. Thome, personal communication, June 2005). ASTER is an on-demand instrument, which means that data are only acquired over a location if a request has been submitted to observe that area. However, many ASTER images are freely available on line through the Land Processes Distributed Active Archive Center (LPDAAC) Data Pool.

This study has four major objectives: 1) development of parametric and non-parametric model able to discriminate among wetland vegetation types using remote sensing data from the ASTER sensor and GIS data layers; 2) determination of which of

the two models is more accurate for mapping wetland presence and type; 3) establishment of which multitemporal remotely sensed data are required for discriminating among wetland vegetation types; and 4) comparison of the results of our models with NWI maps.

Table 4.1. Characteristics of the ASTER sensor.

	Spectral Range (μm)					
VNIR[1] (15 m)	Band 1 0.52 - 0.60	Band 2 0.63 - 0.69	Band 3 0.76 - 0.86	Band 3 0.76 - 0.86		
SWIR[2] (30 m)	Band 4 1.60 - 1.70	Band 5 2.14 - 2.18	Band 6 2.18- 2.22	Band 7 2.23 - 2.28	Band 8 2.29 - 2.36	Band 9 2.36 - 2.43
TIR[3] (90 m)	Band 10 8.12 - 8.47	Band 11 8.47 - 8.82	Band 12 8.92 - 9.27	Band 13 10.20 - 10.90	Band 14 10.90 –11.65	

[1] Visible and near infrared

[2] Short wave infrared

[3] Thermal infrared

4.2.1 CART

CART® (classification and regression trees) is a recently developed non-parametric model that is becoming more and more popular along different disciplines, ranging from medical to ecological applications (De'Ath and Fabricius, 2000; Lewis, 2000; Yohannes and Hoddinott, 2006). CART® provides an accurate and efficient methodology for land cover classification, both at regional and global scales (Friedl and Brodley, 1999; Hansen et al., 2000; Homer et al., 2002). In addition, some studies have shown that CART® can be more accurate than traditional parametric classifiers (Friedl and Brodley, 1999; Pal and Mather, 2003). CART® involves the identification and construction of a binary decision tree using training data samples for which the correct classification is known (Bittencourt and Clarke, 2003). The samples are then used in the production of rule sets, based on the relationship modelled, essentially enabling the software to build a "knowledge base" with little interaction or input from the user (Herold et al., 2003). CART® makes accurate generalizations concerning the relationship of the independent variables and the value of the dependent variable. Since CART® is based on non-

parametric statistics, it does not assume a normal distribution in the available dataset. One of the best known and most used rules for binary recursive partitioning is the Gini splitting rule (Salford System, 2002). Gini's rule looks for the largest class in a database and strives to isolate it from all other classes, tending to create end-cut splits (small nodes with only one target class prevailing) on multilevel targets. Costs are incorporated by adjusting prior probabilities. This method was considered the preferred in this study because net cuts were desired between categories, and no prior and subjective costs were to be attributed to any class.

We utilized the CART 5.0® software (Salford Systems, San Diego, California) to generate the CART model. CART 5.0® is user friendly, and its results are easily interpretable. Nevertheless, CART 5.0® has some limitations. The initial splits largely determine the effectiveness of the tree, since they reduce the greatest variability (Venables and Ripley, 1997; Lawrence et al., 2004). CART® does not allow the user to have full control of the process, limiting possibility for changes. The generated output is standard; it cannot be modified more than growing or pruning the tree.

4.2.2 MULTINOMIAL LOGISTIC REGRESSION

An alternative to CART® is a generalized logit model, in which k+1 possible responses are nominal. This model was introduced by McFadden (1974) as the discrete choice model, and it is also known as multinomial model. The model has the form as shown in equation 4.1:

$$\log\left(\frac{\Pr(Y=i|x)}{\Pr(Y=k+1|x)}\right)=\alpha_i+\beta_i^{'}x, \quad i=1,\ldots,k \qquad \textbf{[Equation 4.1]}$$

where the $\alpha_1, \ldots \alpha_k$, are *k* intercept parameters, and the $\beta_1, \ldots \beta_k$, are *k* vectors of parameters.

A response variable with *k* categories generates *k*-1 equations. Each equation is a binary logistic regression comparing a category with the reference category. The

probability for each category is obtained as in the following equations (Menard, 2002) , where one of the coefficients is set to zero in order to solve the following equations:

$$P(y = x) = \frac{1}{1 + e^{w\beta} + e^{z\beta}} \quad \textbf{[Equation 4.2]}$$

$$P(y = w) = \frac{e^{w\beta}}{1 + e^{w\beta} + e^{z\beta}} \quad \textbf{[Equation 4.3]}$$

$$P(y = z) = \frac{e^{z\beta}}{1 + e^{w\beta} + e^{z\beta}} \quad \textbf{[Equation 4.4]}$$

Logit models give rise to linear log-odds ratios, which facilitate interpretation of the parameters. They have been successfully applied in many fields such as urban land use planning, wildlife habitat modeling, and agricultural land use changes pattern and changes, but little has been published regarding their application to wetlands modeling (Bian and West, 1997; Narumalani et al., 1997; Nelson and Geoghegan, 2002).

4.3 DATA AND METHODS

4.3.1 STUDY AREA

The ASTER scenes cover a 60 x 60 km area in the Coastal Plain of Virginia (figure 4.1) Even though urbanization and agriculture have greatly reduced the number of wetlands, the Coastal Plain contains more than 70% of all the wetlands in Virginia (Tiner and Finn, 1986). The Coastal Plain consists of fluvial and marine deposits, primarily non-lithified. The oldest sediments were deposited during the Cretaceous, but surface deposits near the coast are much younger (5,000-25,000 years B.C.); (Eick, 2006). In the study area, the elevation has a mean of 33 m above the mean sea level, with a maximum elevation of 105 m. The Coastal Plain is crossed by numerous rivers and streams that have a high degree of sinuosity as they cross the middle and lower Coastal Plain. The sinuosity of the stream favours the formation of wetlands of variable nature: emergent, scrub and shrub, and forested wetlands. The topography of the area also allows the formation of mineral flat wetlands, which may be located far from water bodies.

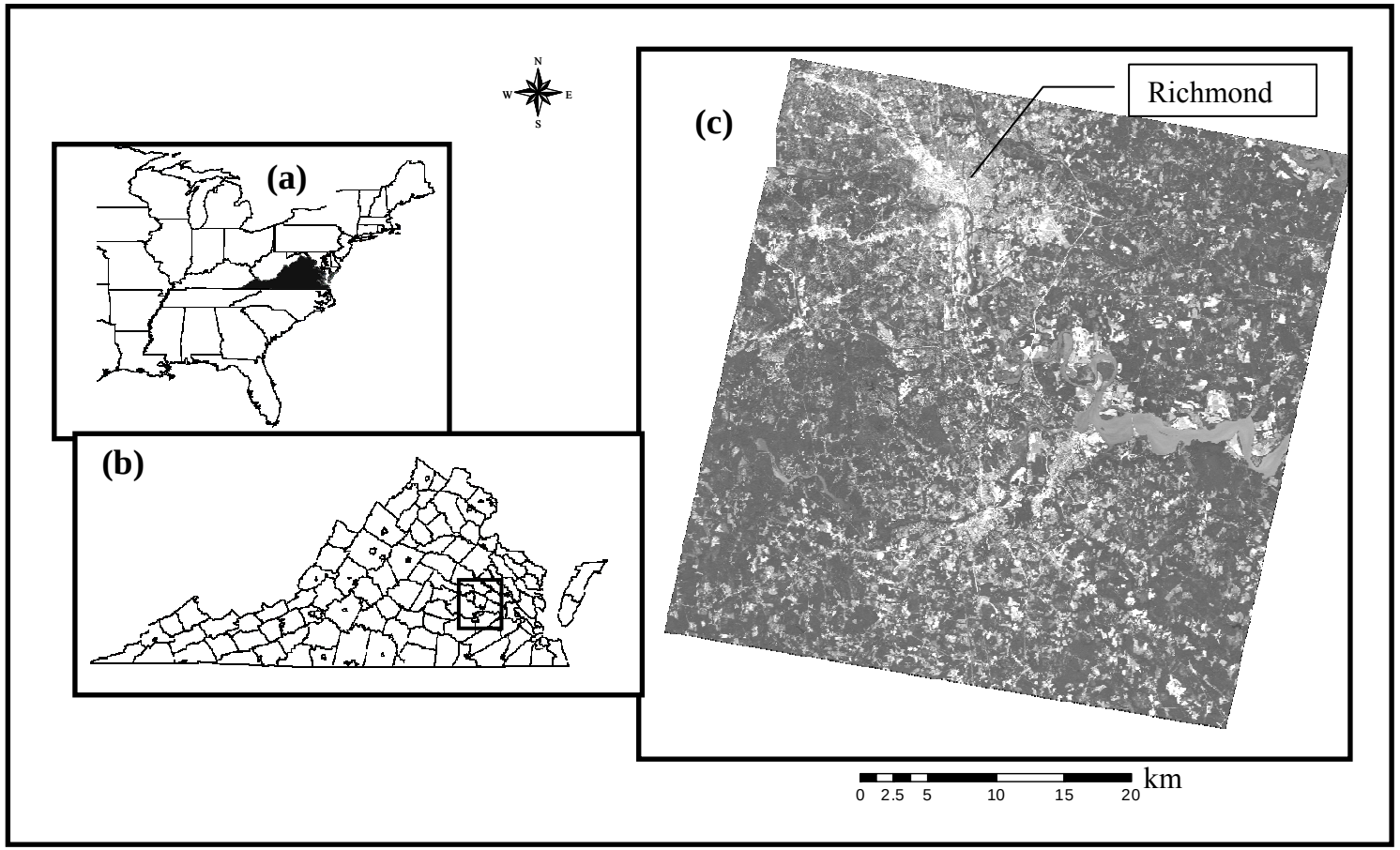

Figure 4.1. Location of the study area. Map of the United States, with Virginia highlighted in bold (a); Map of Virginia. The black square identifies the location of the study area (b); Study area, equivalent to one ASTER scene (c). The image corresponds to Band 2 (0.63-0.69 μm) from the March scene.

4.3.2 DATA

We used CART® and generalized logit models to discriminate among uplands[1] and three types of wetlands: woody wetlands, emergent wetlands, and open water. Woody wetland included all Palustrine Forested Wetlands plus the Scrub and Shrub Wetlands, as defined by the Cowardin Classification system (1979). The water class encompassed rivers and streams not covered by vegetation; this category corresponds to the Lacustrine and Riverine Wetlands in the Cowardin System. Emergent Wetlands belong to the Palustrine Emergent Cowardin category.

Among the remotely sensed data, we selected two ASTER scenes. The first scene was acquired on 6 March 2005, and the second one on 16 October 2005 (respectively AST_L1B.3: 2028411439, and AST_L1B.3:2028019676). The multispectral range of ASTER bands covers values between 0.52 μm and 2.43 μm; however we used only the first five bands that cover the spectrum from the visible to shortwave infrared range (0.52-2.185 μm). We chose this range because longer wavelength bands may be affected by spectral crosstalk phenomena (Iwasaki and Tonooka, 2005). We georeferenced the images to the Universal Transverse Mercator 1983 North American Datum (UTM NAD 83) projection using a first order polynomial transformation. Twenty ground control points (RMSE = 0.80 m) and twenty check points (RMSE = 0.85 m) were selected. The ASTER science team provided us with solar irradiance values that we used to convert the ASTER bands to top-of-atmosphere reflectance. Solar irradiance values are provided in table 4.2. We resampled all the bands to 15 m to match the pixel resolution of the first three ASTER bands.

In the models, we used digital soil data obtained from the Soil Survey Geographic Database (SSURGO), hydrographical data from the National Hydrography Database (NHD), a 10 m DEM developed from Virginia Base Mapping Program (VBMP) DTMs, the slope of the terrain calculated from the 10 m DEM, and a wetness index, computed according to Gessler et al. (1995).

---

[1] In this study, we refer to upland as any land that is not a wetland.

Table 4.2. Solar irradiance values for ASTER.

Band	Solar Irradiance (W/m^2 micrometer)
1	1846.9
2	1546.0
3	1117.6
4	232.5
5	80.32
6	74.92
7	69.20
8	59.82
9	57.32

The Soil Survey Geographic Database (SSURGO) was designed by the Natural Resources Conservation Service primarily for farm and ranch, landowner/user, township, county, and parish natural resource planning and management. We used SSURGO data to obtain information about the hydric properties of the soils in our study area. Wetlands soils are characterized by the presence of hydric soils. We based the distinction of hydric and non-hydric soil on the percentage of hydric composition that NRCS established for each map unit using aerial photographs and field survey. SSURGO refers to soils with a hydric composition greater than 85% as 'hydric'; whereas soils with a composition lower than 55% are 'non-hydric'. We checked the location of the soils with a hydric composition between 55% and 85% using topographic maps and fine resolution digital orthophotos (scale 1:1,200 and 1:2,400). We found these soils either on urban areas or on river-beds. We assigned those on urban areas to the non-hydric group, and the ones on river-beds to the hydric group.

We collected hydrographical data from the NHD. The NHD contains information about surface water features such as lakes, ponds, streams, rivers, springs and wells. We used a 10-m DEM developed from the Virginia Base Mapping Program. The VBMP DEMs provide the highest resolution terrain model currently available statewide (Futrell and Sforza, 2004). The data came as mass points and break lines. Mass points are three-

dimensional elevation points spaced across the surface on a regular grid or at random intervals as necessary for properly modeling the earth surface (VBMP, 2003).

VBMP points and lines were grouped in tiles. About 900 tiles covered the study area, but more tiles were collected around the edges of the study area to avoid an "edge-effect" problem (Butler et a., 1998). Each tile has about 100 elevation points, thus the study area had a total of 90,000 points. Even though the number of total points was high, elevation points were not available for the entire study area. Data for Chesterfield County were not available, and in the other counties some tiles were missing. A comprehensive TIN was created using the 3-D Analyst Extension™ in ArcMap 9.1® (Environmental Systems Research Institute, Inc., Redlands, CA, USA), and subsequently converted to a grid file for obtaining a DEM with a 10-m horizontal resolution. A comprehensive TIN was created using the 3-D Analyst Extension™ in ArcMap 9.1® (Environmental Systems Research Institute, Inc., Redlands, CA, USA), and subsequently converted to a DEM with a 10 m horizontal resolution using the Spatial Analyst Extension™ in ArcMap 9.1® (Environmental Systems Research Institute, Inc., Redlands, CA, USA). We tested the vertical resolution of our DEM against the geodetic control network provided by the National Geodetic Survey, as suggested by Maune et al. (2001). We collected 773 points, resulting in an RMSE of 1.96 m (table 4.3).

Table 4.3. Vertical accuracy of the DEM generated from the VBMP dataset compared to the geodetic control network points.

RMSE (m)	Mean (m)	Median (m)	Skew	Std. Dev.	# of Points
1.96	0.43	0.20	1.87	1.92	773

We used the DEM to calculate the slope of the terrain, and the wetness index (WI). The wetness index is a function of the upstream contributing area and the slope of the landscape. Moore et al. (1993) used the compound topographic index to describe the effects of topography on location and size of saturated areas. It is a refinement of upslope catchment area that better characterizes the spatial variability of soil properties due to

surface hydrology (Moore et al. 1993). The WI is calculated using the catchment area along with the slope as show in equation 4.5:

$$WI = \ln\left(\frac{A}{\tan\beta}\right) \qquad \textbf{[Equation 4.5]}$$

where β = slope, and A = catchment area.

We obtained NWI data from the U.S. Fish and Wildlife Service Wetlands Geodatabase. The data came in shape file format, carrying information on the location and the vegetation composition of the wetland according to the Cowardin classification system (Cowardin et al., 1979). Even though NWI provides data at the subclass level of the Cowardin classification system, we reclassified the data to obtain four categories that could be used for comparison purposes with the maps obtained by CART and logit model. All areas belonging to the Palustrine Forested wetland class were grouped into woody wetlands, and all the Palustrine Emergent wetlands into emergent wetlands; all the areas belonging to the Riverine and Lacustrine system were grouped into open water category; the non-wetland areas were grouped into the upland category.

4.3.3 EXPERIMENTAL DESIGN

We randomly sampled 870 points without replacement which were labeled as uplands (374), emergent wetlands (127), woody wetlands (280), and open water (89) using topographic maps and digital orthophotographs obtained from the VBMP. The VBMP digital orthophotos were developed using true color, leaf-off, vertical photography acquired in 2002. The source photography was acquired at three scales: 1:4,800 in rural areas, 1:2,400 in urban and suburban areas, and 1:1,200 in areas where localities choose the option to purchase a higher accuracy product (VBMP, 2003). We performed a field survey to validate 15% of the photo-interpreted points. We randomly selected 35 sites from each category and navigated to them in the field using GPS. Uplands, forested wetlands, and water were correctly identified with 100% accuracy; emergent wetlands were identified correctly with 94% accuracy. We proceeded with the construction of the

CART® and multinomial regression model, using a random subset consisting of three quarters of the points to generate the models, and the remaining points to test them. Appendix A shows the coordinates of the points.

4.4 RESULTS

4.4.1 CART

CART® produces a predictor ranking (variable importance) based on the contribution predictors make to the construction of the tree. Variable importance, for a particular predictor, is the sum of the improvement scores that the predictor has when it acts as a primary or surrogate (but not competitor) splitter across all nodes in the tree (Yohannes and Hoddinott, 2006). The list in table 4.5 considers all the variables that are used for producing the probability map. March Bands 3 and NHD contributed the most, followed by March Band 4 and October Band 3. The high position of the ASTER images demonstrates the importance of both satellite imagery and multi-temporal analysis, in which differences over seasons can facilitate the recognition of wetland types due to changes in vegetation and soil moisture content.

To determine the accuracy of the classification, we compiled an error matrix, and determined overall accuracy, $\hat{K}$, producer's and user's accuracy according to Congalton and Green (1999). The producer's accuracy is related to the omission error (producer's accuracy = 1 - omission error). The user's accuracy is related to the commission error (user's accuracy = 1 - commission error). $\hat{K}$ indicates the extent to which the percentage correct values of an error matrix are due to "true" agreement versus "chance" agreement (Lillesand and Kiefer, 2004).

Table 4.4. List of variable selected by the CART® model (a) and by the stepwise regression model (b). In (a) the variables are sorted by the score factor.

(a)		**(b)**		
Variable	Score	Variable	χ-square	p-value
March Band 3	100.00	NHD	35.0.	< 0.0001
NHD	78.3	SSURGO	25.6	< 0.0001
March Band 4	56.6	March Band 1	17.85	0.0005
October Band 3	40.5	October Band 2	15.84	0.0012
		March Band 4	13.58	0.0035
		DEM	13.44	0.0038
		March Band 3	11.52	0.0092
		March Band 2	10.37	0.0157
		Slope	9.54	0.0228

The overall accuracy of the CART® model = 73.3%, and the $\hat{K}$ = 0.59, indicating a moderate agreement (Congalton and Green, 1999) between the classification and the reference data (table 4.5). User's and producer's accuracy are low both for the emergent and the woody category. The producer's accuracy of the emergent wetland class is 57.1%, and the user's accuracy is lower (51.6%), indicating both a large omission and a large commission error. Many of the emergent wetlands were wrongly assigned to the woody wetland class. The producer's accuracy of the woody category is 52.6% and the user's accuracy is 69.7%. For this class, CART® omits more wetlands that in the emergent wetland category. The woody category is mostly misclassified with upland. The water class is confused with woody wetland vegetation, but most of the water sites are correctly recognized (producer's accuracy = 85%). The upland category shows the best results, and when all wetland categories are combined the overall accuracy of the classification rises to 83.5%.

Table 4.5. Accuracy results for CART® obtained using ten nodes in the tree.

Reference Category	Map Category				Row Total	Producer's Accuracy	User's Accuracy
	Emergent	Woody	Water	Upland			
Emergent	16	3	5	4	28	57.1	51.6
Woody	13	60	8	33	114	52.6	69.7
Water	1	5	34	0	40	85.0	72.3
Upland	1	18	0	139	158	88.0	79.0
Column Total	31	86	47	176	340		
Overall Accuracy	73.3						
$\hat{K}$	0.59						

The tree selected for producing a map had a relative cost of 0.465 and ten nodes. Figure 4.2 shows the CART® tree that we used to produce a map through the Knowledge Engineer Classifier in ERDAS Imagine® 9.0 (Leica Geosystems LLC, Norcross, GA, USA). The total probability of each terminal node is cumulative; i.e., it is equal to the sum of probability of each single category. Thus, it may be that a low class probability is still high relative to the other classes. Examining the legend of figure 4.3, the concept is clearer. The light blue area is most probably an emergent wetland, even though P = 0.63. This is because the probability of being woody is much lower (P = 0.26), and the probability of being either water or upland is null. Considering the yellow areas in figure 4.3 there is more doubt. It may be either upland (P = 0.40) or woody (P = 0.35), or emergent (P = 0.25).

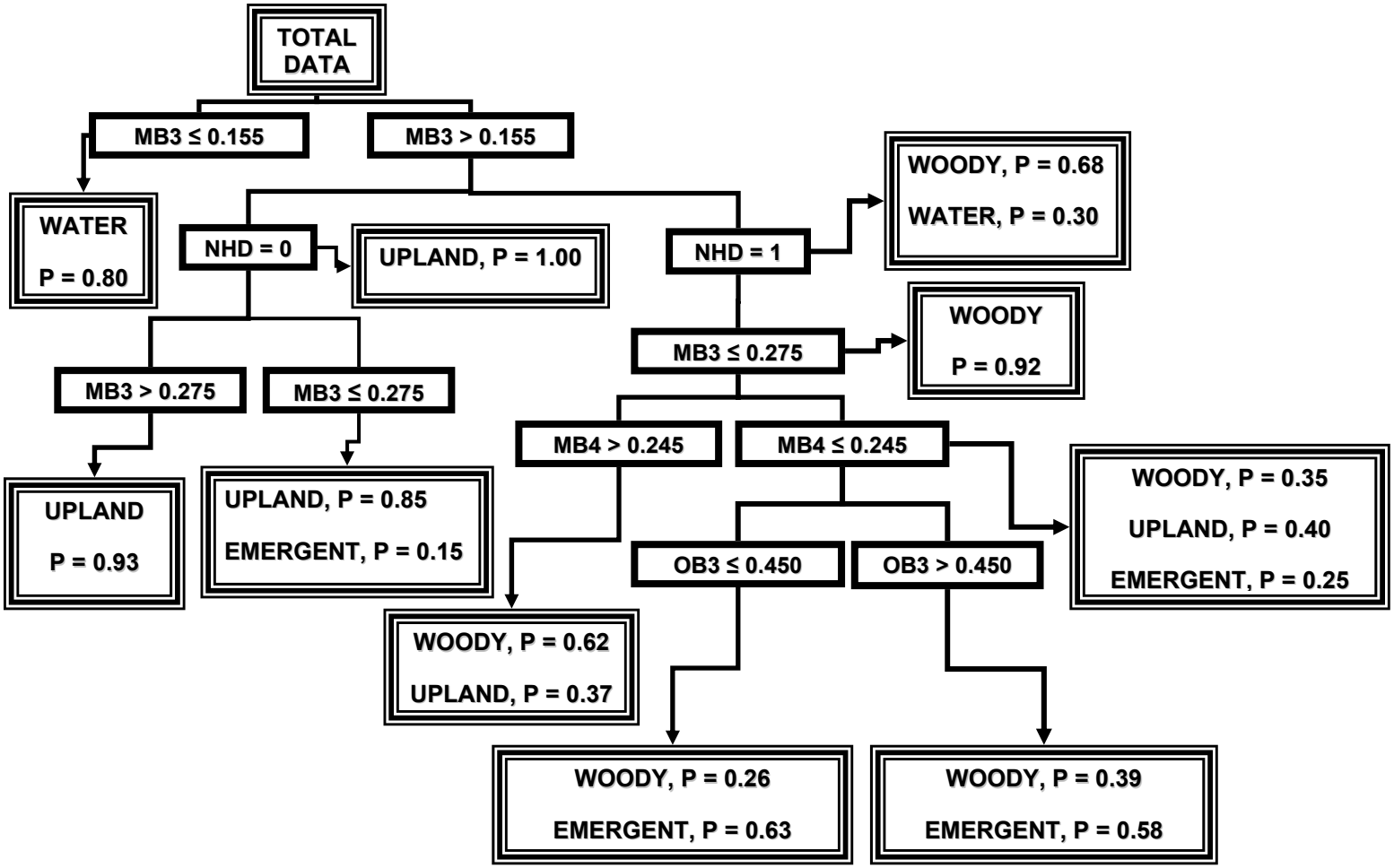

Figure 4.2. CART® tree with ten nodes. MB3 = March Band 3, MB4 = March Band4, October Band 3, NHD = National Hydrography Data. This tree was used for the classification.

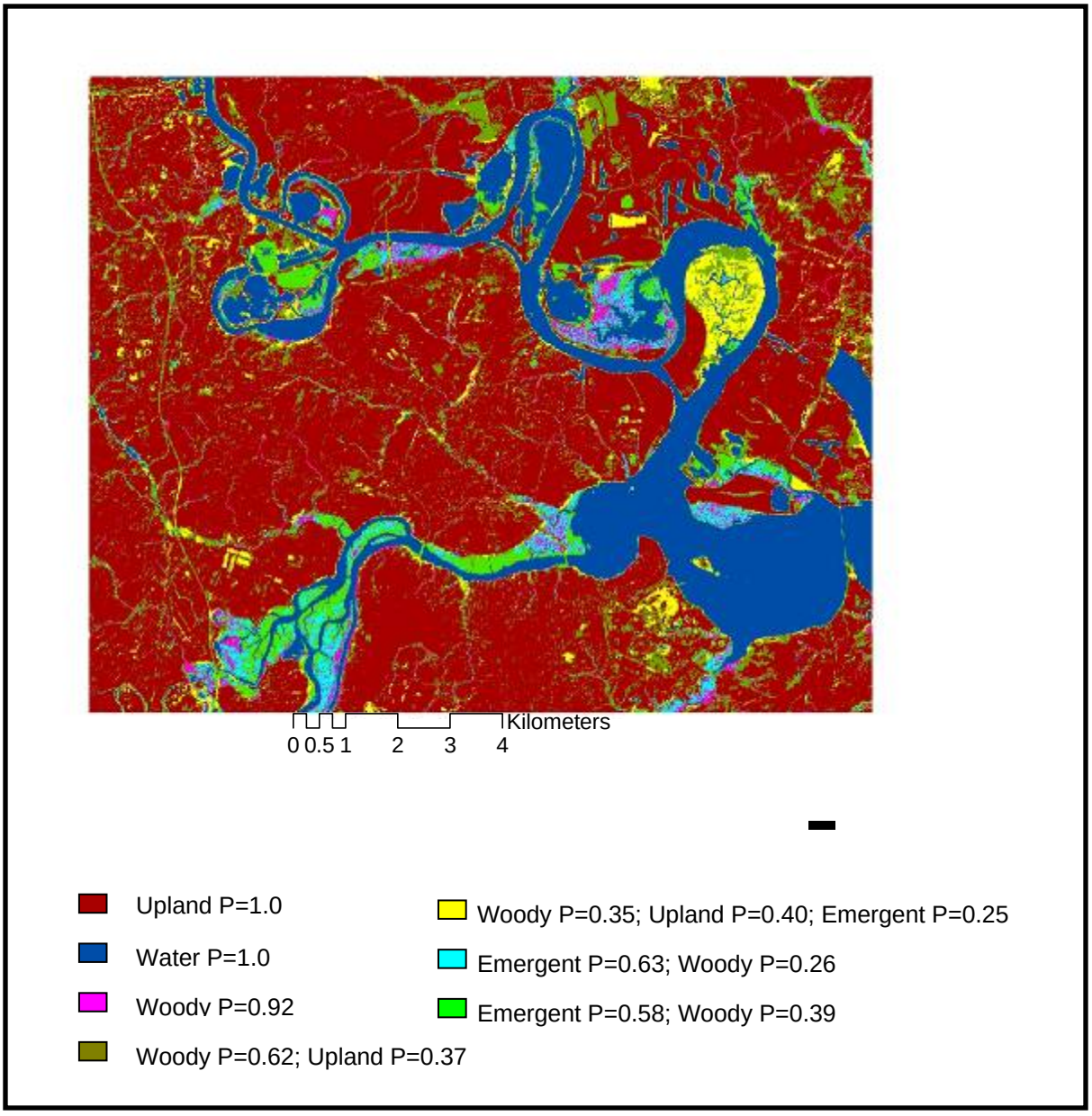

Figure 4.3. Map of the study area centered on the James River obtained by applying the CART® tree with ten nodes.

4.4.2 MULTINOMIAL LOGISTIC REGRESSION

We used SAS 9.1.3 ® (Statistical Analysis System Institute, Inc., Cary, NC, USA) to generate the multinomial logistic regression model. We used the SAS code in Appendix C. Through a stepwise regression, we identified the set of variables that contributed most to the logistic model. The stepwise regression started with fifteen variables: the first five

bands from the ASTER March scene, the first five bands of the ASTER October scene, SSURGO data, NHD data, and elevation data from the DEM, slope data, and data from the wetness index. Among the fifteen variables, the stepwise regression selected only nine (table 4.4). Most of the March image bands were utilized, but only Band 2 from October was selected. Among the GIS data layers, SSURGO soil and NHD water had the highest χ-square statistic, while the lowest χ-square belonged to the Slope variable. Three parameter estimates were assigned to each of these variables. Each estimate corresponded to one category. No parameter estimates were assigned for Woody (Menard, 2001) because it was the reference category. Appendix D shows the parameter estimates for the water, emergent and upland category. Each point within the out of sample dataset had one of four probabilities: one for being upland, one for being emergent, one for being water, and one of being woody wetland. The point was classified according to the highest of the four probabilities. We used the Model Maker tool in ERDAS Imagine® 9.0 (Leica Geosystems LLC, Norcross, GA, USA) to produce the map from the logit model. We defined a class as belonging to a specific category when its probability was 60%, i.e. higher than the sum of the probability of the other three classes when these last ones have each P < 15% (figure 4.4). Only in one case did a class not reach the 60% probability threshold, with 50% probability of being emergent and 50% probability of being upland.

To determine the accuracy of the classification, we compiled a second error matrix (Congalton and Green, 1999). Overall accuracy, user's and producer's accuracy, and $\hat{K}$ are shown in table 4.6. The overall accuracy is 76.7%, with a $\hat{K}$ of 0.64, indicating moderate agreement between the reference data and the classification. The emergent wetland producer's accuracy is very low (40.7%) indicating that most of the emergent wetlands were not identified. On the other hand, the producer's accuracy of the woody wetland is 68.7% and the user's accuracy is 70.5%. Most of the woody wetlands that were wrongly classified were assigned to the upland class. The same is observable in the upland category, in which most of the misclassified sites were assigned to the woody wetland category.

We tested for differences in significance of the two models using McNemar's test (McNemar, 1947). The McNemar χ^2 was 0.89 (p-value = 0.34), indicating that the accuracy of maps produced using the two models are not statistically different.

Table 4.6. Error matrix from the multinomial logit.

Reference Category	Map Category: Emergent	Woody	Water	Upland	Row Total	Producer's Accuracy	User's Accuracy
Emergent	11	9	3	4	27	40.7	57.9
Woody	6	79	5	25	115	68.7	70.5
Water	2	4	33	1	40	82.5	80.5
Upland	0	20	0	138	158	87.3	82.1
Column Total	19	112	41	168	340		
Overall Accuracy	76.7						
$\hat{K}$	0.64						

4.4.3 VISUAL COMPARISON OF MAPS

Figure 4.5 shows two subset locations within the study area. The first location (figure 4.5a, c, and e) was centered on Turkey Island, an area characterized by palustrine wetlands formed within the bends of the James River. The second location was centered on Charles City (figure 4.5b, d, and f). Turkey Island was positively recognized as woody wetland by the logit model. In contrast, CART® did not provide a definitive result. The area might be either upland, or woody or emergent wetland. The map of Charles City shows a large misclassification error in the logit model. Most of the area was classified as emergent wetland, when it was clearly an urban area. Here, the CART® model is more accurate. It classifies most of the area as upland, and only the core of Charles City has an uncertain outcome, with some probability of being either upland, or woody or emergent wetland.

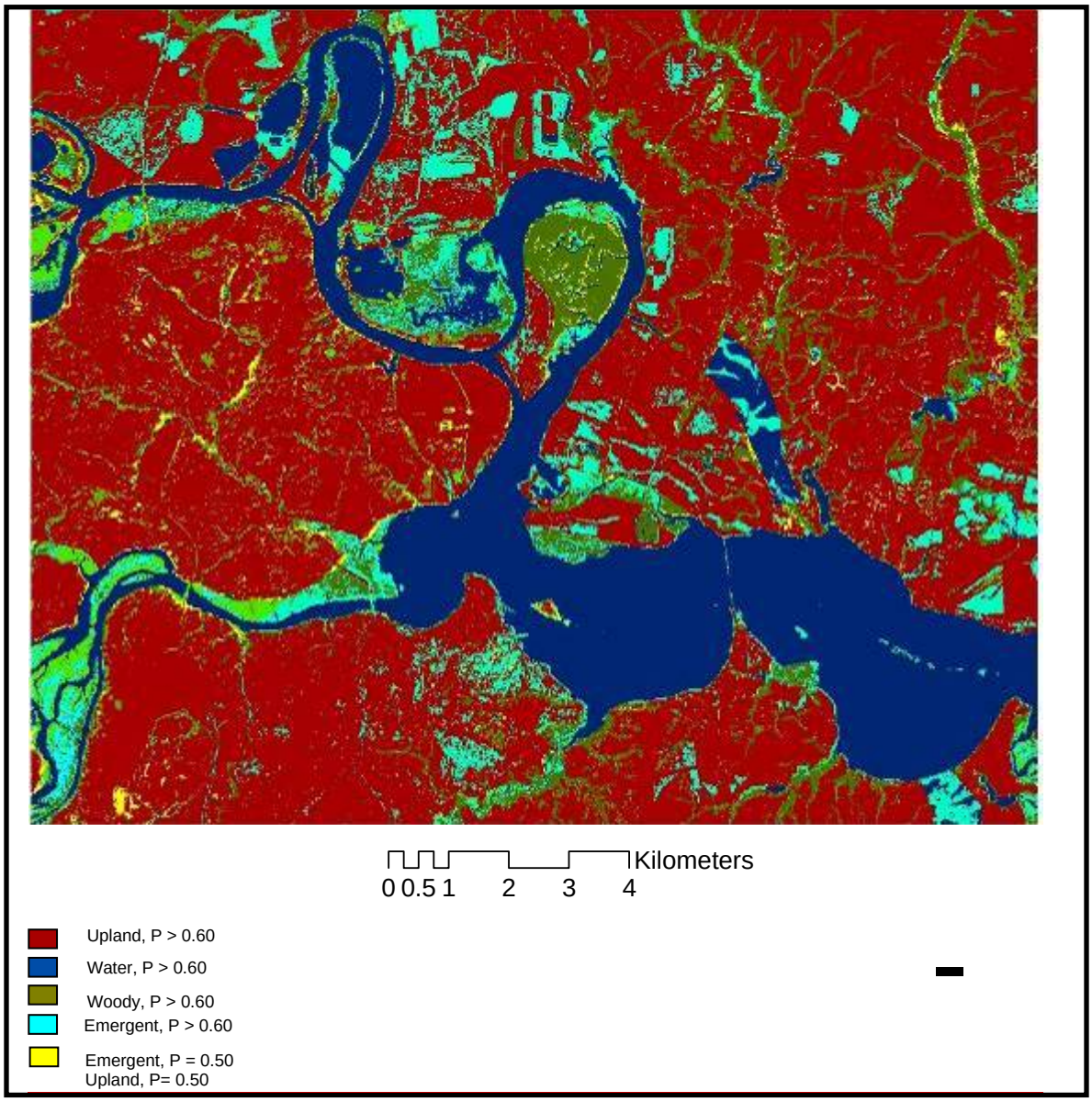

Figure 4.4. Map of the study area centered on the James River obtained by applying the multinomial logistic model.

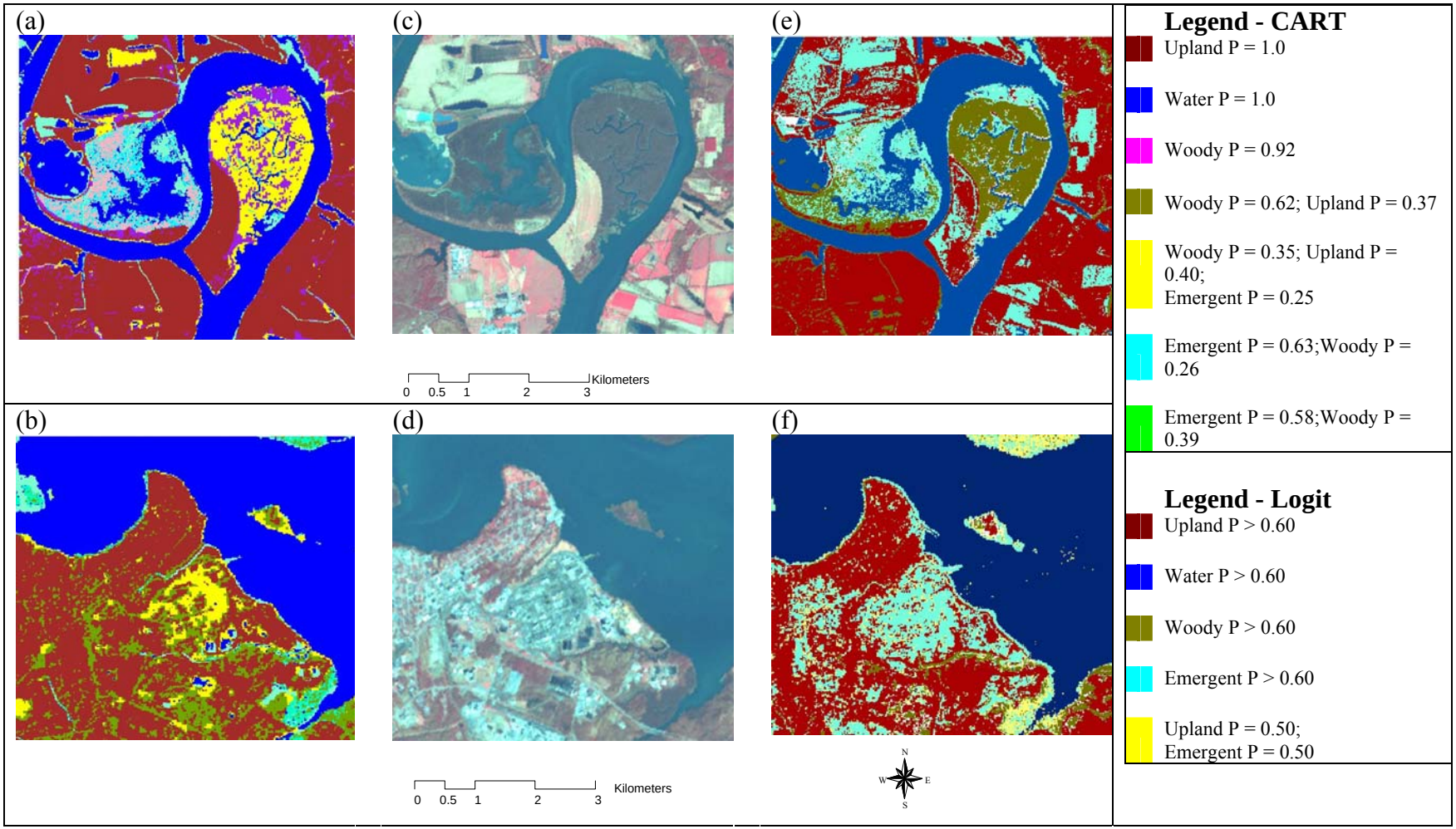

Figure 4.5. Turkey Island classified by CART® (a) and logit (e); Hopewell City classified by CART® (b) and logit(f). ASTER view of Turkey Island and Hopewell City (Bands 3, 2, 1 in R, G, B) (c and d).

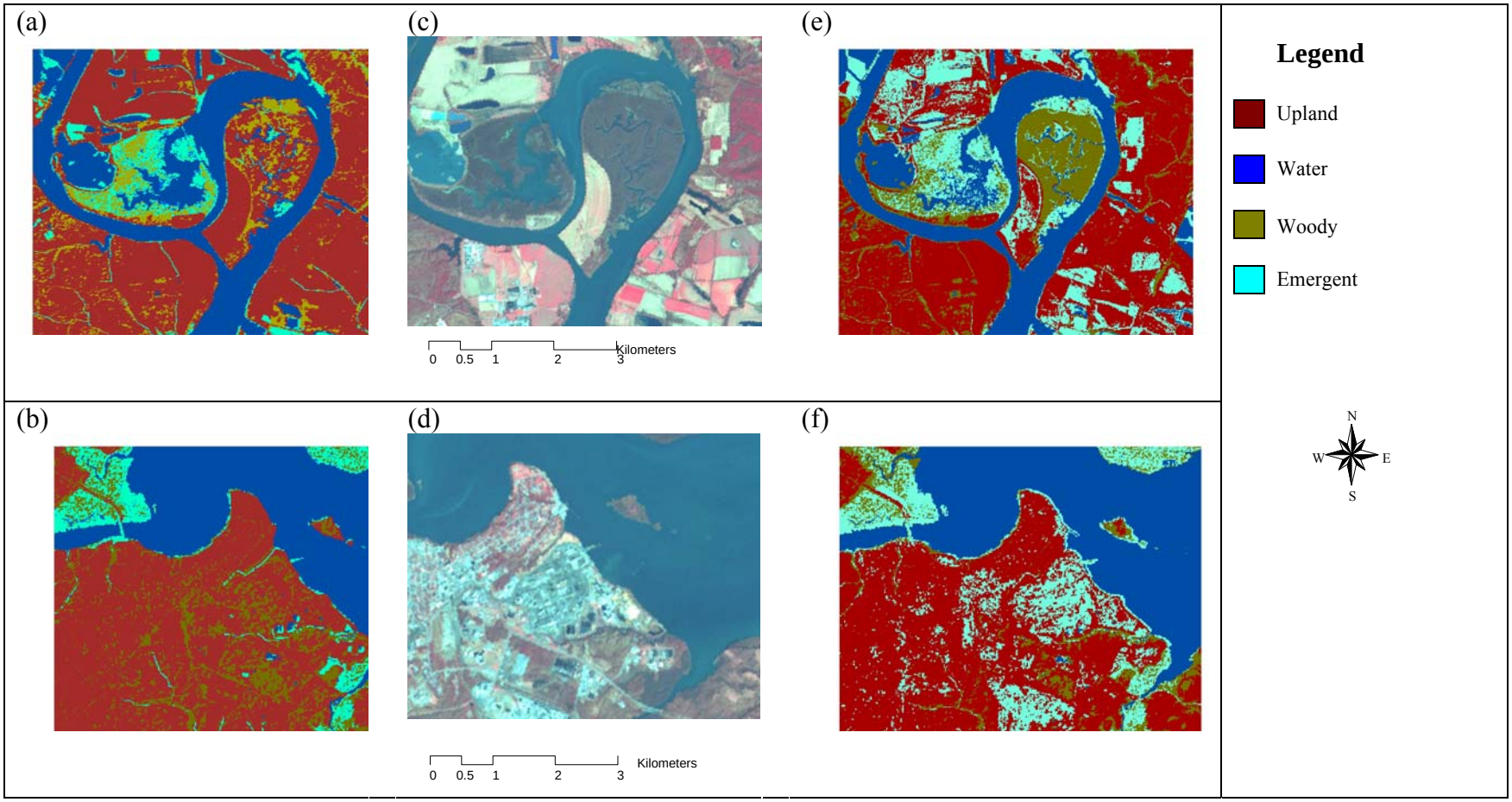

Figure 4.6. Turkey Island classified by CART® (a) and logit (e); Hopewell City classified by CART® (b) and logit(f). ASTER view of Turkey Island and Hopewell City (Bands 3, 2, 1 in R, G, B)(c and d). The maps are based on hard classes whose accuracy was assessed.

4.4.4 NWI

We also used our validation data to assess the accuracy of wetland maps produced by NWI. Table 4.7 shows the resulting error matrix. The overall accuracy is 80.5%, with a moderate agreement between observed and actual data ($\hat{K}$ = 0.69). The producer's accuracy for emergent wetland is low (51.8%), and so is the user's accuracy (63.6%). The woody wetland category is better mapped than the emergent wetland, even if it still suffers from a high omission error (more than 30%). Water and upland are very well recognized by NWI, with producer's accuracies higher than 90%.

We performed a McNemar test between the NWI results and the logistic regression results, as well as between NWI and the CART® results. Table 4.8 shows that the models and the NWI maps are not statistically different. Specifically, NWI and CART® have a χ^2 = 2.03 (p-value = 0.15) that makes them slightly more similar than NWI with the logistic regression (χ^2 = 2.70, p-value = 0.12).

Table 4.7. Error matrix obtained with NWI data.

	Map Category						
Reference Category	Emergent	Woody	Water	Upland	Row Total	Producer's Accuracy	User's Accuracy
Emergent	14	10	1	2	27	51.8	63.6
Woody	4	78	6	27	115	67.8	78.8
Water	0	2	38	0	40	95.0	82.6
Upland	4	9	1	144	158	91.1	83.2
Column Total	22	99	46	173	340		
Overall Accuracy	80.5						
$\hat{K}$	0.69						

Table 4.8. McNemar test resulted between NWI and the two model's accuracy.

McNemar's Test	
NWI–Logistic Regression	
χ^2	2.70
p-value	0.12
Kappa	0.50
NWI-CART	
χ^2	2.03
p-value	0.15
Kappa	0.54

4.5 DISCUSSION AND CONCLUSIONS

As shown by McNemar's test, the two models lead to maps that are not significantly different. Considering emergent wetlands, CART® did a better job than the logit model (17% higher). However, in CART® the emergent class suffered the largest commission error. The logit model identified the woody wetland category over 16% better than CART®. The user's accuracy is very close for both models. The logit model tended to overestimate the amount of emergent wetlands, and CART® underestimated the amount of woody wetlands. CART® did surprisingly well in classifying emergent wetlands compared to NWI, even though NWI had a higher user's accuracy. The regression model obtained the same producer's accuracy for the woody category as NWI, but a lower user's accuracy.

There were several factors affecting the classifications, including the topography of the area. For the logit model, the most pronounced misclassifications were between agricultural fields, parking lots and emergent wetlands. The topography of these sites is extremely similar in the Coastal Plain. They are located on extremely flat areas, where water accumulates easily. It is difficult to discriminate between a crop that has been recently watered, has accumulated water from a recent precipitation, and an emergent wetland where water is present because of the characteristics of a wetland. Some of the agricultural fields in the Coastal Plain of Virginia were originally wetlands converted to agricultural fields. When

soil is plowed when it is easily compacted, develops low infiltration, and becomes susceptible to surface saturation after rainstorms.

The flat topography impedes the 10-m DEM, the slope of the terrain and the wetness index from providing a significant contribution to both statistical models. The wetness index combines local upslope contributing area and slope. When the relief is low, the flow direction cannot be properly determined, thus, the catchment area is imprecise or undefined. The level topography not only negatively affects the logit model for the classification of emergent wetlands, but it also contributes to confusion between upland and wetland forests in the CART® model. In fact, there is little to no difference between the spectral signature of canopy cover in a forested wetland and the one in an upland forest. Help in making this distinction should have come from the information provided by slope, elevation, and wetness index, which provided a minimal contribution in the flat terrain of our study area. A finer digital elevation model may improve the discrimination between upland and wetland forests; however, Zhang and Montgomery (1994) demonstrated that a wetness index generated from a finest grid size (2 m and 4 m grid cell) is not very different from one generated from a 10 m DEM.

Further issues can be reduced by the use of inter-annual images. Already the strong contribution of the two ASTER images demonstrates the importance of a multi-temporal analysis, in which differences over seasons can favor the recognition of types of wetlands due to changes in vegetation and soil moisture content reflectance. In an inter-annual analysis, emergent wetlands show the same vegetation and same reflectance (if not disturbed) when the image is taken over the same month. Agricultural fields, in contrast, will have more phenological differences. The constant inter-annual value of emergent wetlands could then be identified.

Regarding the choice of one statistical model over the other, this would depend on the type of wetlands that the user is primary interested in correctly identifying. If emergent wetlands are more important, CART® performed better. If woody wetlands are more important, the logit model was the better choice. These methods provide promising results when the overall accuracy of the map was considered, because there is sufficient indication of where different types of wetland are located. In addition, they achieved very close results to NWI maps, making them a promising tool for mapping wetland vegetation types over large areas.

5 SUB-PIXEL ANALYSIS OF TREE COVER USING CONTINUOUS FIELD APPROACH AND ASTER DATA

5.1 ABSTRACT

This study presents a model for estimating the density of canopy cover in forested wetlands using data from the Advanced Spaceborne Thermal Emission and Reflection Radiometer (ASTER). Two coincident ASTER scenes were used, acquired in the spring (6 March) and fall (16 October) of 2005 over the Coastal Plain of Virginia, USA. The analysis used the visible and near infrared bands, as well as tasseled cap brightness, greenness, and wetness for each date. In addition, the change in NDVI (ΔNDVI) between the spring and fall scenes was included as an independent variable. Canopy cover was assessed via head-up digitizing on 1:4,000 scale (or better) digital orthophotographs for each of 300 ASTER pixels randomly selected within the bounds of the ASTER scenes. The canopy cover varied as a continuous field between 0% and 100%. All variables, with the exception of band 1 (0.52-0.60 μm) from the March scene, the tasseled cap wetness from both scenes, and ΔNDVI, were inversely related to canopy cover. The final model had an adjusted-R^2 of 0.69 and an RMSE of 2.7% when the canopy cover was less than or equal to 15%, and an adjusted-R^2 of 0.03 and an RMSE of 19.8% when the canopy cover was greater than 15%. While this is a promising result, further research on the impact of water at or above the soil surface and the observed saturation effect is particularly warranted.

5.2 INTRODUCTION

Wetlands are important and complex ecosystems that provide a wide range of services vital to the environment. Wetlands control water storage and indirectly runoff (EPA, 2006), slowing the velocity of water flow and trapping sediments and nutrients, preserving the quality of the water (Mitsch and Gosselink, 1993). Cooper et al. (1987) demonstrated that 85% to 90% of the sediment transported by runoff events is trapped in wooded areas and never reaches major streams. Even though there is still a debate concerning relative effectiveness of grass and forested wetlands, it is evident that forested

wetlands do provide resistance to sediment transport (U.S. E.P.A., 1993). Consequently, it is important to determine the density of trees within forested wetlands.

Most land use and vegetation cover maps are generated using satellite sensors having a coarse resolution that makes it difficult to observe local details (Papadakis et al., 1993; Goodrich et al., 1994; Foody et al., 1996). In addition, some studies indicate a general tendency to underestimate forest cover (Skole and Tucker, 1993), but the contrary has been shown by others (Foody and Cox, 1994).

One method to assess forest density is to look inside each pixel, and determine how much of its reflectance is a consequence of canopy cover and how much is a consequence of other materials. Several techniques have been developed for unmixing a pixel: Foody and Cox (1994) used fuzzy sets to estimate forest cover; Zhu et al. (2001) used isolines in scatter plots of red/infrared space to map vegetation density; Settle and Drake (1993) used linear mixing to determine ground cover proportions; Carpenter et al. (1999) employed neural networks to estimate the mixture of vegetation types within forest stands.

DeFries et al. (2000) generated the first global continuous field product for tree cover, fitting a linear mixture model to a classification output. A continuous field represents the proportion of vegetation cover per pixel, and it is an improvement over discrete land-cover classifications for some applications (Hansen and DeFries, 2004). DeFries et al. (1995, 1997, and 2000) and Hansen et al. (2000, 2002) developed the continuous field approach using coarse resolution data such as the Advanced Very High Resolution Radiometer (AVHRR) and the Moderate-resolution Imaging Spectroradiometer (MODIS). These data are extremely useful for global analysis and regional studies (Boyd et al., 1996; Franklin et al. 2000, 2002), they lose power at scale at which most land management occurs.

We added a double challenge in this study. First, we used the Advanced Spaceborne Thermal Emission and Reflection Radiometer (ASTER) sensor that has much finer resolution than AVHRR and MODIS instruments (10 m pixels versus 1 km and 250 m pixels respectively). Data from ASTER were used for determining the correlation between pixel values and the proportion of tree cover in wetlands, keeping in mind that the finer resolution helps in identifying land characteristics, but it also adds noise due to

the greater spectral variability among pixels. ASTER has been widely utilized for geological studies, but little research has been done over wetlands (Kato et al, 2001; Stefanov et al. 2001; Ford et al., 2003).

The second challenge was determining canopy cover over extremely small plots located in the Coastal Plain of Virginia. The size of the plot allows detecting areas within the forest where there are no trees. Coarser resolution satellites would seldom recognize these areas, because the total reflectance of a pixel results from a combination of the reflectance of each element within the pixel itself (Adams et al., 1986), and the reflectance of small patches of open areas would be overridden by the reflectance of surrounding vegetation. Treeless areas are equally important to recognize as areas where forest is present. As vegetation patches serve as surface obstruction during rainstorm events and sediment transportation, open areas among the patches have just the opposite effect (Ludwig et al., 2004).

5.3 DATA AND METHODS

5.3.1 STUDY AREA

The study area granules cover a portion of the Coastal Plain of Virginia (figure 5.1). The Coastal Plain has a topography that consists of predominantly flat areas with deeply incised estuaries and streams, characterized by the presence of numerous forested wetlands. Forested wetlands are characterized by woody vegetation that is 1.8 m tall or taller (Cowardin et al., 1979). Representative species are Bald Cypress (*Taxodium distichum*), Swamp Tupelo (*Nyssa sylvatica var. biflora*), Yellow Poplar (*Liriodendrom tupilifera*), Water Oak (*Quercus nigra*), and Sweet Gum (*Liquidamber styraciflua*) (Ware, 1970; Russ and Frederick, 1990). Scrub-shrub wetlands are characterized by woody vegetation that is less than 1.8 m tall, including saplings and trees that are small or stunted because of environmental conditions (Cowardin et al., 1979). In this study, we combined both categories when we selected the canopy cover within each plot.

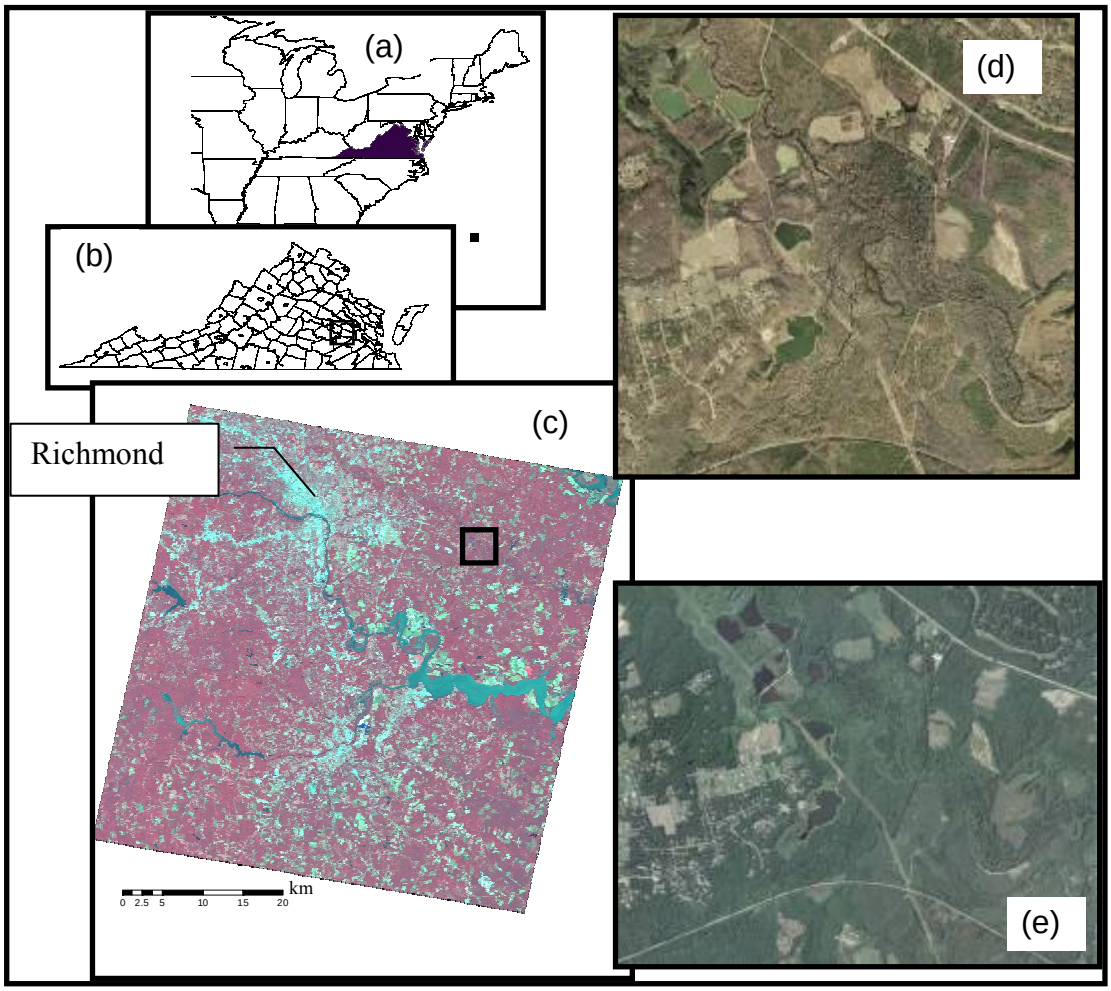

Figure 5.1. A comparison of maps of the study area: (a) map of the east coast of the U.S.A. with Virginia highlighted in bold; (b) county map of the state of Virginia with boundaries of ASTER scene; (c) ASTER granule covering a 60 x 60-km area; (d) example of digital orthophotos from VBMP; (e) example of aerial photos from National Agriculture Imagery Program.

5.3.2 ASTER DATA AND REMOTE SENSING INDICES

The Advanced Spaceborne Thermal Emission and Reflection Radiometer (ASTER) is a cooperative effort between NASA, Japan's Ministry of Economy, Trade and Industry and Japan's Earth Remote Sensing Data Analysis Center. ASTER consists of three separate instrument subsystems (table 5.1): the visible and near infrared (VNIR), the shortwave infrared (SWIR), and the thermal infrared (TIR). The VNIR subsystem operates in three

spectral bands at visible and near-IR wavelengths, with a resolution of 15 m. It consists of two telescopes: one nadir-looking with a three-spectral-band detector, and the other backward-looking that provides a second view of the target area for stereo observations. The SWIR subsystem operates in six spectral bands in the near-IR region through a single, nadir-pointing telescope that provides 30m resolution. The TIR subsystem operates in five bands in the thermal infrared region using a single, fixed-position, nadir-looking telescope with a resolution of 90 m.

The ASTER instrument is still being corrected and improved. For this study, it was suggested that we use images collected after 2003 (K.Thome, personal communication, June 2005). In addition, Iwasaki and Tonooka (2005) found that the ASTER SWIR bands are affected by crosstalk phenomena. Thus, we limited our analysis to the first three ASTER bands (range: 0.52-0.86 μm), and we used two scenes collected in 2005. However, we resampled all the ASTER bands to 15 m, to coincide with the bands that have the smallest resolution. Resampling was necessary for NDVI and tasseled cap calculations.

The first scene from 6 March 2005 (AST_L1B.3:2028411439) was radiometrically- and geometrically-corrected, and projected in UTM zone 18 with the North American 1983 Datum using a first order polynomial transformation. The second scene from 16 October 2005 (AST_L1B.3:2028019676) was registered to the March scene. We selected twenty ground control points (RMSE = 0.80 m) and twenty check points (RMSE = 0.85 m). To reduce the error generated by image registration, registration of multiple data sources should be conducted to achieve sub-pixel accuracy (Dai and Khorram, 1998; Pohl and Van Genderen, 1998). In this study, image registration was particularly important because of the sub-pixel analysis performed. Even though our RMSE error was far from the suggested value of 0.2 (Dai and Khorram, 1998), we did not achieve a finer registration, and a negative impact on the analysis was assumed. We converted the ASTER bands to top of atmosphere reflectance using the solar irradiance values shown in table 5.1.

Table 5.1. Characteristics of the ASTER instrument and solar irradiance values.

	VNIR[1] (μm)	Solar irradiance (W/m^2-μm)	SWIR[2] (μm)	Solar irradiance (W/m^2-μm)	TIR[3] (μm)
Spectral Range	Band 1 0.52 - 0.60	1846.9	Band 4 1.60 - 1.70	232.5	Band 10 8.12 - 8.47
	Band 2 0.63 - 0.69	1546.0	Band 5 2.14 - 2.18	80.32	Band 11 8.47 - 8.82
	Band 3 0.76 - 0.86	1117.6	Band 6 2.18 - 2.22	74.92	Band 12 8.92 - 9.27
			Band 7 2.23 - 2.28	69.20	Band 13 10.25 - 10.95
			Band 8 2.29 - 2.36	59.82	Band 14 10.95 - 11.65
			Band 9 2.36 - 2.43	57.32	
Ground Resolution	15 m		30 m		90 m

[1] Visible and near infrared
[2] Visible and near infrared
[3] Thermal infrared

In addition to the first three bands of the two ASTER images, we computed the delta normalized difference vegetation index (ΔNDVI) by subtracting the NDVI of the March scene from the NDVI of the October scene. ΔNDVI is commonly used for studying vegetation changes over time (Volcani et al., 2005), the effect of flooding over forests and agricultural lands (Michener and Houhoulis, 1997; Pantaleoni et al. 2007), and monitoring regeneration of vegetation (Svoray et al., 2003). We generated a tasseled cap transformation using coefficients developed by Yarbrough et al. (2005). Table 5.2 shows the list of the independent variables.

Table 5.2. List of independent variables used as input in the ordinary least square regression model and their description.

Abbreviation	Description
March scene	
MB1	March band 1
MB2	March band 2
MB3	March band 3
October scene	
OB1	October band 1
OB2	October band 2
OB3	October band 3
ΔNDVI	(October NDVI)-(March NDVI)
Tasseled cap transformation	
MBRIGHT	March brightness
MGREEN	March greenness
MWET	March wetness
OBRIGHT	October brightness
OGREEN	October greenness
OWET	October wetness

5.3.3 EXPERIMENTAL DESIGN

We randomly selected 300 plots over the study area. The coordinates of the plots are provided in Appendix E. Each plot had the area equal to one ASTER pixel in the visible and near infrared range of the spectrum ($225m^2$). We used a forested wetland mask to separate forested wetlands from the rest of the landscape. We obtained the mask from National Wetland Inventory (NWI) digital maps (U.S. Fish and Wildlife Service, 2007). We determined the continuous canopy cover field by manually digitizing the contour of forested wetland canopy cover on digital orthophotographs obtained from the Virginia Base Mapping program (VBMP), as shown in figure 5.3. These orthophotos were developed using true color, leaf-off, vertical photography acquired in 2002. The digital orthophotos have a scale varying from 1:4,800 to 1:1,200 depending on the location (VBMP, 2003). However, only orthophotos at scale 1:4,800 and 1:2,400 were available for our study area. Figure 5.2 shows the index grid for the digital orthophotos used for identifying the points. The largest tiles correspond to orthophotographs at a 1:4,800 scale;

the smallest tiles correspond to orthophotographs at a 1:2,400 scale. We used aerial photographs from the National Agriculture Imagery Program (NAIP) as additional reference. NAIP acquires imagery during the agricultural growing seasons. We used NAIP imagery from 2005 that have a 1-m ground sample distance with a horizontal accuracy that matches to a reference orthoimage within 5 m (U.S.D.A., 2007).

We calculated the canopy cover area using ArcMap 9.1® (Environmental Systems Research Institute, Inc., Redlands, CA, USA). In order to ensure that a pixel interpreted as part of the sample was representative of the surrounding area, we visually verified the position of each sampled pixel on each ASTER scene with respect to the digital orthophotographs. We then generated a point feature for each pixel and assigned the canopy cover value to it.

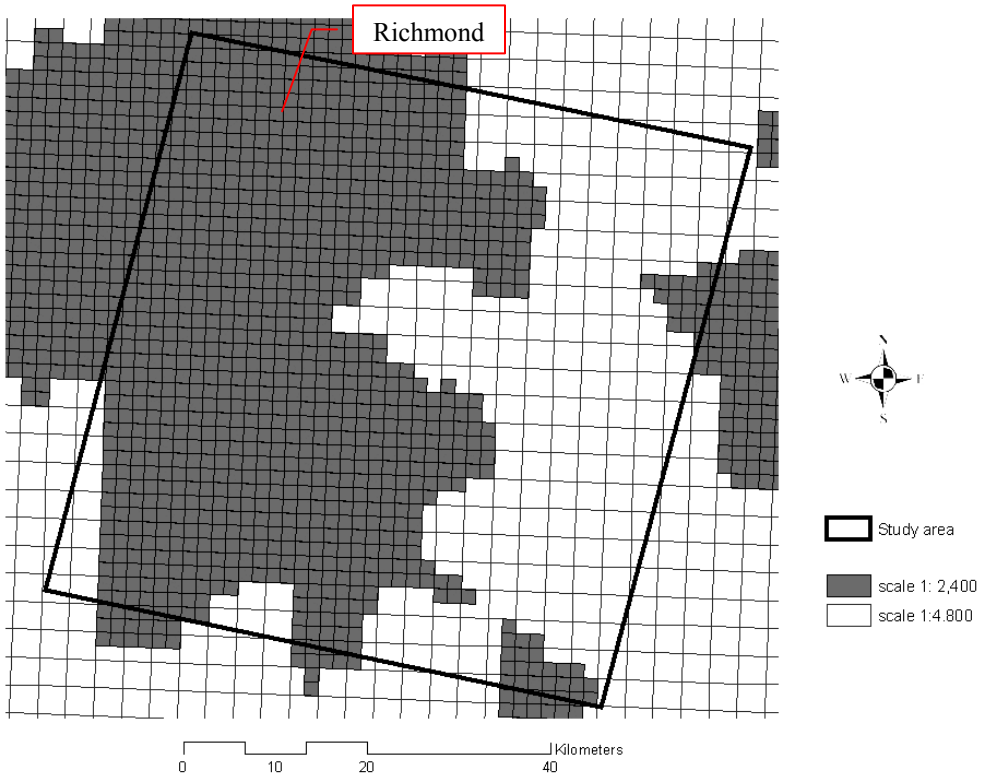

Figure 5.2. 2002 Virginia Base Mapping Program orthotile grid. The dark gray tiles have a 1:2,400 scale, the light gray tiles a 1:4,800 scale. The black frame is the study area.

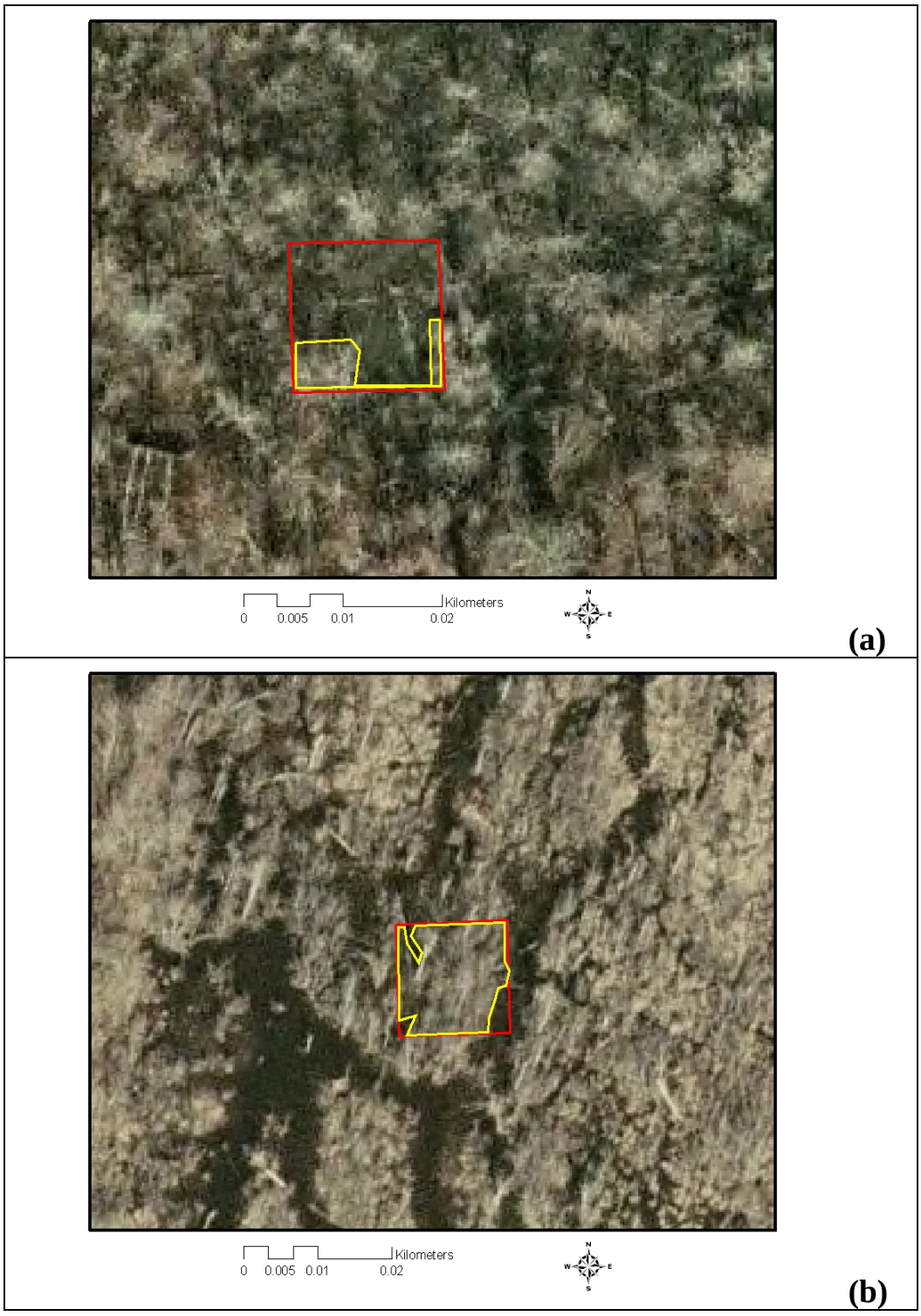

Figure 5.3. Example of digitization of two plots. The red line delineates the boundaries of the plot, and the yellow line the boundaries of the canopy cover. In (a) the canopy cover is 14.8%, and in (b) the canopy cover is 85.5%.

5.3.4 MODEL DEVELOPMENT

We used the sample points to extract the values of the independent variables using Arc Toolbox® (Environmental Systems Research Institute, Inc., Redlands, CA, USA). SAS 9.1.3 ® (Statistical Analysis System Institute, Inc., Cary, NC, USA) was used for the analysis and model development. We calculated a correlation matrix to determine which variables were significantly correlated with canopy cover. Table 5.3 shows that 9 out of the 15 variables were statistically correlated with the canopy cover (p-value < 0.05). We plot the percent canopy cover and October Band 2 (figure 5.4) and the percent of canopy cover and the *ΔNDVI* (figure 5.5).

Table 5.3. Correlation matrix between the area of canopy cover and the independent variables for the entire dataset.

Dependent Variable	Independent Variables	Correlation	p-Value
AREA	OB1	-0.036	0.533
AREA	OB2	-0.360	< .0001
AREA	OB3	-0.153	0.007
AREA	MB1	0.193	< .0001
AREA	MB2	0.001	0.983
AREA	MB3	-0.109	0.052
AREA	*ΔNDVI*	0.371	< .0001
AREA	MBRIGHT	-0.211	< .0001
AREA	MGREEN	-0.235	< .0001
AREA	MWET	0.254	< .0001
AREA	OBRIGHT	-0.263	< .0001
AREA	OGREEN	-0.020	0.730
AREA	OWET	0.092	0.109

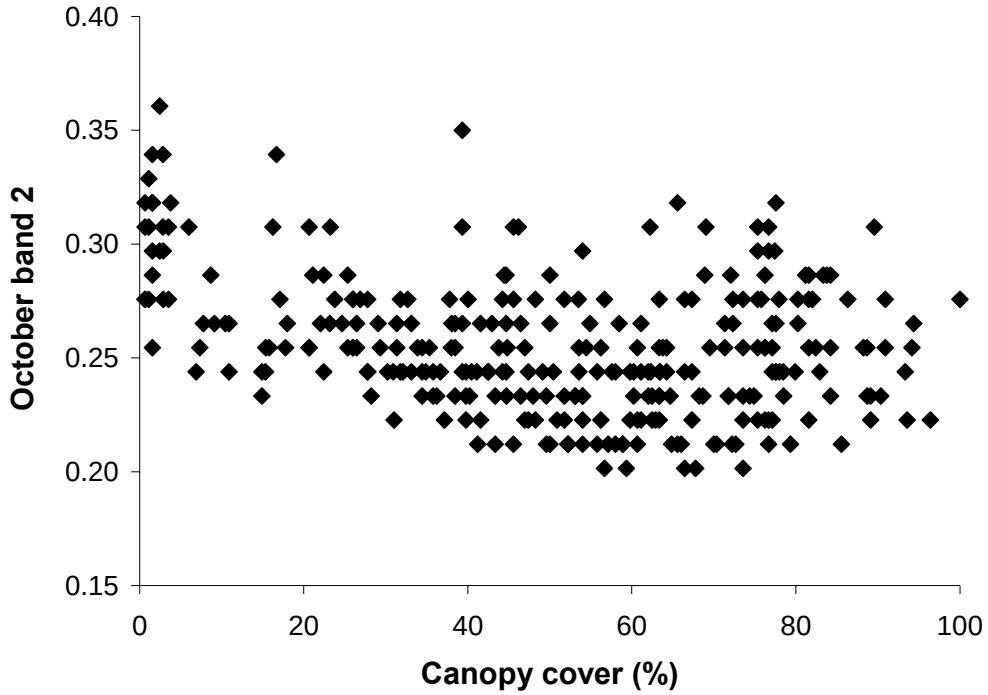

Figure 5.4. Plot of the October Band 2 values over percent of canopy cover.

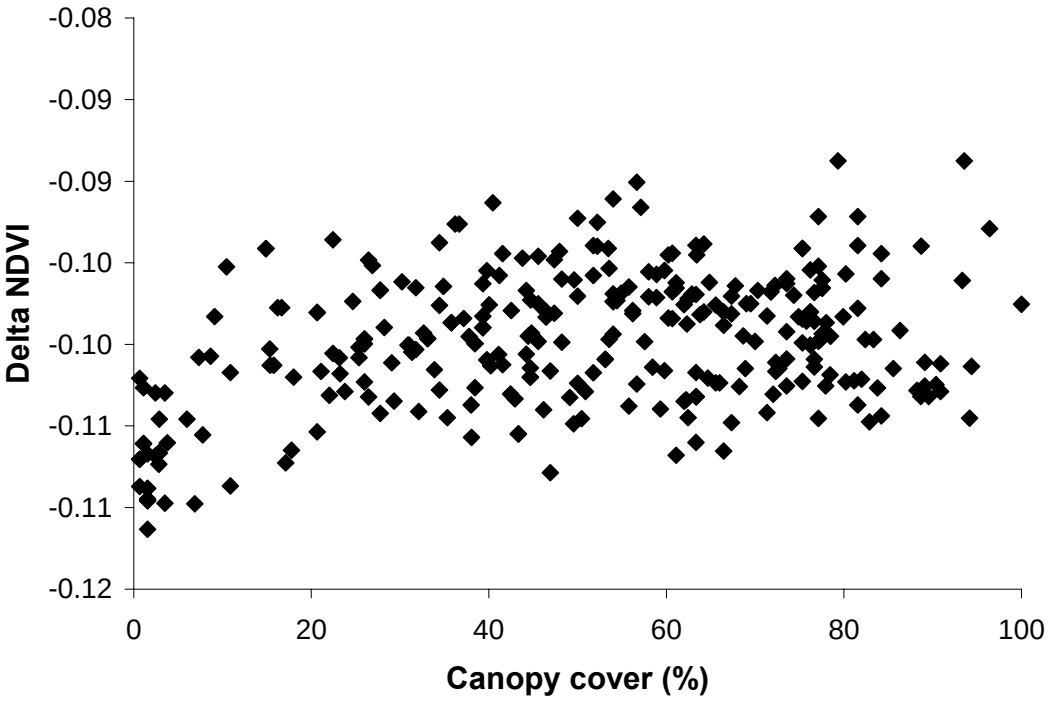

Figure 5.5. Plot of the Delta NDVI values over percent of canopy cover.

We examined the variable inflation factor (VIF) for the nine variables highly correlated with area in order to determine if the model was affected by multicollinearity. A VIF higher than 10 is considered evidence of multicollinearity (Belsley, Kuh, & Welsch, 1980). Table 5.4 shows that half of variables had a VIF much greater than 10. We removed these variables from the model, and we performed a best subset regression using exclusively October band 2, October band 3, March band 3, Delta NDVI, and October tasseled cap brightness. We used the Mallows C_p criterion (Mallows, 1966). The C_p statistic is defined as shown in equation 5.1:

$$C_p = \frac{RSS_p}{\sigma^2} + 2p - n \qquad \textbf{[Equation 5.1]}$$

where n = the number of observations, p = the number of variables in the regression, RSS_p = the residual sum of squares using p variables, and σ^2 = an independent estimate of the error. If the model is satisfactory, C_p will be approximately equal to p.

Table 5.4. Variable inflation values (VIF) and parameter estimates for the nine variables selected by the correlation matrix.

Variable	Parameter estimate	VIF
Intercept	-79.492	0
OB2	-166.404	2.794
OB3	41.699	8.540
MB1	-3654.976	137.300
MB3	-250.161	15.913
ΔNDVI	4.791	1.953
MTAS1	-49857	5322.495
MTAS2	-44373	2269.007
MTAS3	-56606	8886.998
OTAS1	-318.66	7.462

5.4 RESULTS

Our results show that our model requires only three variables: Delta NDVI, October band 2, and March band 3. The Mallows C_p value of 4.32 is close to p, and the adjusted-R^2 of 23.0% and an R^2 of 24.0% (table 5.5). The VIF is lower than 10 for all the variables, and the RMSE value is 22.3%. PExamining the predicted values of canopy cover against the observed values of canopy cover (figure 5.6) in addition to the ΔNDVI vs. canopy cover (figure 5.5), we found that the model appeared to be affected by a saturation effect. In order to address this effect, we separated the group of points into two parts, and we ran two separate models using the same variables selected by the best subset regression: October band 2, October band 3, March band 3, Delta NDVI, and October tasseled cap brightness. The first group had canopy cover between zero and 15%, and the second group had a canopy cover between 16% and 100%. Table 5.6 shows that the first group has an adjusted-R^2 of 69.0% and an R^2 of 72.0%, with RMSE = 2.7% and VIF values lower than 10. The VIF values are lower than 10 also for the second group, but the RMSE value is higher (13.7%), and the adjusted-R^2 and R^2 are extremely low (respectively 3.0% and 4.0%), with RMSE = 19.8%. Figure 5.7 shows the plot of the predicted values canopy cover and the observed values for the two groups.

Table 5.5. Results from the best subset regression analysis for model using all points. For each number of variables only the model resulting in the lowest Mallow C_p is shown.

# of variables	R^2	Adjusted-R^2	Mallows C_p	RMSE	Variables in model
1	0.13	0.13	37.89	23.60	ΔNDVI
2	0.23	0.22	6.84	22.33	ΔNDVI OTAS1
3	0.23	0.22	4.32	22.31	ΔNDVI MB3 OB2
4	0.24	0.23	4.34	22.27	ΔNDVI MB3 OB2 OTAS1
5	0.24	0.22	6.00	22.29	ΔNDVI MB3 OB2 OB3 OTAS1

Table 5.6. Results from the OLS model when only October band 2, March band 3, and Delta NDVI are used for a group of plots that have a canopy cover ≤ 15%.

Variables	Parameter estimate	VIF
Intercept	81.71	0
OB2	-91.39	1.57
MB3	51.04	1.31
ΔNDVI	2.21	1.37
R^2	0.72	
Adjusted- R^2	0.69	
RMSE	2.73	

Table 5.7. Results from the OLS model when only October band 2, March band 3, and Delta NDVI are used for a group of plots that have a canopy cover > 15%.

Variables	Parameter estimate	VIF
Intercept	151.75	0
OB2	-119.07	1.23
MB3	-141.26	1.19
ΔNDVI	1.64	1.09
R^2	0.04	
Adjusted- R^2	0.03	
RMSE	19.79	

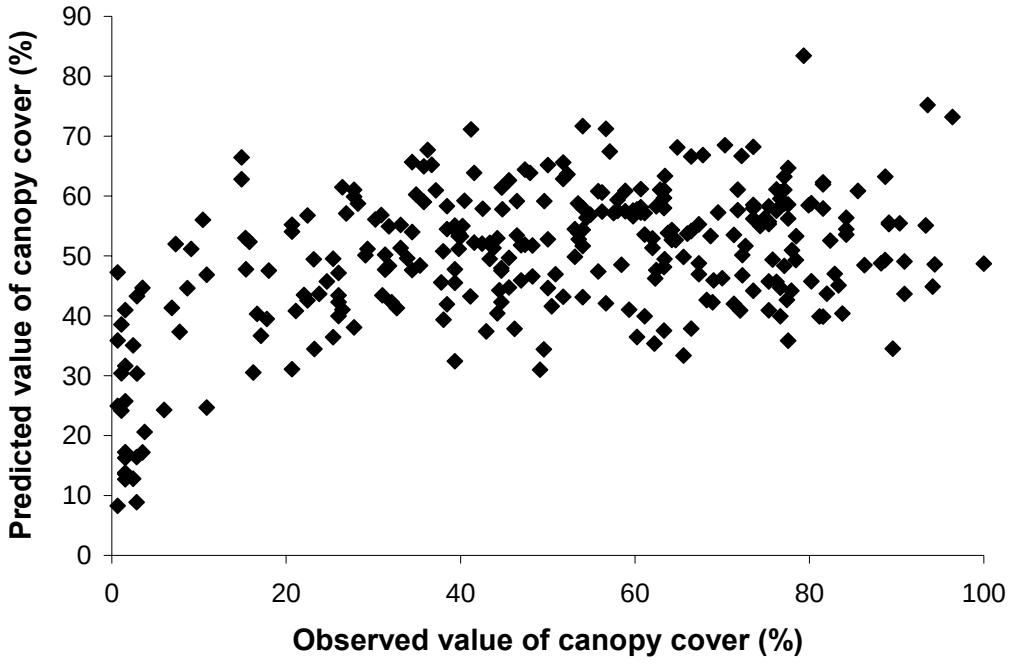

Figure 5.6. Plot of the predicted values of canopy cover versus the observed values of canopy cover.

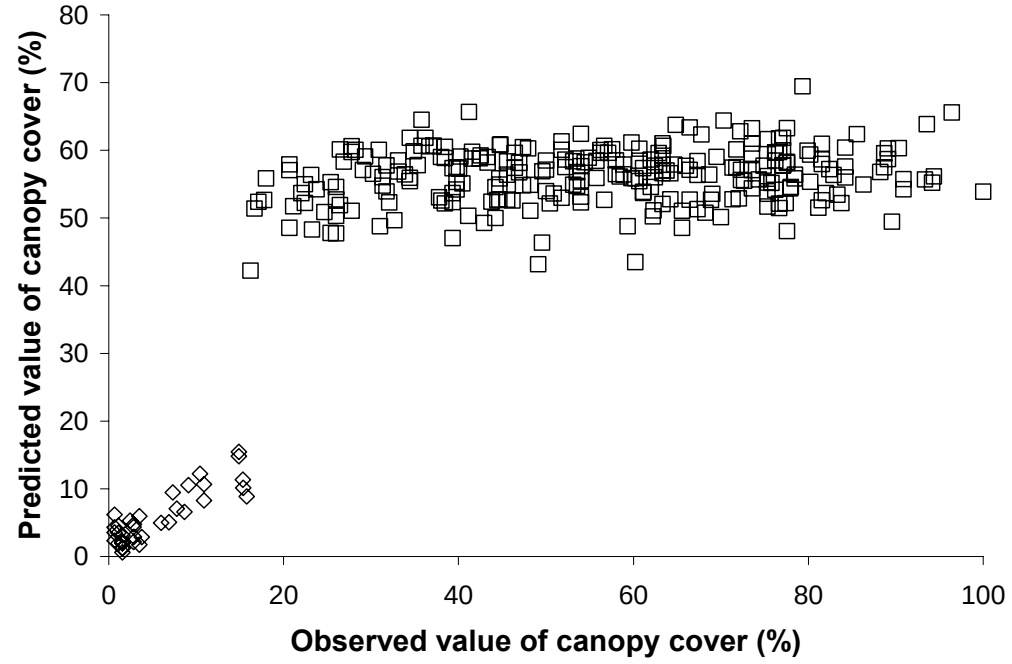

Figure 5.7. Plot of the predicted values of canopy cover versus the observed values of canopy cover for two groups of plots. The diamond symbol corresponds to plots with canopy cover area ≤ 15%, the square symbol corresponds to plots with canopy cover area > 15%.

5.5 DISCUSSION AND CONCLUSIONS

In this study, we found a relationship between canopy cover and the spectral characteristics of the VNIR ASTER bands and derived indices. The literature had already highlighted ΔNDVI as a strong indicator of vegetation characteristics. In our study, this measure was selected as one of the important variables by the model selection criteria, and it also had the highest correlation with canopy cover.

Band 2 from the October scene was negatively correlated with canopy cover. Band 2 corresponds to the red range of the spectrum. Chlorophyll increases red absorption; bare soil increases red reflectance. Thus, the greater the canopy cover, the lower the value of Band 2.

Crist and Cicone (1984) and Crist et al. (1986) reported that the wetness component of the tasseled cap transformation determines the amount of moisture held by soil and vegetation, whereas the greenness component is a measure of the presence and density of green vegetation. Hansen et al. (2000) established that the wetness component was highly correlated with stand age and structural complexity of forest stands. The tasseled cap bands had statistically significant correlations with forested wetland canopy cover; however, the sign of the correlations was not what we expected. The brightness and the greenness components from the March scene had a negative correlation with the canopy cover, whereas the wetness component had a positive correlation. Also, the brightness component from the October scene had a negative correlation.

While we are not completely certain of the causes of the reversed signs of these correlations, it is likely due to the presence of water at or above the soil surface. Water is a strong absorber even in the visible portion of the spectrum, and is almost completely unreflective at the near-IR wavelengths and beyond (Lillesand and Kiefer, 2004). According to Beget and Di Bella (2007), infrared band reflectance and vegetation indices decrease when flooding level increases. As such, the higher the moisture content of the soil, the lower the greenness and brightness components, and the higher the wetness component.

After we addressed the multicollinearity problem, and we reduced the model to its simplest form, we found that ΔNDVI, the red band from October and the NIR band from

the March scene were the most important variables. The combination of these three variables produces good results in plots that have a canopy cover lower than 16%. When canopy cover is higher than 15%, there appears to be no relationship between the ASTER-derived variables and canopy cover. This result is similar, albeit at a lower threshold, to the off-observed saturation effect between vegetation indices such as NDVI and leaf area index (Birky, 2001; Anderson et al., 2004; Wang et al., 2005).

Our conclusion is that ASTER imagery has potential for use in estimating canopy cover within forested and scrub-shrub wetlands, even though further research will be required to address the water absorption and saturation effect problems.

6 SUMMARY AND CONCLUSIONS

In the U.S., determination of wetland location and quantification of wetland gains and losses has become one of the most important goals for federal and state agencies, as well as for private citizens that look to receive permits for transforming the landscape. Most of the agencies rely on NWI maps or local surveys for determining the extent, boundary and vegetation composition of wetlands. For large areas, this process may be expensive, time consuming, and not completely accurate. Remote sensing has potential to overcome most of these issues.

The focus of this research was to investigate the value of the ASTER sensor *per se* and in combination with GIS data layers for determining wetland location and vegetation. The results indicated that ASTER data can be used to estimate boundaries between uplands and wetlands, and to determine vegetation characteristics of wetlands. Even though other satellite sensor may achieve higher accuracies, ASTER balances its mapping ability with overall coverage and costs.

The main objective of this research was to develop robust analysis techniques to facilitate the use of satellite data for predicting wetland extent and composition by focusing on the unique characteristics that frame a wetland. The availability of multi-temporal data was indispensable for determining seasonal characteristics of wetlands, including the changes in soil moisture content and differences in reflectance of vegetation.

Among the input variables, the near-infrared bands were the most useful. The near-infrared band from the spring scene was especially valuable for detecting aquatic habitats. The importance of the near-infrared bands was maintained when the goal of the project narrowed to determine wetland types, but most of the other bands from the March scene were required. The GIS data layers provided results that were somewhat expected. The NHD water and SSURGO soil data were very important for discriminating between upland and wetlands. Nevertheless, their importance was substantially lower once the target was to discriminate among types of wetlands. The DEM, slope and wetness index did not significantly contribute to any of the models generated for this study.

Estimation of canopy cover within pixels has profound implications for watershed management and runoff risk assessment, since forests have a direct effect on sediment movement and precipitation interception (Ewel and Smith, 1992; Mitsch and Gosselink, 1993). Continuous canopy cover was estimated with moderate accuracy using VNIR top-of-atmosphere reflectances and vegetation indices from ASTER as independent variables. When the canopy covered more less than 16% of the plot, the model achived good results. For larger canopy cover, water absorption and a saturation factor likely contributed to lowering the accuracy of the model.

Future investigation should consider the following points: 1) introduce inter-annual satellite data; 2) repeat the CART and logit model models using a high resolution DEM; 3) test the models on areas with topography different from the Coastal Plain.

7 LITERATURE CITED

ACKLESON, S.G., and KLEMAS, V., 1987, Remote-sensing of submerged aquatic vegetation in lower Chesapeake Bay—A comparison of Landsat MSS to TM imagery. *Remote Sensing of the Environment*, **22**, 235–248.

ADAMS, J.B., SMITH, M.O., and JOHNSON, P.E., 1986, Spectral mixture modeling: A new analysis of rock and soil types at the Viking Lander 1 site. *Journal of Geophysical Research*, **91**, 8098–8112.

ALBEROTANZA, L., BRANDO, V.E, RAVAGNAN, G., and ZANDONELLA, A., 1999, Hyperspectral aerial images. A valuable tool for submerged vegetation recognition in the Orbetello Lagoons, Italy. *International Journal of Remote Sensing*, **20**, 523–533.

ANDERSON, M.C., NEALE, C.M. U., Li, F., NORMAN, J.M., KUSTAS, W.P., JAYANTHI, H., and CHAVEZ, J., 2004, Upscaling ground observations of vegetation water content, canopy height, and leaf area index during SMEX02 using aircraft and Landsat imagery. *Remote Sensing of the Environment*, **92**, 447-464.

BAJJOUK, T., POPULUS, J., and GUILLAUMONT, B., 1998, Quantification of subpixel cover fractions using principal component analysis and a linear programming method: application to the coastal zone of Roscoff (France). *Remote Sensing of the Environment*, **64**, 153–165.

BEAUCHAMP, K.H., 1987, A history of drainage and drainage methods. In *Farm drainage in the United States--History, status, and prospects,* G.A. Pavelis, (eds), Miscellaneous Publication no. 1455, pp. 13-29. Washington, D.C., Economic Research Service, U.S. Department of Agriculture.

BEGET, M.E., and DI BELLA, C.M., 2007, Flooding: the effect of water depth on the spectral response of grass canopies. *Journal of Hydrology*, **35**, 285-294.

BIAN, L., and WEST, E., 1997, GIS modeling of elk calving habitat in a prairie environment with statistics. *Photogrammetric Engineering & Remote Sensing*, **63**, 161-167.

BIRKY, A.K., 2001, NDVI and a simple model of deciduous forest seasonal dynamics. *Ecological Modeling*, **143**, 43–58.

BITTENCOURT, H.R., and CLARKE, R.T., 2003, Use of classification and regression trees (CART) to classify remotely-sensed digital images. In *Proceedings. 2003 IEEE International, Istanbul, Turkey* (Geoscience and Remote Sensing Symposium), pp. 3751–3753.

BOYD, D.S., FOODY, G.M., CURRAN, P.J., LUCAS, R.M., and HANZAK, H., 1996, An assessment of radiance in Landsat TM middle and thermal infrared wavebands for the detection of tropical forest regeneration. *International Journal of Remote Sensing*, **17**, 249-261.

BOLSTAD, P., and LILLESAND, T.M., 1992, Rule-based classification models - Flexible integration of satellite imagery and thematic spatial data. *Photogrammetric Engineering & Remote Sensing,* **58**, 965-971.

BOURGEAU-CHAVEZ, L.L., KASISCHKE, E.S., TUCKMAN, M., and MUDD, J.P., 2002, Mapping fire scars in global boreal forests using imaging radar data. *International Journal of Remote Sensing,* **42**, 4211-4234.

BOWERS, S.A., and HANKS, A.J., 1965, Reflection of radiant energy from soil. *Soil Science*, **100**, 130-138.

BRADY, N.C., and WEIL, R.R., 1999, *The Nature and Properties of Soils (*Upper Saddle River, NJ: Prentice-Hall, Inc.).

BRULAND, G.L., and RICHARDSON, C.J., 2004, A spatially explicit investigation of phosphorus sorption and related soil properties in two riparian wetlands. *Journal of Environmental Quality*, **33**, 785-794.

BURDICK, D.M., MENDELSSOHN, I.A., and MCKEE, K.L., 1989, Live standing crop metabolism of marsh grass *Spartina patens* as related to edaphic factors in a brackish, mixed marsh community in Louisiana. *Estuaries,* **12**, 195-204.

BUTLER, J.B., LANE, S.N., and CHANDLER, J.H., 1998, Assessment of DEM quality for characterizing surface roughness using close range digital photogrammetry. *The Photogrammetric Record*, **16**, 271-291.

CARPENTER, G.A., GOPAL, S., MACOMBER, S., MARTENS, S., WOODCOCK, C.E., and FRANKLIN, J., 1999, A neural network method for efficient vegetation mapping. *Remote Sensing of the Environment*,**70**, 326-388.

CARTER, V., MALONE, D.L., and BURBANK, J.H., 1979, Wetland classification and mapping in Western Tennessee. *Photogrammetric Engineering & Remote Sensing*, **45**, 273-284.

CHIRICO, G.B., WESTERN, A.W., GRAYSON, R.B., and BLOSCHL, G., 2005, On the definition of flow width for calculating specific catchment area patterns from gridded elevation data. *Hydrological Processes*, **13**, 2539-2556.

CIVCO, D.L., 1989, Topographic normalization of Landsat Thematic Mapper digital imagery. *Photogrammetric Engineering & Remote Sensing*, **55,** 1303-1309.

COLE, C.A., and SHAFER, D., 2002, Section 404 wetland mitigation and permit success criteria in Pennsylvania, USA, 1986-1999. *Environmental Management,* **30**,508-515.

CONGALTON, R.G., and GREEN, K., 1999, *Assessing the Accuracy of Remotely Sensed Data: Principles and Practices* (London, UK: Lewis Publishers).

COOPER, J.R., GILLIAM, J.W., DANIELS, R.B., and ROBARGE, W.P., 1987, Riparian areas as filters for agricultural sediment. *Soil Society of America*, **51**, 416-420.

COWARDIN, L.M., CARTER, V., GOLET, F.C., and LAROE, E.T., 1979, Classification of wetlands and deepwater habitats of the United States. U.S. Department of the Interior, Fish and Wildlife Service, Washington, D.C. 131 pp.

CRIST, E.P. and CICONE, R.C., 1984, Application of the tasseled cap concept to simulated Thematic Mapper data. *Photogrammetric Engineering & Remote Sensing*, **50**, 343-352.

CRIST, E.P., LAURIN, R., and CICONE, R.C., 1986, Vegetation and soils information contained in transformed Thematic Mapper data. In Proceedings of IGARSS' 86 Symposium, Paris: European Space Agency, 1465-70.

DAHL, T.E, 1990, Wetlands losses in the United States, 1780's to 1980's. U.S. Department of the Interior, Fish and Wildlife Service, Washington, D.C. 21

DAHL, T.E., and JOHNSON, C.F., 1991, Status and trends of wetlands in the conterminous United States: mid-1970's to mid-1980's. U.S. Fish and Wildlife Service, Washington, DC. 28 pp.

DAHL, T.E., and ALLORD, G.J., 1997, Technical aspects of wetlands. History of wetlands in the conterminous United States. United States Geological Survey Water Supply Paper 2425.

DAI, X., and KHORRAM, S., 1998, The effect of image misregistration on the accuracy of remotely sensed change detection. *IEEE Transaction on Geoscience and Remote Sensing*, **36**, 1566-1577.

DE'ATH, G., and FABRICIUS, K.E., 2000, Classification and regression trees: a powerful yet simple technique for ecological data analysis. *Ecology*, **81**, 3178-3192.

DEFRIES, R.S., FIELD, C.B., FUNG, I., JUSTICE, C.O., LOS, S., MATSON, E., and MATTHEW, E., 1995, Mapping the land surface for global atmosphere–biosphere models: towards continuous fields of vegetation's functional properties. *Journal of Geophysical Research*, **100**, 867–920.

DEFRIES R.S., HANSEN, M.C., STEININGER, M., DUBAYAH, R., SOHLBERG, R.S., and TOWNSHED, J.R.G., 1997, Subpixel forest cover in Central Africa from multisensor, multitemporal data. *Remote Sensing of the Environment*, **60,** 228–46.

DEFRIES, RS, HANSEN, M.C., TOWNSHEND, J.R.G., 2000, Global continuous fields of vegetation characteristics: a linear mixture model applied to multi-year 8 km AVHRR data. *International Journal of Remote Sensing*, **21**, 1389–414.

DEFRIES, R. S., HANSEN, M. C., TOWNSHEND, J. R. G., JANETOS, A. C. and LOVELAND, T. R., 2000, A new global 1-km dataset of percentage tree cover derived from remote sensing. *Global Change Biology,* **6**, 247-254.

DOSSKEY, M.G., EISENHAUER, D.E., and HELMERS, M.J., 2005, Establishing conservation buffer using precision information. *Journal of Soil and Water Conservation*, **60**, 349-354.

DOTTAVIO, C.L., and DOTTAVIO, F.D., 1984, Potential benefits of new satellite sensors to wetland mapping. *Photogrammetric Engineering & Remote Sensing*, **50**, 599-606.

DOWNING, D.M., WINER, C., and WOOD, L.D., 2003, Navigating through Clean Water Act jurisdiction: a legal review. *Wetlands*, **23,** 475-493.

EGGERS, S. D., and REED, D. M., 1997, Wetland plants and communities of Minnesota and Wisconsin. U.S. Army Corps of Engineers, St. Paul District, MN, USA.

EICK, M., 2006, CSES 3124, Unpublished Laboratory Guide, Virginia Tech, Blacksburg, VA, USA.

ENVIRONMENTAL LABORATORY, 1987, Wetlands delineation manual. Technical report Y-87-1, US Army Corps of Engineers Waterways Experiment Station, Vicksburg, MS. Available online at: http://el.erdc.usace.army.mil/wetlands/pdfs /wlman87.pdf (accessed 2 May 2007).

EWEL, K.C., and SMITH, J.E., 1992, Evapotranspiration from Florida pond cypress swamps. *Water Resources Bulletin,* **28**, 299-304.

FEDERAL GEOGRAPHIC DATA COMMITTEE, 1992, Application of satellite data for mapping and monitoring wetlands-fact finding report. Wetland Subcommittee. U.S. Fish and Wildlife Service, Reston, VA, USA.

FOODY, G. and CURRAN, P.J., 1994, Estimation of tropical forest extent and regenerative stage using remotely sensed data. *Journal of Biogeography*, **21**, 223-244.

FOODY, G.M., and COX, D.P., 1994, Sub-pixel land cover composition estimation using a linear mixture model and fuzzy membership functions. *International Journal of Remote Sensing* , **15**, 619- 631.

FOODY, G.M., LUCAS, R.M., CURRAN, P.J., and HONZAK, M., 1996, Non-linear mixture modeling without end-members using an artificial neural network. *International Journal of Remote Sensing*, **18**, 937-953.

FORD, A.L.J., FORSTER, R.R., and BRUHN, R.L., 2003, Ice surface velocity patterns on Seward Glacier, Alaska/Yukon, and their implications for regional tectonics in the Saint Alias Mountains. *Annals of Glaciology*, **36**, 21-28.

FRANKLIN, J., WOODCOCK, C.E., AND WARBINGTON, R., 2000, Multi_attribute vegetation maps of forest service lands in California Supporting Resource Management Decisions. *Photogrammetric Engineering & Remote Sensing*, **66**, 1209-1217.

FRANKLIN, S.E., LAVIGNE, M.B., WULDER, M.A., and MCCAFFREY, T.M., 2002, Large-area forest structure change detection: an example. *Canadian Journal of Remote Sensing*, **28**, 588-592.

FRAYER, W.E., MONAHAN, T.J, BOWDEN, D.C., and GRAYBILL, E.A., 1983, Status and trends of wetlands and deepwater habitats in the coterminous United States, 1950s-1970s, Department of Forest and Wood Service, Longmont, CO, USA.

FRIEDL, M.A., BRODLEY, C.E., and STRAHLER, A.H., 1999, Maximizing land cover classification accuracies produced by decision trees at continental to global scale. *IEEE Transactions on Geoscience and Remote Sensing*, **37**, 969-977.

FUTRELL, M. and SFORZA, P., 2004, Converting VBMP digital terrain model to a digital elevation model for raster analysis applications. *The Virginia Geospatial Newsletter*, **2**, 9-10.

GALBRAITH, J.M., DONOVAN, P.F., SMITH, K.M., and ZIPPER, C.E., 2003, Using public domain data to aid in field identification of hydric soils. *Soil Science,* **168**, 563-575..

GESSLER, P.E., MOORE, I.D., MCKENZIE, N.J., and RYAN, P.J., 1995, Soil-landscape modelling and spatial prediction of soil attributes. *International Journal of Geographical Information Systems*, **9**, 421-432.

GOODRICH, D.C., SCHMUGGE, T.J., JACKSON, T.J., UNKRICH, C.L., KEEFER, T.O., PARRY, R., BACH, L.B., AND AMER, S.A., 1994, Runoff simulation sensitivity to remotely sensed initial soil water content. *Water Resources Research*, **30**, 1393-1405.

HANSEN, M.C., DEFRIES, R.S., TOWNSHEND, J.R.G., and SOHLBERG, R., 2000, Global land cover classification at 1 km spatial resolution using a classification tree approach. *International Journal of Remote Sensing*, **21**, 1331–1364.

HANSEN, MC, DEFRIES, R.S., TOWNSHEND, J.R.G., MARUFU, L., and SOHLBERG, R., 2002, Development of a MODIS tree cover validation data set for Western Province, Zambia. *Remote Sensing of the Environment,* **83**, 320–35.

HANSEN, M.C., AND DEFRIES, R.S., 2004, Detecting long-term global forest change using continuous fields of tree-cover maps from 8-km advanced very high resolution radiometer (AVHRR) data for the years 1982-99. *Ecosystems*, **7**, 695-716.

HARVEY, K.R., and HILL, G.J.E., 2001, Vegetation mapping of a tropical freshwater swamp in the northern territory, Australia: a comparison of aerial photography, Landsat TM and SPOT satellite imagery. *International Journal Remote Sensing*, **22**, 2911-2925.

HEIMLICH, R.E., WIEBE, K.D., CLAASSEN, R., GADSBY, D., and HOUSE R.M., 1998, Wetlands and agriculture:private interests and public bBenefits. Agricultural Economics Report No. (AER765) 104 pp.

HEROLD, M., LIU, X.H., and CLARKE, K.C., 2003, Spatial metrics and image texture for mapping urban land-use, *Photogrammetric Engineering & Remote Sensing*, **69**, 991–1001

HESS, L.L., MELACK, J.M.M., Novo, E.M.L., BARBOSA, C.C.F., and GASTIL, M., 2003, Dual-season mapping of wetland inundation and vegetation for the central Amazon basin. *Remote Sensing of the Environment*, **87**, 404-428.

HEWES, L., and FRANDSON P.E., 1952, Occupying the wet prairie: The role of artificial drainage in Story County, Iowa. *Annual Association American Geographer*, **42**, 24-50.

HIRANO, A., MADDEN, M., and WELCH, R., 2003, Hyperspectral image data for mapping wetland vegetation. *Wetlands*, **23**, 2.

HODGSON, M., JENSEN, J.R., MACKEY, H., and COULTER, M.C., 1988, Monitoring wood stork foraging habitat using remote sensing and geographic information systems. *Photogrammetric Engineering & Remote Sensing*, **54**, 1601-1607.

HOMER, C.G., HUANG, C., YANG, L., and WYLIE, B., 2002, Development of a circa 2000 land cover database for the United States. In *Proceedings 2002 ASPRS-ACSM Annual Conference and FIG XXII Congress, Washington, DC,* 2002 (The American Society for Photogrammetry and Remote Sensing), pp. 111–123.

HUNT, E.R., and ROCK, B.N., 1989, Detection of changes in leaf water content using near- and middle-infrared reflectances. *Remote Sensing of the Environment*, **30**, 43-54.

HUPP, C.R., 1986, Upstream variation in bottomland vegetation patterns, northwestern Virginia. *Bulletin of the Torrey Botanical Club*, **113**, 421-430.

HYPERSPECTRAL DATA INTERNATIONAL, 2004, Bulletin. Available online at: http://www.hdi.ns.ca/news/news.archive.2004.php (accessed 7 May 2007)

IWASAKI, A., and TONOOKA, H., 2005, Validation of a crosstalk correction algorithm for ASTER/SWIR. *IEEE Transactions on Geoscience and Remote Sensing*, **43**, 2747-2751.

JACOBSON, G.L., WEBB, T., and GRIMM, E., 1987, Patterns and rates of vegetation change during the glaciation of eastern America. In *North America and Adjacent Oceans During the Last Deglaciation*, W.F. Ruddiman and H.E. Wright Jr (eds), pp. 277–288 (Boulder, Colorado, Geological Society of America).

JACOBSON, J.E., RITTER, R.A., and KOELN, G.T., 1987. Accuracy of thematic mapper derived wetlands as based on national wetland inventory data. In *Proceedings of the ASPRS/ACSM/WFPLS Fall Convention, Falls Church, VA.* 11 p.

JENSEN, J.R., MACKEY, H.E., CHRISTENSEN, E.J., and SHARITZ, R.R., 1987, Inland wetland change detection using aircraft MSS data. *Photogrammetric Engineering & Remote Sensing*, **53**, 521-529.

JOHNSTON, R.M., and BARSON, M.M., 1993, Remote sensing of Australian wetlands: an evaluation of Landsat TM data for inventory and classification. *Australian Journal of Marine and Freshwater Research*, **44**, 223-232.

KATO, M., SONOBE, T., OYANAGI, M., YASUOKA, Y., TAMURA, M., and HAYASHI, M., 2001, ASTER data utilization for wetland mapping and forest mapping. Paper presented at the 22nd Asian Conference on Remote Sensing, 5-9

November 2001, Singapore. Copyright © 2001 CRISP, National University of Singapore; SISV; AARS.

KUDRAY, G.M., and GALE, M.R., 2000. Evaluation of National Wetland Inventory maps in a heavily forested region in the Upper Great Lakes. *Wetlands*, **20**, 581-587.

KUZILA, M.S., RUNDQUIST, D.C., and GREEN, J.A, 1991, Methods for estimating wetland loss: the Rainbasin region of Nebraska, 1927–1981. *Journal of Soil and Water Conservation*, **46**, 441–445.

LAWRENCE, R., BUNN, A. POWELL, S., and ZAMBON, M., 2004, Classification of remotely sensed imagery using stochastic gradient boosting as a refinement of classification tree analysis. *Remote Sensing of the Environment*, **90**, 331–336.

LEWELLYN, D.W., SHAFFER, G.P., CRAIG, N.J., CREASMAN, L., PASHLEY, D., SWAN, M., and BROWN, C., 1995, A decision-support system for prioritizing restoration sites on the Mississippi River alluvial plain. *Conservation Biology,* **10**, 1446-1455.

LEWIS, R.J., 2000, An introduction to classification and regression tree (CART) analysis. Presented at the 2000 Annual Meeting of the Society for Academic Emergency Medicine, San Francisco, California.

LILLESAND, T.M., and KIEFER, R.W., 2004, *Remote Sensing and Image Interpretatio. 5th Edition* (New York, NY: John Wiley & Sons, Inc.).

LOBELL, D.B., and ASNER, G.P., 2002, Moisture effect on soil reflectance. *Soil Science Society of America Journal*, **66**, 722-727.

LOVELAND, T.R., REED, B.C., BROWN, J.F., OHLEN, D.O., ZHU, Z., YANG, L., and MERCHANT, J.W., 2000, Development of a global land cover characteristics

database and IGBP Discover from 1 km AVHRR data. *International Journal of Remote Sensing*, **21**, 1303–1330.

LUDWIG, J.A., WILCOX, B.P., BRESHEARS, D.D., TONGWAY, D.J., and IMESON, A.C., 2004, Vegetation patches and runoff-erosion as interacting ecohydrological process in semiarid landscapes. *Ecology*, **86**, 288-297.

LYON, J.G., and MCCARTHY, J., 1995, *Introduction to Wetlands and Environmental Applications of GIS* (Boca Raton, FL: John G. Lyon and Jack McCarthy).

MACDONALD, DETTWILER and ASSOCIATES (MDA), 2007, Products and service. Available on line at: http://gs.mdacorporation.com/products/sensor/index.asp (accessed 20 July 2007).

MACKEY, H.E., 1990, Monitoring seasonal and annual wetland changes in a freshwater marsh with SPOT HRV data. In *Proceedings of the American Society for Photogrammetry and Remote Sensing*, **4**, 283-292.

MADER, S.F., 1991, Forested wetlands classification and mapping--A literature review. Technical Bulletin no. 606, 99 p. (New York, NY: National Council of the Paper Industry for Air and Stream Improvement, Inc.)

MALLOWS, C.L., 1973, Some comments on CP. *Technometrics*, **15**, 661-675.

MAUNE, D.F., MAITRA, J.B., and MCKAY, E.J., 2001, *Accuracy standards, digital elevation model technologies and applications.* In *The DEM Users Manual*, pp. 61–82 (Bethesda, MD: American Society for Photogrammetry and Remote Sensing)

MCCAULEY, L.A. and JENKINS, D.G., 2005, GIS based estimates of former and current depressional wetlands in an agricultural landscape. *Ecological Applications*, **15**, 1199-1208.

MCFADDEN, D., 1974, Conditional logit analysis of qualitative choice behavior. In *Frontiers in Economics*, P. Zarembka (ed), pp. 105-142 (New York, NY: Academic Press).

MCNEMAR, Q., 1947, Note on the sampling error of the difference between correlated proportions or percentages. *Psychometrika*, **12,** 153-157.

MELACK, J.M., and HESS, L.L., 1998, Recent advances in remote sensing of wetlands. In *Modern Trends in Ecology and Environment*, R.S. Ambasht (eds), p155-170 (The Netherlands: Backhuys Publisher).

MENARD, S.W., 2001, Applied logistic regression analysis. In *Sage University Papers Series on Quantitative Applications in the Social Sciences*, Thousand Oaks, CA.

MERTES, L. A. K., DUNNE, T., and MARTINELLI, L.A., 1996, Channel-floodplain geomorphology along the Solimões-Amazon River, Brazil. *Geological Society of America Bulletin*, **108**, 1089-1107.

MESSINA, M.G, and CONNER, W.H., 2000, *Southern Forested Wetlands*. *Ecology and Management*. (Boca Raton, FL: Lewis Publishers/CRC Press).

MICHENER, W.K., and HOUHOULIS, P., 1997, Detection of vegetation changes associated with extensive flooding in a forested ecosystem. *Photogrammetric Engineering & Remote Sensing,* **63**, 1363–1374.

MITSCH, W.J., and GOSSELINK, J.G., 1993, *Wetlands*. 2nd ed. (New York, NY: Van Nostrand Reinhold).

MOORE, I.D., GESSLER, P.E., NIELSEN, G.A., and PETERSON, G.A., 1993, Soil attribute prediction using terrain analysis. *Soil Science Society of America Journal*, **57**, 443–452.

MORAN, P.A.P., 1950, Notes on continuous stochastic phenomena. *Biometrika,* **37,** 17-23.

MUMBY, P.J., GREEN, E.P., EDWARDS, A.J., and. CLARK, C.D., 1999, The cost-effectiveness of remote sensing for tropical coastal resources assessment and management. *Journal of Environmental Management*, **55**, 157–166.

NARUMALANI, S., JENSEN, J.R., ALTHAUSEN, J.D., BURKHALTER, S., and MACKEY, H.E., 1997, Aquatic macrophysics modeling using GIS and logistic multiple regression. *Photogrammetric Engineering & Remote Sensing*, **63**, 41-49.

NATIONAL WETLAND INVENTORY, 1995, 905-FW 1 Policy. Division of Habitat Conservation. Available at: http://www.fws.gov/policy/905fw1.html (accessed 20 July 2007).

NELSON, G.C., and GOEGHEGAN, J., 2002, Deforestation and land use change: sparse data environments. *Agricultural Economics*, **27**, 201-216.

NOVO, E.M., and SHIMABUKURO, Y.E., 1997, Identification and mapping of the Amazon habitats using a mixing model. *International Journal of Remote Sensing*, **18**, 663–670.

O'HARA, C.G., 2001, Remote sensing and geospatial applications for wetland mapping and assessment. Computational Geospatial Technologies Center, Mississippi State University.

PAL, M., and MATHER, P.M., 2003, An assessment of effectiveness of decision-tree methods for land cover classification. *Remote Sensing of the Environment*, **86**, 554–65.

PANTALEONI, E., ENGEL, B.A., and JOHANNSEN, C.J., 2007. Identifying agricultural flood damage using Landsat imagery. *Journal of Precision Agriculture*, **8**, 27-36.

PAPADAKIS, I., NAPIORKOWSKI, J., and SCHULTZ, G.A., 1993, Monthly runoff generation by non-linear model using multispectral and multitemporal satellite imagery. *Advance in Space Research*, **13**, 181-186.

POHL, C., and VAN GENDEREN, J.L., 1998, Multisensor image fusion in remote sensing: concepts, methods and applications, *International Journal of Remote Sensing*, **19**, 823-854.

QUINN, J.M., 2001, Band combinations. Available online at : http://web.pdx.edu/ ~emch/ip1/bandcombinations.html (accessed 25 April 2007).

REED, P.B., Jr., 1988, National list of plant species that occur in wetlands: 1988 National Summary. U.S. Fish and Wildlife Service, Washington, DC, USA.

RICE, S. K., and PEET, R.K., 1997, Vegetation of the lower Roanoke River floodplain. Report to The Nature Conservancy, Durham, NC.

RUSS, L., and FREDERICK, D.J., 1990, Bottomland hardwood restoration in the southeastern United States. In Proceedings of the 1st annual meeting of the Society for Ecological Restoration, Oakland, CA, 1989. H. Glenn, T. Bonnicksen (eds.) (Restoration `89: the new management challenge: The University of Wisconsin Arboretum, Society for Ecological Restoration), pp. 292-300.

SALFORD SYSTEM, 2002, An implementation of the original CART methodology. Salford System, San Diego, California. Available on line at: http://www.salfordsystems.com/cart.php (accessed 7 May 2007).

SCHABENBERGER, O., and PIERCE, F.J. 2001, *Contemporary Statistical Models for the Plant and Soil Sciences* (Boca Raton, FL: CRC Press LLC).

SETTLE, J., AND DRAKE, N.A., 1993, Linear mixing and the estimation of ground cover proportions. *International Journal of Remote Sensing,* **14**, 1159–77.

SHARITZ, R.R., and MITSCH, W.J., 1993, Southern hardwood forests. In *Biodiversity of the Southeastern United States: Lowland Terrestrial Communities*. W. H, Martin, S. G. Boyce, and A. C. Echternacht (eds), pp311-372 (New York, NY: John Wiley and Sons).

SILVESTRI, S., MARANI, M., SETTLE, J. BENVENUTO, F., and MARANI, A., 2002, Salt marsh vegetation radiometry: data analysis and scaling. *Remote Sensing of the Environment*, **80**, 473-482.

SKIDMORE, E.L., DICKERSON, J.D., and SHIMMELPFENNIG, H., 1975, Evaluating surface-soil water content by measuring reflectance. *Soil Science Society of America Journal*, **39**, 238-242.

SKOLE, D., AND TUCKER, C., 1993, Tropical deforestation and habitat fragmentation in the Amazon: satellite data from 1978± 1988. *Science*, **260**, 1905-1910.

SLAUGHTER, D.C., PELLETIER, M.G., UPADHYAYA, S.K., 2001, Sensing soil moisture using NIR spectroscopy. *Applied Engineering in Agriculture*, **17**, 241.

SMITH, R.L., 1997, The resilience of bottomland hardwood wetlands soils following timber harvest. M. S. Thesis. The University of Mississippi, MS, USA.

SOIL SURVEY STAFF, 1999, Soil taxonomy: A basic system of soil classification for making and interpreting soil surveys. In *Agric. Handbook,* USDA Natural Resources Conservation Service, pp. 869 (Washington, D.C.: U.S. Government Printing Office).

STAUNTON, F.T., circa 1950, Pothole drainage and its effect on wildlife. Unpublished report, Dept Wildlife and Fish Science, San Diego State University, Brookings, CA.

STEFANOV, W.L., CHRISTENSEN, P.R., and RAMSEY, M.S., 2001, Remote sensing of urban ecology at regional and global scales: Results from the Central Arizona-Phoenix LTER site and ASTER urban environmental monitoring program. In *Remote Sensing of Urban Areas*, C. Jürgens (eds), pp. 313-321 (Munich, Germany: Regensburger Geographische Schriften).

STOLT, M.H., and BAKER, J.C., 1995, Evaluation of NWI maps to inventory wetlands in the southern Blue Ridge of Virginia. *Wetlands*, **15**, 346-353.

SUGUMARAN, R., HARKEN, J., and GERJEVIC, J., 2004, Using remote sensing data to study wetland dynamics in Iowa. Iowa Space Grant (Seed) Final Technical Report.

SVORAY, T., SHOSHANY, M., AND PEREVOLOTSKY, A., 2003, Monitoring the response of spatially complex vegetation formations to human intervention: a case study from Mediterranean rangelands. *Journal of Mediterranean Ecology*, **4**, 3–12.

SWARTWOUT D. J., MACCONNELL, W. P., and FINN J. T., 1981, An evaluation of the National Wetlands Inventory in Massachusetts. p. 685–691. In *Proceedings of the In-Place Resource Inventories Workshop,* Orono, ME, USA.

TAN, Q., SHAO, Y., YANG, S., and WEI, Q., 2003, Wetland vegetation biomass using Landsat-7 ETM+ Data. *Remote Sensing of the Environment*, 2629-2631.

TINER, R., and FINN, J.T., 1986, Status and recent trends of wetlands in five mid-atlantic states: Delaware, Maryland, Pennsylvania, Virginia, and West Virginia. Technical Report. U.S. Fish and Wildlife Service, Newton Corner, MA, USA.

TINER, R.W., 1990, Wetlands of the United States. U.S. Fish and Wildlife Service, Washington, DC, USA.

TINER, R.W., 1996, National water summary on wetland resources. U.S. Geological Survey Water-Supply Paper 2425, pp. 431, Washington, DC, USA.

TINER, R.W., 1999, *Wetland indicators: a guide to wetland identification, delineation, classification, and mapping* (Boca Raton, FL, Lewis Publishers).

TOWNSEND, P.A. and WALSH, S.J., 2001, Remote sensing of forested wetlands: application of multitemporal and multispectral satellite imagery to determine plant community composition and structure in southeastern USA. *Plant Ecology*, **157,** 129-149.

TRAVAGLIA, C., and MACINTOSH, H., 1997, Wetlands monitoring by ERS synthetic aperture radar (SAR) data in Zambia. *RCS Serie,* **69**.

U.S.C.O.E., 1995, Section 404 of the Clean Water Act. Available online at: http://www.wetlands.com/regs/sec404fc.htm (accessed 11 July 2007).

U.S.D.A., 2007, National Agriculture Imagery Program. Available at: http://165.221.201.14/NAIP.html (accessed 20 July 2007).

U.S.E.P.A., 1977, Federal water pollution control. Guidelines for specification of disposal sites for dredged or fill material. Act. 40 CFR Part 230 Section 404(b)(1).

U.S.E.P.A., 1993, The role and function of forest buffers in the Chesapeake Bay basin for non-point source management. Chesapeake Bay Program Forestry Work Group. Publication U.S. EPA CBP/TRS 91/93. Annapolis, MD.

U.S.E.P.A., 2002, Federal water pollution control act. 33 U.S.C. §§ 1251-1387, October 18, 1972.

U.S.F.W.S., 2007, Providing wetland information to the American people. Available online at: http://www.fws.gov/nwi/ (accessed 20 July 2007).

V.B.M.P., 2003, Handbook: Overview. Available online at : http://www.vgin.virginia.gov/VBMP/VBMP.html (accessed 25 April 2007).

VENABLES, W.N., and. RIPLEY, B.D., 1999, *Modern Applied Statistics with S-Plus. Third Edition* (New York, NY: Springer Verlag).

VOLCANI, A., KARNIELI, A., AND SVORAY, T., 2005, The use of remote sensing and GIS for spatio-temporal analysis of the physiological state of a semi-arid forest with respect to drought years. *Forest Ecology and Management*, **215,** 239-250.

WANG, Y., and SUN, D., 2005, The ASTER tasseled cap interactive transformation using Gramm-Schmidt method. MIPPR 2005: SAR and Multispectral Image processing, In *Proceedings of the SPIE*, 6043.

WARE, S.A., 1970, Southern mixed hardwood forest in the Virginia Coastal Plain. *Ecology,* **51**,921-924.

WARTHON, C.H., KITCHENS, M.W., PENDLETON, E.C., and SIPE, T.W., 1982, The ecology of bottomland hardwood swamps of the southeast—a community profile. US Fish and Wildlife Service, Office of the Biological Survey, Washington, DC, USA.

WELCH, R., REMILLARD, M., and ALBERTS, J., 1992, Integration of GPS, remote sensing and GIS techniques for coastal resource management. *Photogrammetric Engineering & Remote Sensing*, **58**, 1571-1578.

WERNER, H., 2005, Assessment of National Wetland Inventory maps for Sequoia and Kings Canyon National Parks, 2000–2001. Sequoia and Kings Canyon National Parks, Three Rivers , CA : unpublished report.

WHITE, D.A., DARWIN, S.P., and THIEN, L.B., 1983, Plants and plant communities of Jean Lafitte National Historical park, Louisiana. *Tulane Studies in Zoology and Botany* **24**, 100–129.

WICKWARE, G. M. and HOWARTH P. J., 1981, Change detection in the Peace-Athabasca delta using digital Landsat data. *Remote Sensing of the Environment*, **11**, 9-25.

WILEN, B.O., and PYWELL, H.R., 1992, Remote sensing of the Nation's wetlands, National Wetlands Inventory. In *Proceedings of the Forest Service Remote Sensing Applications Conference*, 4th biennial, Orlando, FL, 1992.

WILEN, B.O., CARTER, V., and JONES, J.R., 2002, Wetland mapping inventory, National Water Summary on Wetland Resources, *United States Geological Survey Water Supply, Paper 242.*

WOLTER, P.T., MLADENOFF, D.J., HOST, E.G., and CROW, T.R., 1995, Improved forest classification in the northern lake states using multi-temporal Landsat imagery. *Photogrammetric Engineering & Remote Sensing*, **61**, 1129-1143.

WRIGLEY, N., 1985, *Categorical Data Analysis for Geographer and Environmental Scientists* (London and NY: Longman).

YAMAGATA, Y., 1999, Advanced remote sensing techniques for monitoring complex ecosystems: spectral indices, unmixing, and classification of wetlands. Research Report from the National Institute for Environmental Studies, Japan (in Japanese), **141**, 1-7.

YAMAGATA, Y., and SUGITA, M., 1999, Land cover monitoring with a vegetation-soil-water index. *Mire of Japan*, **15**, 105-108.

YOHANNES, Y., and HODDINOTT, J., 2006, Classification and regression trees: an introduction. Technical Guide No.3. International Flood Policy Research Institute. Washington, DC, USA.

APPENDIX A -- COORDINATES OF THE 870 POINTS RANDOMLY SELECTED AND USED IN THE LOGIT MODEL, AND IN THE CART AND LOGIT MODELS. BINARY CLASSIFICATION: 1 = WETLAND, 2 = UPLAND.

ID	X-coord	Y-coord	Binary Classification	Wetland type
1	294972.568	4140230.363	1	Emergent
2	313535.544	4127288.531	1	Emergent
3	307552.211	4136026.792	1	Emergent
4	307695.123	4133988.191	1	Emergent
5	314942.351	4149857.591	1	Emergent
6	305793.200	4152848.182	1	Emergent
7	309870.426	4126595.626	1	Emergent
8	316924.145	4124549.649	1	Emergent
9	266774.218	4115209.150	1	Emergent
10	317100.092	4129751.318	1	Emergent
11	307096.610	4135428.975	1	Emergent
12	296535.695	4132573.534	1	Emergent
13	262587.753	4118767.903	1	Emergent
14	308268.932	4133458.610	1	Emergent
15	315957.863	4115310.637	1	Emergent
16	305582.810	4154843.520	1	Emergent
17	309976.120	4151575.180	1	Emergent
18	310030.360	4154154.380	1	Emergent
19	310420.260	4152057.160	1	Emergent
20	315589.750	4160460.240	1	Emergent
21	319089.130	4144746.230	1	Emergent
22	319460.060	4144479.600	1	Emergent
23	320621.260	4157196.710	1	Emergent
24	322969.840	4158229.020	1	Emergent
25	324911.390	4151376.940	1	Emergent
26	301010.383	4109928.653	1	Emergent
27	306113.727	4124750.917	1	Emergent
28	308529.499	4123771.171	1	Emergent
29	304357.068	4119540.568	1	Emergent
30	304343.131	4119542.224	1	Emergent
31	307908.706	4114752.379	1	Emergent
32	307927.306	4114744.572	1	Emergent
33	301616.900	4114165.721	1	Emergent
34	310306.118	4113797.474	1	Emergent
35	316680.579	4133927.835	1	Emergent
36	316889.740	4133808.266	1	Emergent
37	319424.916	4130834.518	1	Emergent
38	314163.718	4127378.124	1	Emergent
39	312839.970	4111773.129	1	Emergent

ID	X-coord	Y-coord	Binary Classification	Wetland type
40	301010.383	4109928.653	1	Emergent
41	306113.727	4124750.917	1	Emergent
42	308529.499	4123771.171	1	Emergent
43	304357.068	4119540.568	1	Emergent
44	304343.131	4119542.224	1	Emergent
45	307908.706	4114752.379	1	Emergent
46	307927.306	4114744.572	1	Emergent
47	301616.900	4114165.721	1	Emergent
48	310306.118	4113797.474	1	Emergent
49	316680.579	4133927.835	1	Emergent
50	316889.740	4133808.266	1	Emergent
51	319424.916	4130834.518	1	Emergent
52	314163.718	4127378.124	1	Emergent
53	309419.705	4126407.561	1	Emergent
54	318595.765	4161482.474	1	Emergent
55	319366.626	4161271.446	1	Emergent
56	323359.818	4159539.180	1	Emergent
57	323379.108	4159605.375	1	Emergent
58	320996.036	4159067.889	1	Emergent
59	320964.876	4159052.210	1	Emergent
60	300075.010	4108199.965	1	Emergent
61	300064.674	4108137.683	1	Emergent
62	300317.305	4155430.848	1	Emergent
63	299563.196	4155406.942	1	Emergent
64	315636.963	4123535.004	1	Emergent
65	303021.817	4157147.976	1	Emergent
66	303039.268	4157130.244	1	Emergent
67	318595.765	4161482.474	1	Emergent
68	319366.626	4161271.446	1	Emergent
69	323359.818	4159539.180	1	Emergent
70	323379.108	4159605.375	1	Emergent
71	320996.036	4159067.889	1	Emergent
72	320964.876	4159052.210	1	Emergent
73	300075.010	4108199.965	1	Emergent
74	300064.674	4108137.683	1	Emergent
75	300317.305	4155430.848	1	Emergent
76	299563.196	4155406.942	1	Emergent
77	315636.963	4123535.004	1	Emergent
78	303021.817	4157147.976	1	Emergent
79	303039.268	4157130.244	1	Emergent
80	306128.014	4115023.269	1	Emergent
81	309419.705	4126407.561	1	Emergent
82	286100.001	4148554.833	1	Emergent
83	318595.765	4161482.474	1	Emergent
84	319366.626	4161271.446	1	Emergent

ID	X-coord	Y-coord	Binary Classification	Wetland type
85	323359.818	4159539.180	1	Emergent
86	323379.108	4159605.375	1	Emergent
87	320996.036	4159067.889	1	Emergent
88	320964.876	4159052.210	1	Emergent
89	290477.265	4109562.175	1	Emergent
90	300075.010	4108199.965	1	Emergent
91	300064.674	4108137.683	1	Emergent
92	289602.484	4105752.835	1	Emergent
93	290795.522	4105007.443	1	Emergent
94	291933.321	4104477.900	1	Emergent
95	292658.429	4104125.954	1	Emergent
96	298174.365	4103666.311	1	Emergent
97	267340.844	4122977.985	1	Emergent
98	270228.933	4117608.433	1	Emergent
99	270215.294	4117614.862	1	Emergent
100	300317.305	4155430.848	1	Emergent
101	299563.196	4155406.942	1	Emergent
102	315636.963	4123535.004	1	Emergent
103	303021.817	4157147.976	1	Emergent
104	303039.268	4157130.244	1	Emergent
105	296054.307	4124715.132	1	Emergent
106	294366.123	4121702.950	1	Emergent
107	298924.221	4116495.220	1	Emergent
108	289029.441	4113166.169	1	Emergent
109	296140.993	4132116.863	1	Emergent
110	298690.985	4139466.195	1	Emergent
111	298688.470	4139467.309	1	Emergent
112	285497.137	4150819.643	1	Emergent
113	285477.436	4150881.359	1	Emergent
114	301010.383	4109928.653	1	Emergent
115	306113.727	4124750.917	1	Emergent
116	308529.499	4123771.171	1	Emergent
117	304357.068	4119540.568	1	Emergent
118	304343.131	4119542.224	1	Emergent
119	307908.706	4114752.379	1	Emergent
120	307927.306	4114744.572	1	Emergent
121	301616.900	4114165.721	1	Emergent
122	310306.118	4113797.474	1	Emergent
123	316680.579	4133927.835	1	Emergent
124	316889.740	4133808.266	1	Emergent
125	319424.916	4130834.518	1	Emergent
126	314163.718	4127378.124	1	Emergent
127	312839.970	4111773.129	1	Emergent
128	298425.125	4129960.168	0	Upland

ID	X-coord	Y-coord	Binary Classification	Wetland type
129	320389.350	4144413.453	0	Upland
130	311417.998	4137992.358	0	Upland
131	300924.912	4149983.488	0	Upland
132	318378.590	4146439.175	0	Upland
133	303909.564	4138869.081	0	Upland
134	305769.466	4139607.825	0	Upland
135	294432.659	4150446.583	0	Upland
136	308575.788	4151880.590	0	Upland
137	303723.781	4155042.244	0	Upland
138	307207.281	4140667.693	0	Upland
139	291920.443	4147179.800	0	Upland
140	308713.137	4136798.221	0	Upland
141	284023.540	4110206.085	0	Upland
142	301532.430	4153838.990	0	Upland
143	307773.132	4139207.114	0	Upland
144	324978.587	4156181.822	0	Upland
145	305450.314	4115286.107	0	Upland
146	293135.455	4120385.735	0	Upland
147	279247.770	4114776.264	0	Upland
148	296854.783	4139761.387	0	Upland
149	313115.898	4156028.691	0	Upland
150	305186.157	4145982.615	0	Upland
151	282379.389	4151076.365	0	Upland
152	322071.131	4145744.923	0	Upland
153	298685.690	4116298.807	0	Upland
154	290409.227	4105848.335	0	Upland
155	297027.181	4154578.227	0	Upland
156	260625.676	4116712.456	0	Upland
157	318238.855	4147144.550	0	Upland
158	311318.341	4140448.235	0	Upland
159	312014.102	4119144.647	0	Upland
160	266897.672	4112978.541	0	Upland
161	290978.269	4148030.545	0	Upland
162	311746.102	4137568.276	0	Upland
163	294395.141	4123914.246	0	Upland
164	317219.998	4151437.130	0	Upland
165	297777.937	4115730.722	0	Upland
166	311875.464	4138694.902	0	Upland
167	304083.664	4150802.126	0	Upland
168	299281.876	4136674.520	0	Upland
169	309577.072	4109442.279	0	Upland
170	319455.384	4156215.150	0	Upland
171	317916.922	4152963.669	0	Upland
172	267035.743	4114420.131	0	Upland

ID	X-coord	Y-coord	Binary Classification	Wetland type
173	292066.814	4144778.263	0	Upland
174	296741.194	4124111.734	0	Upland
175	312544.231	4115527.282	0	Upland
176	287020.531	4151699.977	0	Upland
177	282234.163	4110014.805	0	Upland
178	265208.037	4113730.657	0	Upland
179	263083.672	4117406.644	0	Upland
180	297411.078	4131171.281	0	Upland
181	267680.874	4109338.532	0	Upland
182	296441.519	4123041.088	0	Upland
183	302119.208	4146351.255	0	Upland
184	302945.122	4138928.697	0	Upland
185	290877.633	4150606.232	0	Upland
186	261529.931	4119521.609	0	Upland
187	313232.920	4110541.092	0	Upland
188	313591.293	4128531.820	0	Upland
189	300755.508	4128407.195	0	Upland
190	301037.615	4152518.442	0	Upland
191	317806.041	4122318.543	0	Upland
192	297196.769	4131411.986	0	Upland
193	314384.871	4137400.912	0	Upland
194	295801.329	4104329.507	0	Upland
195	260533.341	4115445.016	0	Upland
196	289406.914	4111331.109	0	Upland
197	307677.465	4113551.398	0	Upland
198	303750.574	4129878.331	0	Upland
199	308636.583	4119528.345	0	Upland
200	294178.050	4150985.687	0	Upland
201	309616.498	4143126.456	0	Upland
202	308652.699	4119519.264	0	Upland
203	296934.241	4110968.223	0	Upland
204	301711.863	4158256.063	0	Upland
205	315874.424	4160192.074	0	Upland
206	317993.755	4125851.305	0	Upland
207	296472.897	4120624.377	0	Upland
208	280678.412	4154673.727	0	Upland
209	278715.901	4118034.754	0	Upland
210	290605.241	4105537.970	0	Upland
211	314338.782	4124192.225	0	Upland
212	296895.708	4143017.004	0	Upland
213	312094.016	4156364.574	0	Upland
214	322004.403	4159017.178	0	Upland
215	319964.147	4155968.468	0	Upland
216	295502.659	4151238.924	0	Upland

ID	X-coord	Y-coord	Binary Classification	Wetland type
217	297451.481	4148021.703	0	Upland
218	291455.414	4119413.140	0	Upland
219	303229.071	4147125.331	0	Upland
220	291509.431	4118702.978	0	Upland
221	276145.127	4111486.502	0	Upland
222	279969.735	4151834.343	0	Upland
223	314365.190	4150006.917	0	Upland
224	304501.171	4116180.762	0	Upland
225	294130.984	4154610.754	0	Upland
226	321747.430	4155643.391	0	Upland
227	316306.512	4161907.820	0	Upland
228	263713.543	4114732.675	0	Upland
229	305434.867	4147281.896	0	Upland
230	294296.822	4104377.554	0	Upland
231	262254.306	4119673.229	0	Upland
232	295133.697	4154765.478	0	Upland
233	304241.443	4135199.488	0	Upland
234	316746.966	4149424.583	0	Upland
235	317223.180	4130243.893	0	Upland
236	277024.527	4118427.996	0	Upland
237	295056.854	4114105.209	0	Upland
238	302575.258	4147453.742	0	Upland
239	321679.985	4144325.978	0	Upland
240	290785.111	4109674.910	0	Upland
241	297122.876	4106543.678	0	Upland
242	289481.402	4110769.348	0	Upland
243	302967.417	4126121.301	0	Upland
244	317554.474	4159685.261	0	Upland
245	313113.283	4156230.084	0	Upland
246	282549.070	4113116.045	0	Upland
247	299280.741	4109406.169	0	Upland
248	290761.392	4141075.603	0	Upland
249	295171.644	4146667.358	0	Upland
250	292877.607	4117572.216	0	Upland
251	283364.916	4113615.964	0	Upland
252	302161.957	4136651.075	0	Upland
253	312868.955	4150650.060	0	Upland
254	282933.302	4105702.452	0	Upland
255	261060.389	4116747.402	0	Upland
256	292908.174	4105359.916	0	Upland
257	309200.703	4113292.877	0	Upland
258	297128.990	4104101.218	0	Upland
259	313954.997	4129846.275	0	Upland
260	268337.275	4113246.952	0	Upland

ID	X-coord	Y-coord	Binary Classification	Wetland type
261	268584.254	4112707.951	0	Upland
262	315684.337	4118396.097	0	Upland
263	266247.748	4118182.792	0	Upland
264	264041.059	4121545.309	0	Upland
265	319009.496	4132396.106	0	Upland
266	305479.290	4148296.446	0	Upland
267	283169.087	4153590.211	0	Upland
268	278418.860	4113803.900	0	Upland
269	310792.158	4140064.991	0	Upland
270	317757.561	4143057.497	0	Upland
271	279224.693	4113349.848	0	Upland
272	295226.061	4151594.694	0	Upland
273	298578.568	4111241.232	0	Upland
274	298224.765	4128633.643	0	Upland
275	314180.602	4134157.365	0	Upland
276	322313.700	4153924.888	0	Upland
277	301719.158	4106432.873	0	Upland
278	311386.427	4118938.540	0	Upland
279	312447.233	4162922.824	0	Upland
280	295845.287	4110062.414	0	Upland
281	270899.842	4108844.251	0	Upland
282	306017.719	4140835.954	0	Upland
283	301963.225	4136792.842	0	Upland
284	306090.153	4132574.603	0	Upland
285	260745.450	4118084.390	0	Upland
286	265845.290	4115170.870	0	Upland
287	266060.870	4120007.390	0	Upland
288	266737.360	4115467.900	0	Upland
289	267136.750	4121920.170	0	Upland
290	267690.440	4112052.040	0	Upland
291	268469.170	4127486.860	0	Upland
292	268470.050	4125447.180	0	Upland
293	268624.680	4126599.560	0	Upland
294	269328.640	4117726.330	0	Upland
295	270755.170	4117522.290	0	Upland
296	274699.350	4122537.000	0	Upland
297	277062.050	4107651.190	0	Upland
298	277104.670	4118662.720	0	Upland
299	277714.100	4111402.130	0	Upland
300	280302.360	4108224.450	0	Upland
301	282539.020	4118079.710	0	Upland
302	282589.170	4109534.890	0	Upland
303	282635.930	4153250.880	0	Upland
304	283230.080	4151356.730	0	Upland

ID	X-coord	Y-coord	Binary Classification	Wetland type
305	284011.950	4151515.940	0	Upland
306	284451.460	4151428.230	0	Upland
307	284804.490	4118322.600	0	Upland
308	287157.770	4146304.790	0	Upland
309	287823.760	4113457.350	0	Upland
310	288849.840	4105687.400	0	Upland
311	289695.380	4144204.270	0	Upland
312	290085.540	4112787.990	0	Upland
313	290663.770	4149087.400	0	Upland
314	291013.990	4147250.720	0	Upland
315	291218.070	4110830.390	0	Upland
316	291874.430	4122135.850	0	Upland
317	291934.420	4141174.350	0	Upland
318	292178.090	4113288.250	0	Upland
319	293868.120	4118173.640	0	Upland
320	294213.060	4125616.200	0	Upland
321	294381.500	4150394.060	0	Upland
322	295516.370	4117404.850	0	Upland
323	295559.500	4116300.990	0	Upland
324	295882.310	4109921.600	0	Upland
325	296008.190	4110330.480	0	Upland
326	296270.390	4114780.890	0	Upland
327	296950.360	4110959.140	0	Upland
328	297058.310	4138027.040	0	Upland
329	297233.920	4112038.870	0	Upland
330	297416.830	4117173.690	0	Upland
331	297449.110	4109758.490	0	Upland
332	297984.150	4156038.210	0	Upland
333	298293.210	4118679.080	0	Upland
334	298359.790	4145893.150	0	Upland
335	298587.830	4143031.390	0	Upland
336	298640.180	4149870.910	0	Upland
337	298670.760	4142127.930	0	Upland
338	299026.080	4154651.450	0	Upland
339	299120.890	4108656.580	0	Upland
340	301020.230	4145970.880	0	Upland
341	301671.560	4125132.150	0	Upland
342	301942.860	4135535.020	0	Upland
343	302472.960	4156567.790	0	Upland
344	302599.790	4125848.640	0	Upland
345	303173.300	4150435.430	0	Upland
346	303323.300	4125081.120	0	Upland
347	304615.590	4153720.460	0	Upland
348	305167.390	4152110.720	0	Upland

ID	X-coord	Y-coord	Binary Classification	Wetland type
349	305248.590	4123676.430	0	Upland
350	305262.290	4134716.490	0	Upland
351	305339.520	4140578.350	0	Upland
352	305399.540	4153699.220	0	Upland
353	305448.540	4120844.860	0	Upland
354	305538.580	4139786.460	0	Upland
355	305561.730	4139888.850	0	Upland
356	305832.530	4151895.880	0	Upland
357	306657.090	4151231.350	0	Upland
358	306779.570	4139087.220	0	Upland
359	307405.180	4121461.690	0	Upland
360	308378.290	4118474.370	0	Upland
361	308746.310	4125863.940	0	Upland
362	309007.930	4152785.600	0	Upland
363	309291.670	4124277.170	0	Upland
364	309335.690	4119654.220	0	Upland
365	309347.890	4119207.520	0	Upland
366	309480.590	4144722.420	0	Upland
367	309845.740	4123005.360	0	Upland
368	310062.460	4155110.240	0	Upland
369	310843.140	4136877.540	0	Upland
370	311113.570	4147840.680	0	Upland
371	311298.430	4120787.400	0	Upland
372	311852.520	4116556.770	0	Upland
373	311984.690	4155666.480	0	Upland
374	312073.940	4163333.080	0	Upland
375	312198.270	4132315.520	0	Upland
376	312358.610	4162294.130	0	Upland
377	312469.280	4120807.400	0	Upland
378	312740.570	4132689.680	0	Upland
379	312997.330	4148433.100	0	Upland
380	313877.040	4128210.880	0	Upland
381	313922.340	4128665.160	0	Upland
382	314413.260	4125109.870	0	Upland
383	314677.780	4140220.310	0	Upland
384	314694.250	4118993.950	0	Upland
385	314817.810	4142994.620	0	Upland
386	314985.070	4143420.160	0	Upland
387	315369.620	4154958.740	0	Upland
388	315383.550	4154870.920	0	Upland
389	315506.630	4117296.710	0	Upland
390	315895.010	4142587.580	0	Upland
391	315957.770	4136274.750	0	Upland
392	316273.690	4116624.600	0	Upland

ID	X-coord	Y-coord	Binary Classification	Wetland type
393	316323.620	4142106.170	0	Upland
394	316536.210	4138547.770	0	Upland
395	316550.140	4139939.360	0	Upland
396	316659.590	4121405.150	0	Upland
397	317471.290	4158452.650	0	Upland
398	319843.490	4156636.210	0	Upland
399	320560.060	4149994.970	0	Upland
400	320602.400	4136136.700	0	Upland
401	322093.710	4157807.330	0	Upland
402	322651.300	4149856.230	0	Upland
403	322682.620	4156315.970	0	Upland
404	323847.390	4154340.210	0	Upland
405	324077.830	4151131.600	0	Upland
406	325452.500	4156154.690	0	Upland
407	326066.240	4156448.620	0	Upland
408	326368.540	4155838.470	0	Upland
409	316297.196	4119110.139	0	Upland
410	305672.443	4143475.753	0	Upland
411	299777.079	4124046.018	0	Upland
412	306082.604	4117156.667	0	Upland
413	282488.960	4113309.850	0	Upland
414	289757.060	4121329.700	0	Upland
415	297004.120	4150193.000	0	Upland
416	299128.920	4147716.280	0	Upland
417	305167.390	4152110.720	0	Upland
418	305262.290	4134716.490	0	Upland
419	312358.610	4162294.130	0	Upland
420	315369.620	4154958.740	0	Upland
421	315895.010	4142587.580	0	Upland
422	318132.192	4128833.142	0	Upland
423	276568.718	4118950.871	0	Upland
424	276045.914	4113533.529	0	Upland
425	298636.975	4154291.353	0	Upland
426	298666.884	4154314.439	0	Upland
427	316297.196	4119110.139	0	Upland
428	305672.443	4143475.753	0	Upland
429	299777.079	4124046.018	0	Upland
430	293796.279	4117730.448	0	Upland
431	296364.796	4114393.314	0	Upland
432	289074.967	4113165.193	0	Upland
433	292926.340	4146857.460	0	Upland
434	306082.604	4117156.667	0	Upland
435	283731.509	4107958.933	0	Upland
436	294433.158	4108185.551	0	Upland

ID	X-coord	Y-coord	Binary Classification	Wetland type
437	295105.556	4152179.660	0	Upland
438	303674.440	4117850.960	0	Upland
439	310323.210	4149128.576	0	Upland
440	303496.659	4133611.676	0	Upland
441	305029.492	4137268.900	0	Upland
442	281262.493	4150991.166	0	Upland
443	304217.045	4138426.579	0	Upland
444	267483.510	4110648.128	0	Upland
445	306043.727	4136271.332	0	Upland
446	305819.548	4137045.755	0	Upland
447	301765.738	4136767.930	0	Upland
448	297499.379	4109229.770	0	Upland
449	308800.108	4125012.575	0	Upland
450	306071.716	4134734.405	0	Upland
451	311011.740	4116335.305	0	Upland
452	304555.336	4136924.494	0	Upland
453	285539.246	4148661.716	0	Upland
454	293777.005	4110644.514	0	Upland
455	280746.352	4152952.150	0	Upland
456	304197.159	4135651.629	0	Upland
457	305651.648	4137417.092	0	Upland
458	311188.036	4115797.896	0	Upland
459	282743.424	4149666.157	0	Upland
460	312149.864	4152873.477	0	Upland
461	308668.553	4132531.138	0	Upland
462	305701.085	4137258.586	0	Upland
463	316310.706	4136722.116	0	Upland
464	279607.458	4149423.405	0	Upland
465	302989.226	4135127.284	0	Upland
466	308689.383	4132993.133	0	Upland
467	304449.009	4135094.623	0	Upland
468	285775.241	4147598.933	0	Upland
469	316045.492	4136013.937	0	Upland
470	282614.706	4148770.819	0	Upland
471	302458.167	4135744.575	0	Upland
472	316438.188	4135784.603	0	Upland
473	303224.278	4136377.455	0	Upland
474	280445.702	4150158.977	0	Upland
475	307555.112	4138550.136	0	Upland
476	311817.797	4153214.558	0	Upland
477	284218.125	4150977.189	0	Upland
478	315844.016	4135574.520	0	Upland
479	293197.134	4110861.700	0	Upland
480	302261.666	4135261.376	0	Upland

ID	X-coord	Y-coord	Binary Classification	Wetland type
481	282043.529	4151492.703	0	Upland
482	280830.927	4152207.870	0	Upland
483	279116.199	4149690.447	0	Upland
484	304917.246	4137795.764	0	Upland
485	311332.137	4152879.206	0	Upland
486	284093.757	4150596.682	0	Upland
487	304883.352	4138739.352	0	Upland
488	316746.622	4136020.242	0	Upland
489	283947.013	4148200.635	0	Upland
490	280739.823	4152917.423	0	Upland
491	306736.455	4137918.745	0	Upland
492	280719.000	4150980.391	0	Upland
493	297019.624	4109487.757	0	Upland
494	279614.286	4152128.901	0	Upland
495	305811.145	4138686.862	0	Upland
496	281278.660	4151217.636	0	Upland
497	316353.295	4138283.226	0	Upland
498	295565.747	4110113.757	0	Upland
499	280919.539	4152257.726	0	Upland
500	308816.779	4151231.102	0	Upland
501	311099.430	4114273.003	0	Upland
502	281751.886	4150924.922	0	Upland
503	292385.388	4119009.092	1	Water
504	304009.833	4114751.376	1	Water
505	309680.780	4125724.519	1	Water
506	298641.228	4138637.521	1	Water
507	293691.761	4140060.126	1	Water
508	298129.209	4132362.384	1	Water
509	325064.380	4159364.748	1	Water
510	304611.371	4123381.784	1	Water
511	309382.885	4155622.951	1	Water
512	298230.618	4137565.578	1	Water
513	305262.751	4131412.970	1	Water
514	319307.005	4145545.207	1	Water
515	310158.409	4130143.248	1	Water
516	296372.912	4138416.047	1	Water
517	281705.958	4114278.858	1	Water
518	307080.772	4129116.908	1	Water
519	302993.549	4131762.933	1	Water
520	306618.095	4131581.683	1	Water
521	270699.939	4125092.996	1	Water
522	287635.916	4106916.664	1	Water
523	302751.403	4133205.360	1	Water
524	296456.259	4140244.669	1	Water

ID	X-coord	Y-coord	Binary Classification	Wetland type
525	305997.111	4129487.273	1	Water
526	295926.545	4142380.463	1	Water
527	315038.079	4146703.902	1	Water
528	298196.218	4137218.073	1	Water
529	303138.506	4155455.989	1	Water
530	301666.064	4133194.185	1	Water
531	303674.735	4140112.454	1	Water
532	303503.304	4139717.989	1	Water
533	308955.010	4160060.721	1	Water
534	325882.085	4157412.280	1	Water
535	300334.452	4138576.812	1	Water
536	296446.049	4140628.216	1	Water
537	295246.354	4139829.686	1	Water
538	299875.707	4139550.505	1	Water
539	265162.640	4112045.730	1	Water
540	288499.270	4141987.690	1	Water
541	290913.810	4104974.670	1	Water
542	291024.480	4142006.930	1	Water
543	295580.780	4140048.290	1	Water
544	295752.340	4140562.630	1	Water
545	297490.090	4138964.620	1	Water
546	298973.550	4126412.460	1	Water
547	299141.820	4138761.210	1	Water
548	299218.570	4137331.100	1	Water
549	300988.500	4137509.190	1	Water
550	304702.610	4132138.700	1	Water
551	306646.320	4131402.540	1	Water
552	317018.530	4125270.920	1	Water
553	324833.710	4159414.110	1	Water
554	324847.380	4159610.250	1	Water
555	325510.740	4156909.240	1	Water
556	301146.759	4109298.942	1	Water
557	314850.658	4133170.937	1	Water
558	317279.448	4129878.011	1	Water
559	319530.430	4128691.492	1	Water
560	316145.125	4126698.319	1	Water
561	317445.074	4125902.473	1	Water
562	299430.096	4134460.129	1	Water
563	294660.200	4140511.590	1	Water
564	301666.064	4133194.185	1	Water
565	303674.735	4140112.454	1	Water
566	303503.304	4139717.989	1	Water
567	308955.010	4160060.721	1	Water
568	325882.085	4157412.280	1	Water

ID	X-coord	Y-coord	Binary Classification	Wetland type
569	300334.452	4138576.812	1	Water
570	296446.049	4140628.216	1	Water
571	295246.354	4139829.686	1	Water
572	299875.707	4139550.505	1	Water
573	281272.249	4148804.356	1	Water
574	286143.838	4147714.915	1	Water
575	285169.878	4145903.161	1	Water
576	287275.828	4143385.863	1	Water
577	287934.439	4143268.721	1	Water
578	289110.660	4141696.610	1	Water
579	288805.009	4141734.879	1	Water
580	289392.736	4141257.136	1	Water
581	301146.759	4109298.942	1	Water
582	314850.658	4133170.937	1	Water
583	317279.448	4129878.011	1	Water
584	319530.430	4128691.492	1	Water
585	316145.125	4126698.319	1	Water
586	317445.074	4125902.473	1	Water
587	287740.205	4106698.924	1	Water
588	269292.740	4126125.837	1	Water
589	289577.239	4105761.058	1	Water
590	294660.200	4140511.590	1	Water
591	299430.096	4134460.129	1	Water
592	279779.433	4117452.123	1	Woody
593	318683.929	4125263.654	1	Woody
594	313798.964	4109113.815	1	Woody
595	317008.745	4137592.337	1	Woody
596	309634.989	4113189.957	1	Woody
597	317853.377	4145042.686	1	Woody
598	312129.552	4115920.871	1	Woody
599	312988.032	4154433.186	1	Woody
600	317776.129	4144415.814	1	Woody
601	287369.509	4108984.576	1	Woody
602	303495.355	4149136.302	1	Woody
603	318825.758	4155483.447	1	Woody
604	298759.437	4137510.123	1	Woody
605	310800.019	4148986.946	1	Woody
606	298992.329	4134523.270	1	Woody
607	310796.429	4158817.207	1	Woody
608	298371.401	4123375.444	1	Woody
609	302144.900	4142806.881	1	Woody
610	324465.933	4150243.213	1	Woody
611	269542.711	4111313.324	1	Woody
612	286410.651	4111486.281	1	Woody

ID	X-coord	Y-coord	Binary Classification	Wetland type
613	300852.372	4112628.473	1	Woody
614	304398.142	4155760.585	1	Woody
615	301107.708	4117703.521	1	Woody
616	320307.310	4144855.123	1	Woody
617	290582.296	4150552.095	1	Woody
618	309406.845	4132649.643	1	Woody
619	301246.636	4118236.386	1	Woody
620	313270.909	4128213.569	1	Woody
621	293867.462	4113860.557	1	Woody
622	299292.269	4130356.495	1	Woody
623	288551.978	4106478.298	1	Woody
624	309274.127	4126607.818	1	Woody
625	307366.503	4140128.733	1	Woody
626	309500.735	4141201.147	1	Woody
627	271303.775	4118714.688	1	Woody
628	311276.499	4125593.679	1	Woody
629	307679.163	4147291.859	1	Woody
630	301198.565	4117692.735	1	Woody
631	302847.234	4113453.741	1	Woody
632	303352.508	4140612.584	1	Woody
633	290315.003	4153191.444	1	Woody
634	308880.118	4150892.241	1	Woody
635	300887.055	4138341.605	1	Woody
636	306378.739	4110185.160	1	Woody
637	314495.250	4130250.999	1	Woody
638	308425.969	4129821.533	1	Woody
639	298012.291	4138668.237	1	Woody
640	275617.682	4118590.770	1	Woody
641	300767.556	4134290.547	1	Woody
642	280369.561	4116913.280	1	Woody
643	297901.150	4138241.945	1	Woody
644	302205.342	4139877.124	1	Woody
645	303495.750	4156395.097	1	Woody
646	305597.364	4154468.230	1	Woody
647	303178.681	4149071.349	1	Woody
648	291427.119	4116428.267	1	Woody
649	299630.066	4137831.601	1	Woody
650	322034.804	4160390.962	1	Woody
651	314292.752	4139174.629	1	Woody
652	308619.638	4122085.564	1	Woody
653	300470.800	4122877.169	1	Woody
654	309962.234	4115451.084	1	Woody
655	319376.238	4147463.401	1	Woody
656	303663.179	4112990.637	1	Woody

ID	X-coord	Y-coord	Binary Classification	Wetland type
657	300497.794	4108466.151	1	Woody
658	263580.991	4119631.508	1	Woody
659	308405.250	4128161.271	1	Woody
660	320759.330	4153774.298	1	Woody
661	300886.640	4134100.616	1	Woody
662	306471.093	4152789.680	1	Woody
663	303621.053	4149187.302	1	Woody
664	277501.431	4114463.038	1	Woody
665	302630.717	4107377.916	1	Woody
666	317251.381	4128319.678	1	Woody
667	286771.420	4113157.447	1	Woody
668	280846.342	4115867.835	1	Woody
669	297972.078	4151088.488	1	Woody
670	305916.270	4150086.785	1	Woody
671	314447.744	4109805.895	1	Woody
672	296550.375	4112582.507	1	Woody
673	281761.538	4112983.101	1	Woody
674	312620.753	4135923.158	1	Woody
675	262033.843	4110966.863	1	Woody
676	301155.779	4118247.172	1	Woody
677	301208.769	4108103.406	1	Woody
678	307178.723	4123025.724	1	Woody
679	306315.225	4110588.238	1	Woody
680	262026.786	4111011.650	1	Woody
681	295902.349	4132443.629	1	Woody
682	299639.799	4133054.699	1	Woody
683	310857.126	4115147.077	1	Woody
684	296898.565	4150922.941	1	Woody
685	285573.507	4116610.452	1	Woody
686	302979.727	4155709.231	1	Woody
687	304510.396	4139187.057	1	Woody
688	304484.811	4139132.530	1	Woody
689	303422.638	4158612.913	1	Woody
690	312221.519	4157539.845	1	Woody
691	312248.668	4157533.039	1	Woody
692	307666.728	4154805.518	1	Woody
693	307663.931	4154807.446	1	Woody
694	300743.068	4149947.617	1	Woody
695	300459.098	4141471.022	1	Woody
696	300378.069	4141658.477	1	Woody
697	308343.059	4121730.156	1	Woody
698	308341.700	4121707.849	1	Woody
699	301313.723	4121479.064	1	Woody
700	307965.332	4118869.144	1	Woody

ID	X-coord	Y-coord	Binary Classification	Wetland type
701	307974.726	4118846.648	1	Woody
702	306884.586	4115077.207	1	Woody
703	307081.114	4114806.364	1	Woody
704	301098.332	4111867.066	1	Woody
705	301348.180	4134266.097	1	Woody
706	307608.614	4133285.617	1	Woody
707	302762.377	4107439.679	1	Woody
708	291424.990	4104276.730	1	Woody
709	301591.540	4118122.190	1	Woody
710	307328.290	4115192.440	1	Woody
711	286654.980	4113141.970	1	Woody
712	287680.020	4107013.970	1	Woody
713	289479.050	4109459.290	1	Woody
714	291552.380	4115256.080	1	Woody
715	292170.770	4110011.390	1	Woody
716	294039.460	4115598.080	1	Woody
717	294836.050	4106581.950	1	Woody
718	296278.060	4142507.200	1	Woody
719	296629.670	4127544.910	1	Woody
720	296892.370	4153414.100	1	Woody
721	297077.820	4120928.720	1	Woody
722	297239.290	4112925.560	1	Woody
723	297648.430	4137488.200	1	Woody
724	297788.890	4105476.950	1	Woody
725	298487.770	4133953.240	1	Woody
726	299154.090	4151885.730	1	Woody
727	299781.960	4110462.900	1	Woody
728	299801.380	4108453.610	1	Woody
729	300285.020	4139050.330	1	Woody
730	300317.710	4129978.390	1	Woody
731	300725.290	4122488.040	1	Woody
732	300872.610	4120610.060	1	Woody
733	300911.430	4119609.290	1	Woody
734	301013.560	4149892.390	1	Woody
735	301478.630	4117329.870	1	Woody
736	302501.460	4112630.470	1	Woody
737	302922.380	4156638.960	1	Woody
738	303269.800	4106811.290	1	Woody
739	303417.320	4143879.060	1	Woody
740	304271.570	4154772.120	1	Woody
741	304981.250	4149230.920	1	Woody
742	306093.360	4113976.640	1	Woody
743	306151.790	4149912.330	1	Woody
744	306345.500	4155385.650	1	Woody

ID	X-coord	Y-coord	Binary Classification	Wetland type
745	306458.130	4110058.540	1	Woody
746	306537.080	4110217.640	1	Woody
747	306548.330	4143529.330	1	Woody
748	307143.080	4109955.250	1	Woody
749	307157.370	4151829.240	1	Woody
750	308440.620	4114357.210	1	Woody
751	308513.870	4109177.240	1	Woody
752	308782.270	4140385.490	1	Woody
753	308949.060	4128953.710	1	Woody
754	309188.360	4159403.650	1	Woody
755	311149.580	4108293.000	1	Woody
756	311492.530	4139499.740	1	Woody
757	312282.830	4148063.790	1	Woody
758	313152.290	4125099.980	1	Woody
759	313364.730	4147327.390	1	Woody
760	315244.940	4145485.410	1	Woody
761	315522.290	4155890.270	1	Woody
762	316301.610	4159526.060	1	Woody
763	317756.280	4145201.920	1	Woody
764	318483.570	4144829.910	1	Woody
765	318519.390	4129231.240	1	Woody
766	319533.090	4128542.520	1	Woody
767	320044.490	4137092.770	1	Woody
768	320705.580	4144873.770	1	Woody
769	321181.920	4144114.040	1	Woody
770	322131.060	4143371.430	1	Woody
771	323160.810	4159751.880	1	Woody
772	323382.670	4147005.120	1	Woody
773	323425.880	4160050.020	1	Woody
774	319298.639	4145167.209	1	Woody
775	300685.899	4134268.281	1	Woody
776	303851.880	4112066.471	1	Woody
777	308929.661	4121866.882	1	Woody
778	305704.823	4115707.777	1	Woody
779	310489.020	4113936.303	1	Woody
780	310185.570	4113770.245	1	Woody
781	301112.141	4137297.027	1	Woody
782	323189.521	4145763.467	1	Woody
783	320202.849	4160909.510	1	Woody
784	317451.157	4159157.283	1	Woody
785	300854.830	4153956.118	1	Woody
786	300841.555	4153967.592	1	Woody
787	311990.357	4123320.907	1	Woody
788	312008.816	4123326.011	1	Woody

ID	X-coord	Y-coord	Binary Classification	Wetland type
789	302281.469	4146514.804	1	Woody
790	308929.661	4121866.882	1	Woody
791	305704.823	4115707.777	1	Woody
792	310489.020	4113936.303	1	Woody
793	310185.570	4113770.245	1	Woody
794	296058.990	4121547.760	1	Woody
795	298644.060	4108254.060	1	Woody
796	300317.710	4129978.390	1	Woody
797	302501.460	4112630.470	1	Woody
798	306151.790	4149912.330	1	Woody
799	308949.060	4128953.710	1	Woody
800	315244.940	4145485.410	1	Woody
801	321181.920	4144114.040	1	Woody
802	319298.639	4145167.209	1	Woody
803	300685.899	4134268.281	1	Woody
804	295237.514	4141804.517	1	Woody
805	295003.516	4141705.681	1	Woody
806	295268.093	4141471.040	1	Woody
807	285335.933	4145508.337	1	Woody
808	303851.880	4112066.471	1	Woody
809	276318.469	4107895.730	1	Woody
810	281180.993	4110365.898	1	Woody
811	285579.775	4116566.054	1	Woody
812	296273.625	4143894.114	1	Woody
813	308929.661	4121866.882	1	Woody
814	305704.823	4115707.777	1	Woody
815	310489.020	4113936.303	1	Woody
816	310185.570	4113770.245	1	Woody
817	301112.141	4137297.027	1	Woody
818	309401.228	4128746.590	1	Woody
819	323189.521	4145763.467	1	Woody
820	320202.849	4160909.510	1	Woody
821	317451.157	4159157.283	1	Woody
822	292414.277	4111284.599	1	Woody
823	291162.371	4108774.773	1	Woody
824	291111.044	4107086.176	1	Woody
825	294051.290	4106555.753	1	Woody
826	298554.250	4103979.115	1	Woody
827	298488.323	4103869.714	1	Woody
828	300854.830	4153956.118	1	Woody
829	300841.555	4153967.592	1	Woody
830	311990.357	4123320.907	1	Woody
831	312008.816	4123326.011	1	Woody
832	302281.469	4146514.804	1	Woody

ID	X-coord	Y-coord	Binary Classification	Wetland type
833	304510.396	4139187.057	1	Woody
834	304484.811	4139132.530	1	Woody
835	303422.638	4158612.913	1	Woody
836	312221.519	4157539.845	1	Woody
837	312248.668	4157533.039	1	Woody
838	307666.728	4154805.518	1	Woody
839	307663.931	4154807.446	1	Woody
840	299286.474	4116731.103	1	Woody
841	299174.702	4116731.333	1	Woody
842	298830.787	4115335.182	1	Woody
843	288909.921	4116540.850	1	Woody
844	297976.928	4151117.820	1	Woody
845	297939.023	4151244.365	1	Woody
846	300743.068	4149947.617	1	Woody
847	290375.905	4147554.684	1	Woody
848	290377.206	4147561.137	1	Woody
849	299621.566	4146768.554	1	Woody
850	300459.098	4141471.022	1	Woody
851	300378.069	4141658.477	1	Woody
852	295071.965	4140811.204	1	Woody
853	309541.209	4109892.680	1	Woody
854	308343.059	4121730.156	1	Woody
855	308341.700	4121707.849	1	Woody
856	301313.723	4121479.064	1	Woody
857	307965.332	4118869.144	1	Woody
858	307974.726	4118846.648	1	Woody
859	306884.586	4115077.207	1	Woody
860	307081.114	4114806.364	1	Woody
861	301098.332	4111867.066	1	Woody
862	277245.390	4111187.187	1	Woody
863	288283.847	4108643.010	1	Woody
864	284110.828	4106251.073	1	Woody
865	284115.331	4106287.797	1	Woody
866	307608.614	4133285.617	1	Woody
867	303051.722	4135038.231	1	Woody
868	302762.377	4107439.679	1	Woody
869	297812.861	4109245.031	1	Woody
870	276282.571	4112164.423	1	Woody

APPENDIX B -- SAS CODE FOR COMPUTING THE CANONICAL DISCRIMINANT ANALYSIS AND MACRO FOR PLOTTING THE CANONICAL VARIABLES.

```
/*CANONICAL DISCRIMINANT ANALYSIS*/

proc candisc data=sample ncan=3 out=outcan;
var March_b1 March_b2 March_b3 March_b4 March_b5
Oct_b1 Oct_b2 Oct_b3 Oct_b4 Oct_b5 ssurgo nhd dem slope wi;
class BinClass;
run;

/* For plotting the results of the Canonical Discriminant
Analysis*/


%plotit(data=outcan,plotvars=Can3 Can1 , labelvar=blank,
symvar=binclass, typevar=binclass,
symsize=1, symlen=4, tsize=1.5, exttypes=binclass, ls=100,
           plotopts=vaxis=-3 to 10 by 3, vtoh=,
extend=close);

%plotit(data=outcan,plotvars=Can2 Can1 , labelvar=blank,
symvar=binclass, typevar=binclass,
symsize=1, symlen=4, tsize=1.5, exttypes=binclass, ls=100,
           plotopts=vaxis=-3 to 10 by 3, vtoh=,
extend=close);

%plotit(data=outcan,plotvars=Can2 Can3 , labelvar=blank,
symvar=binclass, typevar=binclass,
symsize=1, symlen=4, tsize=1.5, exttypes=binclass, ls=100,
           plotopts=vaxis=-3 to 10 by 3, vtoh=,
extend=close);
```

APPENDIX C -- SAS CODE USED TO DEVELOP THE MULTINOMIAL LOGISTIC REGRESSION MODEL.

```
/*Multinomial logistic regression*/

proc logistic data=temp order=internal;
model class=mb1 mb2 mb3 mb4 mb5 oct1 oct2 oct3 oct4 oct5
dem slope wi nhd ssurgo/  selection=stepwise link=glogit;
ods output parameterestimates=odds;
run;

data odds1;set odds;
odds=exp(estimate);
run;

proc print data=odds1;
  var response estimate odds;
run;
```

APPENDIX D -- PARAMETER ESTIMATES OF THE VARIABLES SELECTED BY THE STEPWISE REGRESSION USED IN THE MULTINOMIAL LOGISTIC REGRESSION.

Variable	Response	Estimate	Wald χ-Square	p-value
Intercept	Emergent	5.496	2.119	0.146
Intercept	Upland	-17.811	11.719	0.001
Intercept	Water	-28.891	0.016	0.901
March_1	Emergent	-51.131	6.656	0.010
March_1	Upland	36.455	2.402	0.121
March_1	Water	54.643	5.115	0.024
March_2	Emergent	62.256	8.238	0.004
March_2	Upland	3.196	0.022	0.881
March_2	Water	-27.071	0.938	0.333
March_3	Emergent	1.848	0.081	0.776
March_3	Upland	18.047	9.074	0.003
March_3	Water	-12.463	2.110	0.146
March_4	Emergent	-17.745	7.831	0.005
March_4	Upland	-1.522	0.052	0.820
March_4	Water	-28.079	9.283	0.002
Oct_2	Emergent	15.786	12.427	0.000
Oct_2	Upland	1.767	0.132	0.716
Oct_2	Water	-4.994	0.322	0.570
DEM	Emergent	-0.017	8.191	0.004
DEM	Upland	-0.003	0.460	0.498
DEM	Water	0.015	3.563	0.059
Slope	Emergent	-0.094	3.776	0.052
Slope	Upland	-0.072	4.675	0.031
Slope	Water	-0.057	1.936	0.164
NHD	Emergent	1.064	2.097	0.148
NHD	Upland	-3.882	29.523	< .0001
NHD	Water	10.063	0.004	0.950
SSURGO	Emergent	-2.253	9.027	0.003
SSURGO	Upland	-2.540	21.345	< .0001
SSURGO	Water	10.896	0.004	0.948

APPENDIX E -- COORDINATES OF THE 300 PLOTS RANDOMLY SELECTED TO DETERMINE PERCENT OF CANOPY COVER IN FORESTED WETLANDS.

ID	AREA (m^2)	AREA (%)	X-Coord	Y-Coord
1	88.50	39.33	307156.22	4151841.91
2	105.60	46.93	307816.60	4151242.56
3	107.90	47.96	307200.94	4151918.43
4	151.50	67.33	305687.57	4152849.13
5	117.50	52.22	307171.71	4151109.93
6	188.50	83.78	305761.12	4152893.36
7	154.50	68.67	307981.71	4150913.16
8	110.50	49.11	307232.04	4151094.51
9	142.50	63.33	307125.17	4151107.90
10	111.50	49.56	307216.94	4151169.78
11	179.80	79.91	306013.72	4152789.19
12	90.10	40.04	305970.32	4152713.98
13	93.50	41.56	306001.14	4152263.77
14	137.50	61.11	306991.63	4151364.59
15	90.50	40.22	307847.04	4151274.20
16	121.50	54.00	307108.84	4151124.51
17	120.50	53.56	307112.42	4151469.23
18	174.50	77.56	307953.33	4150898.55
19	100.50	44.67	305657.19	4152908.38
20	112.50	50.00	307098.22	4151109.21
21	147.50	65.56	305835.54	4152711.19
22	121.50	54.00	307020.07	4151348.81
23	169.50	75.33	305896.00	4152292.94
24	172.50	76.67	305836.48	4152878.55
25	80.50	35.78	307499.46	4151782.42
26	77.50	34.44	307832.53	4151274.27
27	100.50	44.67	307201.36	4151844.21
28	183.50	81.56	305925.32	4152309.37
29	173.50	77.11	305746.89	4152909.30
30	142.50	63.33	305612.53	4152729.50
31	121.50	54.00	307212.45	4151108.11
32	140.00	62.22	305701.64	4152817.21
33	92.50	41.11	307079.85	4151155.41
34	174.20	77.42	305745.34	4152847.87
35	106.60	47.38	307185.78	4151845.85
36	162.70	72.31	305743.69	4152771.81
37	145.90	64.84	308025.63	4150854.11
38	160.50	71.33	307770.76	4151318.93
39	91.00	40.44	307036.77	4151212.58
40	125.50	55.78	307143.13	4151092.79
41	148.50	66.00	308087.73	4150824.25
42	141.50	62.89	307125.40	4151904.01
43	74.50	33.11	307426.10	4151828.83
44	134.50	59.78	306016.42	4152250.00
45	169.50	75.33	307529.33	4151828.49

ID	AREA (m^2)	AREA (%)	X-Coord	Y-Coord
46	108.50	48.22	307109.25	4151110.37
47	169.50	75.33	307771.92	4151362.65
48	155.00	68.89	305822.44	4152772.82
49	165.50	73.56	307784.83	4151288.21
50	89.50	39.78	308022.85	4150826.37
51	161.50	71.78	307966.87	4150794.81
52	171.50	76.22	307996.87	4150821.54
53	162.70	72.31	306016.69	4152218.69
54	142.50	63.33	307019.86	4151365.17
55	160.50	71.33	305582.15	4152745.13
56	119.50	53.11	307068.07	4151511.97
57	114.50	50.89	307098.36	4151121.45
58	136.50	60.67	308039.20	4150883.76
59	86.50	38.44	305790.90	4152832.71
60	119.50	53.11	307128.80	4151120.95
61	152.50	67.78	307981.63	4150778.32
62	117.50	52.22	307109.23	4151092.79
63	149.50	66.44	305684.30	4152908.03
64	171.50	76.22	305628.33	4152712.36
65	142.70	63.42	307082.85	4151377.55
66	126.50	56.22	307530.16	4151708.03
67	100.80	44.80	305760.86	4152757.75
68	71.50	31.78	305850.28	4152352.92
69	147.50	65.56	307215.40	4151136.88
70	136.50	60.67	307155.01	4151167.38
71	210.00	93.33	307755.02	4151349.00
72	210.50	93.56	307934.80	4150899.24
73	204.50	90.89	305714.69	4152895.67
74	63.50	28.22	305892.87	4152697.74
75	93.50	41.56	307141.87	4151919.30
76	62.50	27.78	307112.25	4151409.56
77	97.50	43.33	307756.43	4151273.59
78	58.50	26.00	307200.66	4151213.08
79	59.50	26.44	307156.50	4151379.06
80	57.10	25.38	307201.61	4151303.56
81	62.50	27.78	307128.59	4151409.36
82	60.50	26.89	307154.90	4151363.37
83	1.50	0.67	308296.61	4150779.40
84	1.50	0.67	308281.17	4150734.06
85	35.50	15.78	307440.82	4151723.25
86	1.50	0.67	305850.80	4152997.22
87	46.50	20.67	307126.17	4151498.15
88	36.50	16.22	307037.32	4151092.33
89	1.50	0.67	305850.30	4152983.85
90	2.50	1.11	305566.25	4152849.08
91	57.10	25.38	305583.20	4152923.37
92	37.50	16.67	305985.70	4152773.54
93	38.50	17.11	305700.64	4152923.20
94	52.10	23.16	305822.47	4152849.04
95	40.00	17.78	305924.78	4152699.63
96	52.30	23.24	306092.43	4152893.73

ID	AREA (m^2)	AREA (%)	X-Coord	Y-Coord
97	58.50	26.00	307139.84	4151198.39
98	50.50	22.44	305567.11	4152878.02
99	62.50	27.78	305655.82	4152863.52
100	53.50	23.78	305700.50	4152908.82
101	46.50	20.67	305595.38	4152757.55
102	58.50	26.00	305669.56	4152759.19
103	55.50	24.67	307051.05	4151199.81
104	2.50	1.11	308281.51	4150748.38
105	59.50	26.44	305612.78	4152905.98
106	58.50	26.00	305625.72	4152879.08
107	46.50	20.67	305746.26	4152789.31
108	47.50	21.11	305670.58	4152877.65
109	49.60	22.04	305655.33	4152775.95
110	40.50	18.00	307471.54	4151827.83
111	50.50	22.44	307095.33	4151183.41
112	2.50	1.11	305882.97	4153057.85
113	3.50	1.56	308371.70	4150748.47
114	3.50	1.56	308312.87	4150778.80
115	3.50	1.56	308298.40	4150749.30
116	3.50	1.56	308299.18	4150718.08
117	3.50	1.56	306016.02	4152308.87
118	3.50	1.56	305879.96	4152263.11
119	3.50	1.56	305867.93	4153013.68
120	3.50	1.56	308356.93	4150749.84
121	5.50	2.44	305610.66	4152834.47
122	5.50	2.44	308252.46	4150764.38
123	6.40	2.84	308355.86	4150778.36
124	6.40	2.84	308282.03	4150762.51
125	6.50	2.89	305582.58	4152849.52
126	6.50	2.89	305880.45	4153028.60
127	7.90	3.51	308295.54	4150734.88
128	7.90	3.51	307156.38	4151348.58
129	8.50	3.78	308356.07	4150763.05
130	13.50	6.00	308340.82	4150764.58
131	15.50	6.89	307184.48	4151439.54
132	16.50	7.33	307155.90	4151440.27
133	17.50	7.78	307170.18	4151318.78
134	19.50	8.67	305625.71	4152772.32
135	20.50	9.11	307185.99	4151393.65
136	23.50	10.44	307199.52	4151288.40
137	24.50	10.89	308265.58	4150794.12
138	24.50	10.89	305549.38	4152819.04
139	33.50	14.89	307126.53	4151530.02
140	33.50	14.89	307170.51	4151305.05
141	34.50	15.33	307126.25	4151467.49
142	34.60	15.38	307155.33	4151393.27
143	71.50	31.78	307155.47	4151857.31
144	79.50	35.33	307156.58	4151830.24
145	95.50	42.44	307486.46	4151813.94
146	99.50	44.22	306976.72	4151348.38
147	100.62	44.72	307096.85	4151512.32

ID	AREA (m^2)	AREA (%)	X-Coord	Y-Coord
148	74.50	33.11	307081.04	4151515.77
149	72.20	32.09	307185.25	4151831.55
150	96.60	42.93	307170.05	4151392.89
151	68.00	30.22	307168.06	4151918.06
152	76.20	33.87	307502.64	4151709.42
153	83.60	37.16	307412.09	4151782.79
154	70.50	31.33	305610.66	4152876.56
155	98.50	43.78	307095.79	4151136.61
156	70.50	31.33	305656.51	4152894.02
157	95.70	42.53	307412.16	4151797.06
158	86.50	38.44	307097.70	4151347.97
159	99.50	44.22	307082.34	4151121.10
160	88.50	39.33	305865.86	4152308.42
161	65.40	29.07	305655.69	4152729.18
162	100.00	44.44	305639.88	4152924.20
163	92.70	41.20	307154.35	4151303.11
164	85.50	38.00	305970.68	4152309.40
165	85.60	38.04	307142.30	4151859.39
166	73.50	32.67	307126.89	4151213.31
167	78.50	34.89	307081.62	4151531.28
168	69.50	30.89	307471.49	4151814.03
169	88.50	39.33	307397.12	4151782.65
170	69.80	31.02	307173.20	4151209.08
171	86.50	38.44	307035.69	4151871.83
172	77.50	34.44	307245.57	4151137.64
173	88.50	39.33	305971.42	4152743.78
174	102.50	45.56	307183.48	4151122.68
175	89.50	39.78	308058.46	4150840.42
176	89.50	39.78	307170.56	4151121.28
177	85.00	37.78	305567.58	4152894.01
178	100.50	44.67	307516.96	4151722.32
179	80.50	35.78	307156.97	4151423.63
180	81.50	36.22	307172.44	4151288.56
181	102.50	45.56	305820.25	4152862.72
182	66.00	29.33	305669.90	4152695.40
183	82.50	36.67	305566.58	4152803.88
184	77.50	34.44	305579.05	4152772.37
185	97.50	43.33	307845.60	4151241.95
186	111.60	49.60	307219.93	4151182.54
187	106.60	47.38	307799.71	4151348.51
188	102.50	45.56	305580.69	4152697.99
189	137.50	61.11	307229.68	4151107.15
190	131.50	58.44	307185.82	4151379.83
191	137.50	61.11	305866.10	4152910.36
192	127.50	56.67	305656.54	4152849.22
193	104.50	46.44	305642.46	4152895.04
194	132.50	58.89	307245.65	4151122.88
195	108.50	48.22	307097.09	4151213.79
196	132.50	58.89	307168.24	4151168.77
197	116.50	51.78	305657.60	4152923.33
198	136.50	60.67	307020.11	4151844.85

ID	AREA (m^2)	AREA (%)	X-Coord	Y-Coord
199	127.50	56.67	307183.92	4151109.17
200	103.90	46.18	305955.34	4152789.38
201	128.50	57.11	307034.68	4151122.56
202	122.50	54.44	307083.21	4151365.27
203	121.50	54.00	308027.57	4150898.69
204	135.50	60.22	307228.26	4151170.30
205	133.50	59.33	307229.78	4151211.06
206	121.50	54.00	305943.35	4152307.83
207	116.50	51.78	307006.84	4151333.77
208	129.50	57.56	305641.41	4152727.82
209	126.50	56.22	307995.94	4150898.13
210	120.30	53.47	307172.00	4151335.93
211	104.50	46.44	306976.98	4151377.39
212	112.50	50.00	305582.10	4152893.91
213	123.50	54.89	305956.00	4152308.23
214	120.50	53.56	307066.07	4151332.80
215	113.50	50.44	307081.21	4151919.96
216	130.50	58.00	307230.58	4151122.81
217	134.50	59.78	307243.84	4151107.88
218	135.50	60.22	307140.65	4151169.48
219	125.50	55.78	306991.08	4151393.63
220	116.50	51.78	307126.07	4151333.19
221	112.50	50.00	305941.33	4152323.12
222	130.50	58.00	307020.40	4151379.87
223	105.60	46.93	307020.84	4151857.28
224	153.50	68.22	308086.78	4150853.28
225	165.50	73.56	307982.25	4150763.79
226	172.50	76.67	307200.88	4151902.53
227	174.50	77.56	305896.63	4152279.14
228	156.40	69.51	305909.67	4152351.86
229	161.50	71.78	307874.75	4151245.32
230	165.50	73.56	307366.58	4151722.27
231	163.50	72.67	307201.89	4151170.34
232	140.20	62.31	307755.32	4151363.27
233	170.50	75.78	305775.89	4152877.15
234	167.30	74.36	307994.10	4150809.46
235	162.10	72.04	305729.74	4152743.89
236	149.50	66.44	307935.69	4150853.10
237	168.50	74.89	307982.99	4150838.29
238	176.50	78.44	307966.10	4150883.29
239	142.50	63.33	305729.53	4152817.34
240	174.50	77.56	307126.56	4151828.17
241	165.50	73.56	307053.87	4151861.88
242	143.50	63.78	307081.94	4151407.83
243	162.50	72.22	308055.60	4150763.39
244	144.50	64.22	307081.29	4151438.45
245	149.50	66.44	307200.92	4151889.54
246	144.50	64.22	307020.31	4151166.73
247	165.50	73.56	305852.56	4152862.92
248	172.50	76.67	307184.50	4151889.62
249	142.60	63.38	305567.02	4152756.55

ID	AREA (m^2)	AREA (%)	X-Coord	Y-Coord
250	169.50	75.33	305941.39	4152293.84
251	172.50	76.67	305925.02	4152293.59
252	171.50	76.22	305746.30	4152743.42
253	174.50	77.56	305715.50	4152787.34
254	171.50	76.22	305760.73	4152906.58
255	145.50	64.67	308069.48	4150793.61
256	151.50	67.33	305971.56	4152294.44
257	140.50	62.44	307184.84	4151906.04
258	169.50	75.33	305834.33	4152864.41
259	157.50	70.00	307247.44	4151213.23
260	142.50	63.33	305776.13	4152758.82
261	139.50	62.00	307051.18	4151874.97
262	158.20	70.31	307200.42	4151876.04
263	155.30	69.02	305849.83	4152713.10
264	151.50	67.33	307168.40	4151198.27
265	173.50	77.11	307831.43	4151332.82
266	183.50	81.56	307108.59	4151333.26
267	183.50	81.56	307114.74	4151873.93
268	184.50	82.00	305866.91	4152833.54
269	185.40	82.40	305911.77	4152323.36
270	173.50	77.11	305599.27	4152728.09
271	194.20	86.31	306015.74	4152772.43
272	173.50	77.11	307803.65	4151227.83
273	198.50	88.22	305897.63	4152352.31
274	178.50	79.33	307064.34	4151844.00
275	211.83	94.15	305716.19	4152865.09
276	175.36	77.94	305728.16	4152863.48
277	212.32	94.37	305595.38	4152714.03
278	200.50	89.11	307997.75	4150837.45
279	182.60	81.16	305717.68	4152818.37
280	180.50	80.22	305762.14	4152834.04
281	183.50	81.56	305716.32	4152805.51
282	199.50	88.67	305835.72	4152816.86
283	216.90	96.40	307007.31	4151529.94
284	201.50	89.56	306016.50	4152745.62
285	186.50	82.89	305762.00	4152743.27
286	180.50	80.22	305867.24	4152353.44
287	189.50	84.22	307755.55	4151319.03
288	175.50	78.00	308024.86	4150763.37
289	199.56	88.69	307965.85	4150837.48
290	176.60	78.49	308010.44	4150898.17
291	225.00	100.00	305910.89	4152774.79
292	192.50	85.56	307818.65	4151228.44
293	187.50	83.33	305762.04	4152878.51
294	204.50	90.89	307950.51	4150869.37
295	189.50	84.22	305777.64	4152924.21
296	140.50	62.44	307036.75	4151921.61
297	139.50	62.00	308041.41	4150763.91
298	203.31	90.36	305700.15	4152788.79
299	200.50	89.11	307833.16	4151228.37
300	189.50	84.22	305745.70	4152699.63

8 VITA

Name **Eva Pantaleoni**

Research experience:
- Remote sensing and GIS applications in soils, wetland, forestry, and agriculture,
- Multispecrtral sensors, ASTER, Landsat, algorithm development for image processing, vegetation and soil extraction and assessment
-spatial statistics, spatial analysis techniques, sources of spatial data

Positions held:

August 2004-May 2007 Graduate Research and Teaching Assistant, Department of Crop and Soil Environmental Science, Virginia Tech, VA, USA

May 2005- August 2005 Programmer Analyst, Geography Department, Virginia Tech, VA, USA

August 2002-May 2004 Teaching Assistant, Italian Department, Purdue University, IN,USA /

June 2001-June 2002 Executive secretary, ESN-Bologna, Bologna, Italy

September 1999- December 1999 Student assistant, Department of Pharmaceutical Science, Katholieke Universiteit Leuven, Belgium

Education:

-Ph.D. (spring 2007), Dept. of Crop and Soil Environmental Science, Virginia Tech.
Course concentrations: soils, wetlands, remote sensing, GIS, spatial data analysis
Masters in Earth Observation (2004), Dep. Agricultural and Biological Engineering, Purdue University, IN, USA
Laurea (2001), Faculty of Natural Science, University of Bologna, Bologna, Italy

Eva Pantaleoni